

STRUCTURAL AND MAGNETIC PROPERTIES OF EXCHANGE BIASED CoO/Co
MULTILAYERS



by
Ekrem Sınır


Submitted to Graduate School of Natural and Applied Sciences
in Partial Fulfillment of the Requirements
for the Degree of Doctor of Philosophy in
Physics

Yeditepe University
2017

STRUCTURAL AND MAGNETIC PROPERTIES OF EXCHANGE BIASED CoO/Co
MULTILAYERS

APPROVED BY:

Assist. Prof. Dr. Ercüment Akat
(Thesis Supervisor)


.....

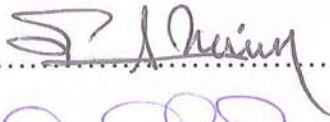
Assoc. Prof. Dr. Numan Akdoğan
(Thesis Co-Supervisor)


.....

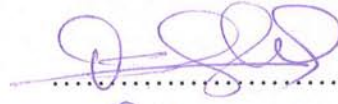
Prof. Dr. Merih Serin


.....

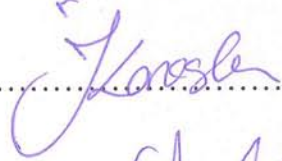
Assoc. Prof. Dr. Ertan Akşahin


.....

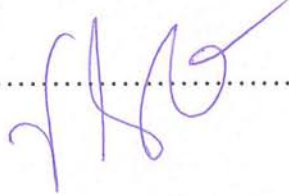
Assoc. Prof. Dr. Osman Öztürk


.....

Assoc. Prof. Dr. Şerife İpek Karaaslan


.....

Assoc. Prof. Dr. Vildan Üstoğlu Ünal


.....

DATE OF APPROVAL: / / 2017

ACKNOWLEDGEMENTS

I would like to thank my co-advisor Assoc. Prof. Dr. Numan Akdoğan from Gebze Technical University Physics Department for giving me the chance to be part of his research team of young, dynamic and very friendly colleagues. Starting from the beginning, Prof. Akdoğan gave me all the advice, help, motivation and opportunity needed to realize the work mentioned in this thesis. He made all the difference...

I would also like to thank Asst. Prof. Dr. Ercüment Akat for shouldering the responsibility of being my advisor at Yeditepe University for the thesis work which I mostly conducted at Gebze, for his trust, support, discussions and help that he provided. He has been a great teacher in the PhD classes, always keen on the mathematical, scientific and most importantly on the personal integrity. He has always welcomed me as a colleague and treated me not less than a friend. His support will never be forgotten.

I am grateful to my colleagues Dr. Erdem Demirci and Dr. Mustafa Öztürk in the research team of Assoc. Prof. Dr. Numan Akdoğan, for the kind and full support during my time in the laboratory. They have helped with the measurements, data analysis and above all with the difficulties faced in this study. I feel myself quite lucky to have known and worked with such kind, hard-working and helpful students of science. Always grateful...

Special thanks are due to Assoc. Prof. Dr. Osman Öztürk and Assoc. Prof. Dr. Mustafa Erkovan for the growth of the samples studied in this work and for their XPS analyses conducted at Surface Physics Laboratory of Gebze Technical University.

I thank all the professors of Yeditepe University Physics Department including Ahmet İnce, Rabia İnce, Necdet Aslan, Ömür Akyüz and Avadis Simon Hacınlıyan. I also would like to thank Assoc. Prof. Dr. Ertan Akşahin and Assoc. Prof. Dr. Ş. İpek Karaaslan and Assoc. Prof. Dr. Vildan Üstoğlu Ünal from Yeditepe, Prof. Dr. Merih Serin from Yıldız Technical University and Assoc. Prof. Dr. Osman Öztürk from Gebze Technical University for being members of my thesis progress and defense committees, for all their support and advice. The research assistants of Physics Departments, my colleagues during my

employment at Yeditepe, my classmates and former assistants: Mehmet K. Torun, Eylem Gülçe Çoker, Fatma Melda Patan Alper, Türkay Toklu, Michael Feeney, Kenan Şentürk, Murat Erentürk and Tuba Şen are all to be remembered with kind memories.

I thank Prof. Dr. Bekir Aktaş and Assoc. Prof. Dr. Mustafa Özdemir for their kindness to attend my thesis progress committees, for their time, discussions we had and guidance they provided.

Special thanks are to my friends Aykut Tekman and Ekim Ateşer for always being there for me and my family and for sharing joys and griefs of life. Mert Ener, a social science graduate in love of natural sciences, tackled some technical details and helped me a lot during our study nights and even run some codes for the little problems I faced.

My colleagues at TÜBİTAK UME, Dr. Yasin Durgut, Ahmet Türk and Dr. Mustafa Arıkan, I thank you all for your support, patience and kindness.

I am also grateful to my high school biology teacher Ayfer Özgül and her family for their continuous support starting from my high school years up to my university graduation.

I would like to thank TÜBİTAK BİDEB for supporting my studies with a five year PhD scholarship in 2211 Domestic Graduate Scholarship Program.

My parents Ali and Ayfer Sınır, brothers Erdem, Kerem and Levent Sınır, my uncle Mahmut Sınır and the rest of the Sınır family, Hasan and Nimet Azkırın, Ayten-Ahmet-Burçak-Altay Ecevit: the members of the family I was raised in and Alaattin Topçu, Nasiye Topçu, Murat Topçu, Nisan Topçu, members of the family I was accepted in, I love you all..

And finally and most importantly I would like to express the greatest of all appreciation to my wife and great friend of life Burcu Topçu Sınır, for always supporting me and for her love. I wouldn't be able to think of a life without you. Thank you for everything and especially for being the mother of our lovely kids Evren and Uzay. Love forever...

ABSTRACT

STRUCTURAL AND MAGNETIC PROPERTIES OF EXCHANGE BIASED CoO/Co MULTILAYERS

In this study, the exchange bias properties of four multilayer stack samples of Antiferromagnetic (AFM) CoO and Ferromagnetic (FM) Co in the [CoO/Co]_n thin film form with n = 1, 2, 3 and 5 are studied. Ferromagnetic resonance (FMR) measurements were carried out to investigate the magnetic anisotropies of the samples and vibrational sample magnetometry (VSM) was employed to probe the exchange bias properties. Out-of-plane FMR studies yielded an increasing number of resonance peaks as “n” increased and in-plane FMR measurements resulted in a uniaxial in-plane magnetic anisotropy for the samples. Low temperature VSM measurements provided shifted hysteresis curves, a sign of exchange bias, with a stepwise character. Observed steps are believed to be due to magnetization reversals of individual FM layers with varying thicknesses, each of which is pinned through two interfaces from above and below with two AFM layers, except the uppermost FM Co layer with a single AFM neighbour. TEM images provided FM-AFM layer thicknesses, which are important on the pinning of each FM layer by neighbouring AFM layers. X-Ray Photoelectron Spectroscopy (XPS) measurements of cobalt-oxide layer show that the oxidation states Co⁺² and Co⁺³ coexist in the AFM layer which is an indication that different phases of cobalt-oxide, CoO and Co₃O₄, are existing in the layer. These different phases of cobalt oxide are thought to be responsible for the observed blocking temperature of the exchange biased system lower than the bulk Néel temperature of AFM CoO, in addition to the effect of thickness of the AFM layer.

Along with the main experimental studies, a theoretical account of the Ferromagnetic Resonance in a single FM layer was conducted that leads to the fundamental resonance condition in FMR. After fundamental resonance condition of FMR was obtained, effort has been devoted to systems composed of many FM layers (a multilayer structure) generally separated by nonmagnetic spacer layers and a matrix model have been developed to solve the system of equations that can then be used to calculate the dynamic susceptibility and can be utilized for the computer simulation of FMR experiments.

ÖZET

EXCHANGE BIAS ETKİSİ ALTINDAKİ CoO/Co ÇOKLU KATMANLARIN YAPISAL VE MANYETİK ÖZELLİKLERİ

Bu çalışmada $[\text{CoO}/\text{Co}]_n$ ($n = 1, 2, 3$ ve 5) ince film yapısında Antiferromanyetik (AFM) CoO ve Ferromanyetik (FM) Co içeren dört adet çok katmanlı örneğin exchange bias özellikleri çalışılmıştır. Ferromanyetik Rezonans (FMR) ölçümleri gerçekleştirilerek örneklerin manyetik anizotropileri araştırılmış, Titreşimli Örnek Manyetometresi (VSM) kullanılarak exchange bias özellikleri incelenmiştir. Düzlem-dışı FMR çalışmalarından “n” arttıkça artan sayıda rezonans tepeleri elde edilmiş, düzlem-içi FMR ölçümlerinden de örnekler için film düzleminde tek-eksenel bir manyetik anizotropi elde edilmiştir. Düşük sıcaklık VSM ölçümleri, basamaklı yapıda ve exchange biasın işareti olan kaymış histerisis eğrileri vermiştir. Gözlemlenen basamakların, tek bir AFM komşuya sahip en üst FM Co katmanı dışında, her biri yukarıdan ve aşağıdan iki ara yüzey üzerinden iki AFM katman tarafından kilitlenen değişik kalınlıktaki FM katmanların bireysel manyetizasyon tersinmelerinden kaynaklandığı düşünülmektedir. Geçirimli elektron mikroskobu (TEM) görüntüleri, her bir FM katmanın komşu AFM katmanlar tarafından kilitlenmesinde önem arz eden FM – AFM kalınlıklarını ortaya koymuştur. CoO tabakasına ait X-ışını fotoelektron spektroskopisi (XPS) ölçümleri, kobalt oksitin CoO ve Co_3O_4 gibi farklı fazlarının varlığının işareti olan Co^{+2} and Co^{+3} oksidasyon fazlarının AFM katmanda birlikte var olduğunu göstermiştir. Kobalt oksitin bu farklı fazlarının, AFM tabaka kalınlığının etkisine ek olarak, exchange bias sisteminde gözlemlenen ve yığın yapıdaki AFM CoO’in Néel sıcaklığından daha düşük olan engelleme sıcaklığından sorumlu olduğu düşünülmektedir.

Ana deneysel çalışmalarla birlikte, tek bir FM katman için temel FMR rezonans koşulunu sağlayan teorik bir çalışma yapılmıştır. FMR için temel rezonans şartı elde edildikten sonra, genellikle manyetik-olmayan ara katmanlarla ayrılmış birçok FM katmandan oluşan sistemler (bir çoklu katman yapısı) çalışılmış ve dinamik uygunluğu hesaplamak için ve FMR deneylerinin bilgisayar benzetimlerinde kullanılabilecek bir matris modeli geliştirilmiştir.

TABLE OF CONTENTS

ACKNOWLEDGEMENTS	iii
ABSTRACT.....	v
ÖZET	vi
LIST OF FIGURES	ix
LIST OF TABLES	xii
LIST OF SYMBOLS/ABBREVIATIONS.....	xiii
1. INTRODUCTION.....	1
2. BASICS OF MAGNETISM.....	4
2.1. MAGNETIC MOMENT.....	4
2.2. ZEEMAN INTERACTION	7
2.3. MAGNETIC MATERIALS.....	10
2.3.1. Diamagnets and Paramagnets	10
2.3.2. Ferromagnetic, Ferrimagnetic and Antiferromagnetic Materials	11
3. EXCHANGE BIAS	14
3.1. DISCOVERY	14
3.2. BASIC PHENOMENOLOGY.....	15
3.3. IDEAL EXCHANGE BIAS MODEL	16
3.4. GENERAL PROPERTIES OF EXCHANGE BIASED SYSTEMS.....	19
3.4.1. Ferromagnetic Layer Thickness.....	19
3.4.2. Antiferromagnetic Layer Thickness	19
3.4.3. Interface Roughness.....	20
3.4.4. Blocking Temperature	20
3.4.5. Cooling Field	20
3.4.6. Training Effect.....	21
4. THEORETICAL WORK ON FERROMAGNETIC RESONANCE.....	22
4.1. FUNDAMENTAL THEORY OF FERROMAGNETIC RESONANCE	23
4.1.1. Magnetic Moment and Angular Momentum	23
4.1.2. Equation of Motion and Damping	24

4.1.3.	Effective Magnetic Field Derived From Energy Density	26
4.1.4.	The Geometry and Energy Terms	28
4.1.5.	Linearization of Equation of Motion	31
4.1.6.	Proposed Solutions	35
4.1.7.	Dynamic Susceptibility and Resonance Condition.....	40
4.2.	FERROMAGNETIC RESONANCE IN MULTILAYER STRUCTURES	45
4.2.1.	Equation of Motion.....	45
4.2.2.	Effective Field and Its Torque	47
4.2.3.	Effects of RF Field and Damping	53
4.2.4.	Matrix Representation of the Magnetization Dynamics	57
4.2.5.	General Rules for Calculating the Nonzero Elements of the Matrix Representation	66
4.2.6.	Extracting Dynamical Magnetic Susceptibility	74
5.	MATERIAL, EXPERIMENTAL WORK AND RESULTS	79
5.1.	SAMPLE PREPARATION	80
5.2.	STRUCTURAL CHARACTERIZATION	81
5.2.1.	X-Ray Photoelectron Spectroscopy (XPS) Measurements.....	81
5.2.2.	Transmission Electron Microscopy (TEM) Measurements.....	82
5.3.	MAGNETIC CHARACTERIZATION	84
5.3.1.	Ferromagnetic Resonance (FMR) Measurements	85
5.3.2.	Vibrational Sample Magnetometry (VSM) Measurements	90
6.	DISCUSSION.....	96
7.	CONCLUSION	100
	REFERENCES	101
	APPENDIX A.....	126

LIST OF FIGURES

Figure 2.1. Schematic representation of spins in a saturated ferromagnet	11
Figure 2.2. Hysteresis curve showing the magnetization response M of the ferromagnet as a function of applied magnetic field.....	12
Figure 2.3. The sketch of antiferromagnetic and ferrimagnetic moments.....	13
Figure 3.1. The hysteresis curves at 77 K of field cooled and zero field cooled FM Co particles embedded in AFM CoO	14
Figure 3.2. Spin configurations of FM and AFM spins at different stages of the hysteresis loop of an FM material in contact with an AFM material when the system is subjected to field cooling procedure	16
Figure 3.3. Geometry for the ideal exchange bias model	17
Figure 4.1. Landau-Lifshitz-Gilbert and Bloch-Bloembergen damping paths.....	26
Figure 4.2. Geometry for the FMR calculations.....	29
Figure 4.3. Components of the magnetization vector.....	47
Figure 4.4. Workflow for the calculation of the dynamical susceptibility	78
Figure 5.1. CoO/Co multilayer thin film structure	79
Figure 5.2. Cluster UHV chamber at Gebze Technical University for magnetron sputtering and surface characterization.....	80

Figure 5.3. XPS survey spectra from the Co-oxide surface and the Co 2p spectral region showing the effects of oxidation.....	82
Figure 5.4. TEM images of [CoO/Co] _n multilayers.....	83
Figure 5.5. Bruker EMX EPR system at Gebze Technical University for FMR measurements.....	85
Figure 5.6. In-plane sample placement and angular sweep for FMR.....	86
Figure 5.7. Out-of-plane sample placement and angular sweep for FMR.....	86
Figure 5.8. In-plane and out-of-plane geometries for FMR measurements.....	87
Figure 5.9. In-plane FMR data for the angular dependence of resonance fields from triple bilayer [CoO/Co] ₃ and quintuple bilayer [CoO/Co] ₅	88
Figure 5.10. The angular dependence of resonance field from FMR data of single bilayer [CoO/Co], double bilayer [CoO/Co] ₂ , triple bilayer [CoO/Co] ₃ , and quintuple bilayer [CoO/Co] ₅ for out-of-plane geometry.....	89
Figure 5.11. A part of out-of-plane collective FMR detailed real spectra of quintuple bilayer [CoO/Co] ₅ taken at varying θ_H	90
Figure 5.12. Quantum Design PPMS (9 T) System at Gebze Technical University for VSM measurements.....	91
Figure 5.13. Measurement protocol for EB measurements with VSM	92
Figure 5.14. The hysteresis loops normalized to saturation magnetization at room temperature (RT) and at 10 K after field cooling of the samples	93

Figure 5.15. Temperature dependence of magnitudes of coercive fields ($-H_{C1}$ and H_{C2}) and exchange bias field ($-H_{EB}$) for $[\text{CoO}/\text{Co}]_n$ multilayers94



LIST OF TABLES

Table 5.1. The TEM measured thicknesses of $[\text{CoO}/\text{Co}]_n$ multilayers	84
---	----



LIST OF SYMBOLS/ABBREVIATIONS

A	Bilinear interlayer exchange coupling constant
\vec{B}	Magnetic induction
e	Fundamental unit of charge (1.6×10^{-19} <i>Coulomb</i>)
E	Volume energy density (energy per unit volume)
g	Spectroscopic splitting factor (Landé-g factor)
\vec{h}	Rf magnetic field
h_θ	θ -component of \vec{h}
h_ϕ	ϕ -component of \vec{h}
\hbar	Reduced Planck constant
h_x^0	Amplitude of rf magnetic field along x -axis
\vec{H}	Magnetic field
H_C	Coercive field
H_{EB}	Exchange bias field
\vec{H}_{eff}	Effective magnetic field
H_{FC}	Cooling field
j	Total angular momentum quantum number for a single electron
J	Total angular momentum quantum number for the atom
\vec{J}	Total angular momentum
J_{INT}	Interfacial interaction constant
kOe	kiloOersted
K	Kelvin
K	Anisotropy constant
l	Orbital angular momentum quantum number for a single electron
\vec{L}	Orbital angular momentum
m	Mass
m_l	Orbital magnetic quantum number
m_s	Spin magnetic quantum number
M	Magnetization (magnetic moment per unit volume)

\vec{M}	Magnetization vector
M_J	Magnetic quantum number for the atom
M_r	Remanent magnetization (remanence)
M_s or M_0	Magnitude of saturation magnetization
m_θ	Dynamic (transverse) component of magnetization in θ direction
m_ϕ	Dynamic (transverse) component of magnetization in ϕ direction
$\vec{M}_{\theta,\phi}$	Dynamic (transverse) magnetization
N	Number of ferromagnetic layers in the multilayer system
P	Power absorbed by the unit volume of the sample
\vec{P}	Generic angular momentum vector
q	Charge
\vec{R}	Damping term
s	Spin angular momentum quantum number for a single electron
\vec{S}	Spin angular momentum
T	Temperature
T_C	Curie temperature
T_N	Néel temperature
T_1	Spin-lattice (longitudinal) relaxation time
T_2	Spin-spin (transverse) relaxation time
U	Energy
V	Volume
Z	Atomic number
α	Gilbert damping constant
γ	Gyromagnetic ratio
ε	Areal energy density (energy per unit area)
$\theta - \phi$	Polar and azimuthal angles of magnetization
$\theta_H - \phi_H$	Polar and azimuthal angles of magnetic field
λ	Landau-Lifshitz damping constant
$\vec{\mu}$	Magnetic moment vector
μ_B	Bohr magneton
μ_0	Magnetic permeability of free space

$\vec{\tau}$	Torque
χ	Magnetic susceptibility
ω	Angular frequency of the driving rf-field
ω_0	Resonance angular frequency
AFM	Antiferromagnetic
Ar ⁺	Argon ion
CGS	Centimeter gram second
Co	Cobalt
CoO	Cobalt Oxide
Co ₃ O ₄	Tricobalt tetraoxide (Cobalt (II) dicobalt (III) tetraoxide)
EB	Exchange bias
EPR	Electron paramagnetic resonance
eV	electron-Volt
FC	Field cooling
FIB	Focused ion beam
FM	Ferromagnetic
FMR	Ferromagnetic resonance
GMR	Giant magnetoresistance
IP	In-plane
LHe	Liquid Helium
MB	Meiklejohn Bean
MRAM	Magnetoresistive random access memory
MTJ	Magnetic tunnel junction
OOP	Out-of-plane
PPMS	Physical property measurement system
RF or rf	Radio (microwave) frequency
RT	Room temperature
sccm	Standard cubic centimeters per minute
Si	Silicon
SWR	Spin wave resonance
TEM	Tunnelling electron microscopy
TMR	Tunnel magnetoresistance

UHV	Ultrahigh vacuum
UV	Ultraviolet
VSM	Vibrational sample magnetometry
XPS	X-ray photoelectron spectroscopy
2-D	2-Dimensional



1. INTRODUCTION

Exchange bias (EB) which was discovered more than half a century ago to occur at a ferromagnetic (FM) – antiferromagnetic (AFM) interface, has played an important role in the pinning of the magnetization state of one of the ferromagnetic layers used in spin valve structures employed in magnetic storage media. Besides the experimental efforts and extensive applications in information storage technology, there is still a lack of a definitive theory able to account for the observed effects. In order to contribute to the ongoing research related to this phenomenon, experimental studies involving varying forms of FM - AFM interfaces have to be performed.

The effect (EB), discovered in 1956 [1] and explained in more detail in 1957 [2] by Meiklejohn and Bean, is a phenomenon observed in structures involving FM-AFM interfaces when the system is cooled down through the Néel temperature (T_N) of the AFM, with the Curie temperature of FM $T_C > T_N$, in the presence of a magnetic field, a procedure called field cooling, or when the system is deposited in a magnetic field [3]. The effect manifests itself as a shift of the hysteresis curve of FM along magnetic field axis generally towards negative field values with an enhanced coercivity defined as the half-width of the hysteresis curve. Since its discovery [1, 2], the effect has been investigated theoretically and experimentally in many papers reviewed in [4-15] and has found a tremendous utility in information storage technology.

Exchange bias has found a great application utility along with the giant magnetoresistance (GMR) [16-26] and tunnel magnetoresistance (TMR) effects [22, 26-42] in the spin based technological device fabrication employing spin-dependent transport [43] leading to spintronics (spin electronics) [44-47] for high density magnetic data storage units, read heads, spin valves, magnetic tunnel junctions (MTJ) and nonvolatile memory devices like magnetoresistive random access memory (MRAM) [48, 49]. However, its microscopic origin is still under debate. The need of strong, controllable, predictable and also low-energy consuming devices for the technology motivates the researchers studying more to understand the scientific basis of this phenomenon.

Exchange bias has been an indispensable tool in the pinning of the magnetization state of the reference layer used in both GMR and TMR based spin-valve structures. The spin-valve term was coined by B. Dieny et al. and it was the first time where EB had been utilized for creating a spin dependent transport [19, 50]. A spin-valve structure is composed of two ferromagnetic layers separated by a nonmagnetic spacer layer. When the nonmagnetic layer is a conductor, a GMR structure is built whereas a very thin insulating layer as a spacer gives rise to a TMR structure. A ferromagnetic reference layer in contact with the antiferromagnetic layer has a single easy direction of magnetization stemming from the unidirectional anisotropy created by the exchange interaction of the FM and AFM spins at the common interface. The electrical resistance of the spin-valve structure is dependent upon the relative orientations of the magnetizations in the FM layers. An external magnetic field can change the magnetization direction of the sensor FM layer whereas the reference layer has its magnetization kept at its easy direction induced by the EB effect. The resistance of the system changes as the angle between the magnetizations of FM layers is changed by the external field. Thus, the spin-valve structure acts a sensor of external fields and can be used to detect the binary information of zeros and ones encoded in the magnetic data storage system. “0” is represented by opposite alignments of the FM magnetizations that causes a high resistance state and “1” is represented by parallel FM magnetizations creating a low resistance state which can be detected by an appropriate electronics circuitry.

Since exchange bias is thought to be an interfacial property, systems composed of more than one FM – AFM interface has gained attention in the scientific community because of the information that can be gathered from such systems. It is mentioned that study of at least a trilayer structure would yield information that is not accessible by a single FM – AFM bilayer [51]. Multilayer studies would enlighten the dependence on atomic scale interface roughness [52, 53], independent exchange bias effects on two FM layers due to a spiraling spin structure in AFM and its thickness dependence [54], parallel-antiparallel EB couplings [55], competition of interfacial exchange and AFM anisotropy and its temperature dependence [56]. In addition to the interfacial properties, these studies also reveal that the AFM bulk structure has also a key role on the EB properties. It is also important to note the simulation studies for the thickness and bilayer number dependence of exchange bias [57].

This thesis work is focused upon thin film bilayers composed of FM Co and AFM CoO prepared in a multilayer fashion. In Section 2, a brief overview of magnetism is given. Section 3 is devoted to the discovery, basic phenomenology, ideal model and general properties of EB and exchange biased systems. In Section 4, a theoretical analysis of one of the experimental techniques used in this work, Ferromagnetic Resonance (FMR), is provided giving the fundamental resonance condition followed by a linearized model of FMR that can be applied to multilayer structures composed of many FM layers and a detailed account is given for the use and range of applicability of the obtained set of equations. Section 5 is devoted to the material, experimental work and results of the multilayer structures of Co/CoO. The experimental findings are discussed in Section 6 followed by the conclusion provided in Section 7. An appendix is also given for some of the magnetic anisotropy energies that can be incorporated into FMR studies.

2. BASICS OF MAGNETISM

There are two macroscopic sources of magnetism: magnets and electric currents. At the microscopic level, however, macroscopic manifestations of magnetism can be understood in three fundamental mechanisms in atoms: the orbital motion of the electrons around the nucleus, their intrinsic angular momentum called spin and a small induced moment as a response to external magnetic fields. The first two contributions are related to what is known as paramagnetism and the third is related to diamagnetism [58]. Individual atoms possess only these above mentioned magnetic classifications. Diamagnetism is inherent to all atoms, therefore, all materials display diamagnetism. Only those atoms, however, which have all their electron shells filled are called diamagnetic. Despite being manifested by all atoms, diamagnetism is a weak effect, except in superconductors, and is overcome by such interactions like paramagnetism or ferromagnetism. The magnetic behaviour of interest, however, is magnetic orders exhibited by structures such as ferromagnets, ferrimagnets and antiferromagnets which require a collection of magnetic moments in an ordered array.

2.1. MAGNETIC MOMENT

The elementary unit of magnetism is the magnetic dipole moment or magnetic moment in short, considering the fact that the magnetic field is created by currents, be it at the atomic level or at the macroscopic realm. If there is a current I flowing around a surface element dA , the magnetic moment is defined as

$$\vec{\mu} = \int d\vec{\mu} = \int I dA \hat{n} \quad (2.1)$$

where \hat{n} is the unit vector along the surface normal as given by the right hand rule for which the normal is defined as the direction pointed by the thumb when the four fingers curl around the current. The unit of magnetic moment is “ $A.m^2$ ” in SI and “emu” (electromagnetic unit) in CGS systems of units. Since magnetism is related to rotating charged particles, there is a relation that connects the magnetic moment to the angular momentum:

$$\vec{\mu}_{orbit} = \gamma \vec{L} \quad (2.2)$$

where \vec{L} represents the orbital angular momentum and γ is the ratio of the magnetic moment to the angular momentum called the gyromagnetic (or magnetogyric) ratio given by

$$\gamma = \frac{q}{2m} \quad (2.3)$$

with q being the charge and m being the mass of the circulating entity. In the case of electrons $q = -e$ in which e is the fundamental unit of electric charge. Due to the negative charge of the electrons, magnetic moment and angular momentum are oppositely directed vectors. It is worth mentioning at this stage that defining $\vec{\mu}$ and γ as given by Equations (2.2) and (2.3) is a more general approach that can be applied to any charge q , but when it comes to electrons, reader can find examples in the literature such that there appears a negative sign in front of γ in Equation (2.2) but then γ itself is given by its absolute value as we shall practise in Section 5.

As pointed out earlier, the magnetic moment is not only caused by the orbital motion but there is an intrinsic angular momentum called spin and therefore it has its own contribution to the magnetic moment:

$$\vec{\mu}_{spin} = \gamma_{spin} \vec{S} \quad (2.4)$$

with \vec{S} being the spin angular momentum. The reason we had to specify a gyromagnetic ratio γ_{spin} for the spin with a subscript is that it is twice the value obtained for the orbital part. Therefore for electrons

$$\vec{\mu}_{orbit} = \gamma \vec{L} = -\frac{e}{2m} \vec{L} = -\frac{e\hbar}{2m} \cdot \frac{1}{\hbar} \cdot \vec{L} = -\frac{\mu_B}{\hbar} \vec{L} \quad (2.5)$$

$$\vec{\mu}_{spin} = \gamma_{spin} \vec{S} = -2 \cdot \frac{e}{2m} \vec{S} = -2 \cdot \frac{e\hbar}{2m} \cdot \frac{1}{\hbar} \vec{S} = -2 \frac{\mu_B}{\hbar} \vec{S} \quad (2.6)$$

where $\hbar = h/2\pi$ is the reduced Planck's constant and $\mu_B (= e\hbar/2m = 9.27 \times 10^{-24} \text{ J/T}$ in SI and $= e\hbar/2mc = 9.27 \times 10^{-21} \text{ erg/Oe}$ in CGS) is the Bohr Magnetron which is the fundamental unit of magnetic moment closely equal to that of a free electron. Equations (2.5) and (2.6) can be cast into a more general form for electrons

$$\vec{\mu} = -g \frac{\mu_B}{\hbar} \vec{P} \quad (2.7)$$

where \vec{P} represents the angular momentum of interest (orbital or spin) and g is called the spectroscopic splitting factor or simply the g -factor. For orbital motion $g_L = 1.00$, and $g_S = 2.0023$ for spin which is usually taken as 2.00.

The magnitude of the orbital angular momentum is given by

$$|\vec{L}| = \sqrt{l(l+1)}\hbar \quad (2.8)$$

where l is the orbital angular momentum quantum number. The allowed values of l are integer values: $0 \leq l \leq n - 1$ determined from the principal quantum number n . For the electron in a Hydrogen atom in ground state, $n = 1$ which then forces $l = 0$ corresponding to the s-orbital. Therefore, the orbital angular momentum is zero for an electron with $n = 1$.

For the magnitude of the spin angular momentum we have

$$|\vec{S}| = \sqrt{s(s+1)}\hbar \quad (2.9)$$

for which the only value to be assumed by the spin quantum number s is $1/2$. The magnitude of the spin angular momentum then becomes $\sqrt{3}\hbar/2$. After defining magnitudes of the orbital and spin angular momenta, the magnitudes of the associated magnetic moments can be given by

$$\mu_{orbit} = g_L \frac{\mu_B}{\hbar} |\vec{L}| = 1 \cdot \frac{\mu_B}{\hbar} \sqrt{l(l+1)}\hbar = \mu_B \sqrt{l(l+1)} \quad (2.10)$$

$$\mu_{spin} = g_S \frac{\mu_B}{\hbar} |\vec{S}| = 2 \cdot \frac{\mu_B}{\hbar} \sqrt{s(s+1)} \hbar = 2\mu_B \sqrt{s(s+1)} = \sqrt{3}\mu_B \quad (2.11)$$

2.2. ZEEMAN INTERACTION

The magnetic moments that we have found in equations (2.10) and (2.11) are valid for the electrons in isolated atoms. The energy of a magnetic moment in a magnetic field is given by

$$U = -\vec{\mu} \cdot \vec{B} \quad (2.12)$$

where $\vec{B} = \vec{H}$ in CGS and $\vec{B} = \mu_0 \vec{H}$ in SI is the applied field. Care should be taken not to confuse μ_0 with magnetic moments because μ_0 is the magnetic permeability of free space. When we consider only the case of the orbital angular momentum of the electron and taking direction of the magnetic field as the z -direction, equation (2.12) calls for the projection of $\vec{\mu}$ along the direction of the magnetic field as required by the dot product:

$$\mu_{orbit,z} = \gamma L_z = -\frac{\mu_B}{\hbar} L_z \quad (2.13)$$

by virtue of equation (2.5). The projection of the orbital angular momentum with magnitude given by equation (2.8) along z -direction is given by

$$L_z = m_l \hbar \quad (2.14)$$

where m_l is the orbital magnetic quantum number restricted to values $-l \leq m_l \leq +l$ changing in integer steps restricting atomic dipole moments to certain values and $2l + 1$ possible orientations of the orbital angular momentum with respect to external magnetic fields leading to space quantization. Insertion of (2.14) into (2.13) gives

$$\mu_{orbit,z} = -\frac{\mu_B}{\hbar} m_l \hbar = -m_l \mu_B \quad (2.15)$$

which then transforms (2.12) into

$$U = m_l \mu_B B \quad (2.16)$$

that adds to the energy of the electrons causing the unperturbed energy levels to change in steps of $\mu_B B$ and lifting the degeneracy. Positive values of m_l correspond to orbital angular momentum projections in the direction of the magnetic field and then the associated magnetic moment components will lie along the negative direction of the external magnetic field. This causes an increase in energy. In the opposite case, energy will be negative for the negative values of m_l for which the magnetic moment projections align with the field. Therefore, originally degenerate energy levels will now be split into $2l + 1$ levels and the transitions between these energy levels will have more spectral lines (equally spaced triplet) than the case of zero applied field consistent with the selection rules. The energy level splittings and the associated transitions between singlet states (zero total spin) involves only the orbital angular momentum and is called the normal Zeeman effect.

The case where the total electron spin in either the initial or final (or both) states involved in the transition is nonzero is called the anomalous Zeeman effect and it can lead to four, six and more lines or triplets with wider spacings. The effect is caused by spin-orbit coupling (LS coupling) which is due to the interaction of the spin of electron with the magnetic field of the nucleus circulating around the electron in electron's rest frame. The spin-orbit interaction depends on the atomic number Z because the current generated by the nucleus is higher for an atom with a greater atomic number and the actual proportionality is Z^4 . In such cases where the effect of both the orbital and spin magnetic moments are to be employed, the total angular momentum \vec{J} of the electrons in the system must be taken into consideration.

In light atoms where Z is small, the spin-orbit interaction is weak and therefore the spin-spin and orbit-orbit interactions are dominant over the spin-orbit coupling. The individual orbital angular momenta are summed up to give a resultant $\vec{L} = \sum_i \vec{l}_i$ and the individual spin angular momenta are coupled to give a total spin angular momentum $\vec{S} = \sum_i \vec{s}_i$. The total angular momentum is then given by $\vec{J} = \vec{L} + \vec{S}$. The LS coupling given in this case is called Russel-Saunders coupling.

In heavy atoms, there is a stronger spin-orbit interaction which then requires to calculate the total angular momentum of individual electrons through $\vec{j}_i = \vec{l}_i + \vec{s}_i$ and then the total angular momentum of all electrons are given by $\vec{J} = \sum_i \vec{j}_i$. This coupling scheme is then called *j-j* coupling.

The total magnetic moment of the atom $\vec{\mu} = \vec{\mu}_{orbit} + \vec{\mu}_{spin}$ is given by

$$\vec{\mu} = -\frac{\mu_B}{\hbar}(g_L\vec{L} + g_S\vec{S}) = -\frac{\mu_B}{\hbar}(\vec{L} + 2\vec{S}) \quad (2.17)$$

where use is made of the fact that $g_L = 1$ and $g_S \cong 2$. Even if the orbital and spin magnetic moments are individually collinear with the corresponding orbital and spin angular momenta, the total magnetic moment is not collinear with the total angular momentum $\vec{J} = \vec{L} + \vec{S}$ but proportional to $\vec{L} + 2\vec{S}$ due to the anomalous g-factor of the electron $g_S \cong 2$.

The magnitude of the total angular momentum is dependent upon the total angular momentum quantum number J and is given by

$$\mu = g\mu_B\sqrt{J(J+1)} \quad (2.18)$$

and the projection of the magnetic moment along the field axis is

$$\mu_z = g\mu_B M_J \quad (2.19)$$

where $M_J = J, J-1, \dots, 0, \dots, -(J-1), -J$ is the quantum number for the projection of total angular momentum onto the field axis and g term in (2.18) and (2.19) is the Landé-g factor given by

$$g = 1 + \frac{J(J+1) + S(S+1) - L(L+1)}{2J(J+1)} \quad (2.20)$$

A final note on the behaviour of a magnetic moment in a magnetic field is the torque applied to it which is given by

$$\vec{\tau} = \vec{\mu} \times \vec{B} \quad (2.21)$$

which leads to the equation of motion

$$\frac{d\vec{\mu}}{dt} = \gamma \vec{\mu} \times \vec{B} \quad (2.22)$$

that will be examined in more detail in Section 4.

2.3. MAGNETIC MATERIALS

Materials can be classified into three major categories depending upon their magnetic behaviour. The first two are diamagnets and paramagnets. The third class of materials is magnetically ordered systems which itself can be divided into subclasses such as ferromagnets, ferrimagnets and antiferromagnets. In the following, brief overview of these materials is presented and reader can refer to [58-63] for a more in-depth study.

2.3.1. Diamagnets and Paramagnets

The magnetic behaviour of diamagnetic and paramagnetic materials are characterized by their response to external magnetic fields through the magnetic susceptibility χ defined by the relation

$$\vec{M} = \chi \vec{B} \quad (2.23)$$

where \vec{M} is the induced magnetization defined as magnetic moment per unit volume and \vec{B} is the applied magnetic field. The diamagnetic and paramagnetic materials are separated by the sign of the magnetic susceptibility. For diamagnets the susceptibility is negative, $\chi < 0$ and for paramagnetic materials it is positive, $\chi > 0$. Therefore the magnetic moments of the individual atoms are forced to align along the direction of the magnetic field for paramagnetic materials and in the opposite direction for diamagnetic materials. The degree of alignment, on the other hand, is quite small and the susceptibility is inversely

proportional to temperature, $\chi \sim 1/T$, for paramagnetic materials and independent of temperature for diamagnetic ones.

Diamagnetic materials are composed of atoms with no unpaired electrons, therefore zero net magnetic moment, whereas for paramagnetic materials atoms do possess a net magnetic moment. The diamagnetic effect which alters the electron trajectories and induces a small negative susceptibility is actually inherent to all atoms but the effect is surpassed in paramagnetic materials due to the higher positive paramagnetic susceptibility.

2.3.2. Ferromagnetic, Ferrimagnetic and Antiferromagnetic Materials

The main difference between the dia(para)magnets and the magnetically ordered systems is that there exist a strong internal interaction between the magnetic moments of individual atoms in the latter class of structures. It is as if there is an internal field responsible for aligning the magnetic moments in an ordered fashion in ferro-, ferri- and antiferromagnetic materials. Such an internal field is called the exchange (or more loosely a molecular) field and the interaction responsible for such a long range order is called the exchange interaction. Exchange interaction is totally a quantum mechanical phenomenon stemming from the Pauli exclusion principle and dependent upon the relative orientations of the neighbouring spins which affects the total electrostatic energy of the system.

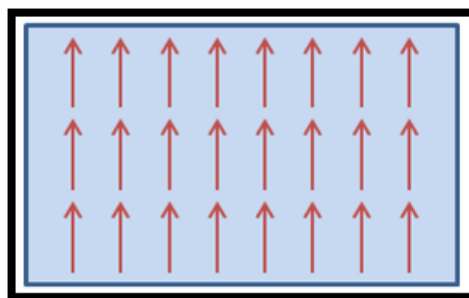


Figure 2.1. Schematic representation of spins in a saturated ferromagnet

Ferromagnetic materials are characterized by spontaneous magnetization, alignment of constituent spins even in the absence of an external field. There exists a critical temperature called Curie temperature T_C and the material manifests paramagnetic

behaviour above this temperature. One other important property of the ferromagnetic materials is that they show hysteretic behaviour as a function of applied magnetic field.

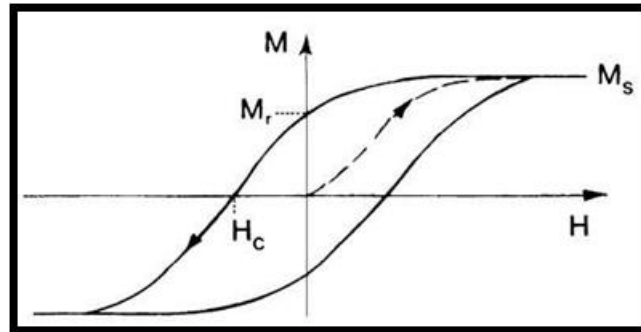


Figure 2.2. Hysteresis curve showing the magnetization response M of the ferromagnet as a function of applied magnetic field H [64].

If the material starts from a zero magnetization state at the origin as in Figure 2.2, magnetization will follow the dashed line called the virgin curve until the material reaches saturation with saturation magnetization M_s . As the field is reversed and reduced to zero, the magnetization does not go back to zero but to a value called remanence M_r . When the direction is reversed, the magnetization will return to zero at a negative field value called the coercive field H_c . Further increase in the strength of the field saturates the sample in the negative direction. As the magnitude of the field is reduced in the negative direction, magnetization passes through $-M_r$ on the M -axis, intersects H -axis at the positive coercive field and saturates back in the positive direction.

Antiferromagnetic materials are actually composed of two sublattices of equal spins oriented in opposite directions so as to produce zero net magnetization. In the ferrimagnetic case, the sublattices have different magnetic moments that cause a net magnetization.

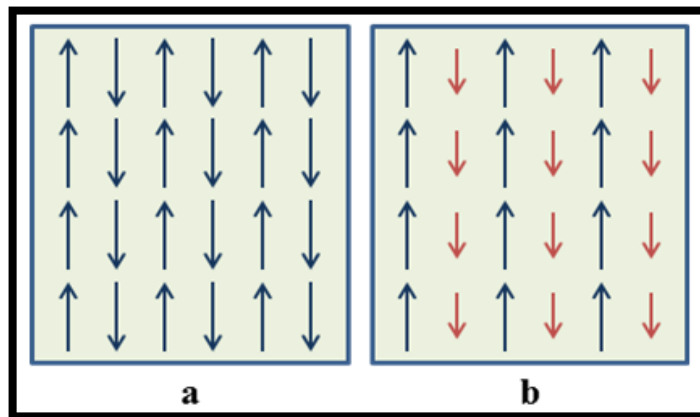


Figure 2.3. The sketch of (a) antiferromagnetic and (b) ferrimagnetic moments

3. EXCHANGE BIAS

3.1. DISCOVERY

The exchange bias effect, also known as unidirectional anisotropy, was discovered when Meiklejohn and Bean were studying fine single domain spherical FM Co particles embedded in their native AFM oxide (CoO) [1, 2, 4]. They first cooled their sample to 77 K and took an hysteresis curve which resulted in an expected magnetization versus magnetic field ($M - H$) curve, symmetric on H axis around $H = 0$ in both positive and negative magnetizations as depicted by the dashed line numbered (2) in Figure 3.1. Then, they went back to the room temperature (RT) and re-cooled their sample to 77 K but this time they applied an external field of 10 kOe during cooling of the sample (field cooling procedure). What they observed was an $M - H$ curve shifted in opposite direction to the cooling field and an enhanced loop width in H-axis (half of which is called the “coercivity”) as depicted by solid curve numbered (1) in Figure 3.1.

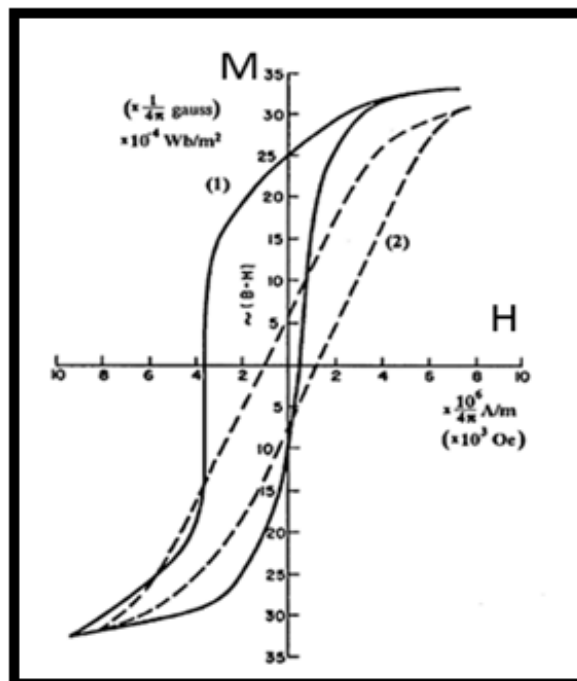


Figure 3.1. The hysteresis curves at 77 K of field cooled (1) and zero field cooled (2) FM Co particles embedded in AFM CoO [1, 6].

3.2. BASIC PHENOMENOLOGY

The origin of exchange bias is related to interfacial magnetic coupling between FM and AFM layers across their common interface [9]. In order to have at least a qualitative understanding of the exchange bias phenomenon, this exchange coupling of FM-AFM spins at the interface is assumed. The critical temperature below which ferromagnetic order takes place in FM materials is called the Curie temperature T_C , while the critical temperature for antiferromagnetic order in AFM materials is called the Néel temperature T_N . If a magnetic field is applied to the FM-AFM system in a temperature range $T_N < T < T_C$, the FM spins line up with this external field while AFM spins are randomly oriented (Figure 3.2.(i)). When the system is now cooled to a temperature $T < T_N$ in the presence of the external field (field cooling procedure), antiferromagnetic order starts manifesting itself in AFM material and the AFM spins at the interface couple to the FM spins next to them ferromagnetically (or antiferromagnetically depending upon the type of interaction) due to the exchange interaction. The other spin planes in AFM now follow the AFM order so as to produce zero net magnetization in AFM (Figure 3.2.(ii)). When the magnetic field direction is reversed, the FM spins try to rotate to the new direction of the magnetic field. However, due to the strong anisotropy and low susceptibility of the AFM material, AFM spins remain almost rigid (Figure 3.2.(iii)). Due to the exchange coupling between the FM and AFM spins at the interface, AFM spins exert a microscopic torque to FM spins tending to keep them in their original direction which was the direction of the initial cooling field. This creates one stable configuration of the FM spins in the original cooling field, hence the term “unidirectional anisotropy” is coined. Then the negative magnetic field value needed to reverse the FM spins becomes larger to overcome the microscopic torque (Figure 3.2.(iv)). Once the magnetic field is reversed back to the original direction, it requires a lesser field to rotate FM spins into their original direction because now the torque on FM spins due to AFM spins are in the same direction of the external field (Figure 3.2.(v)). The system then behaves as if there is an internal biasing field causing the hysteresis loop to shift in the magnetic field axis and we have “exchange bias”. The initial uniaxial anisotropy of two equally favourable directions on the same axis is now converted into a single direction leading to a unidirectional anisotropy.

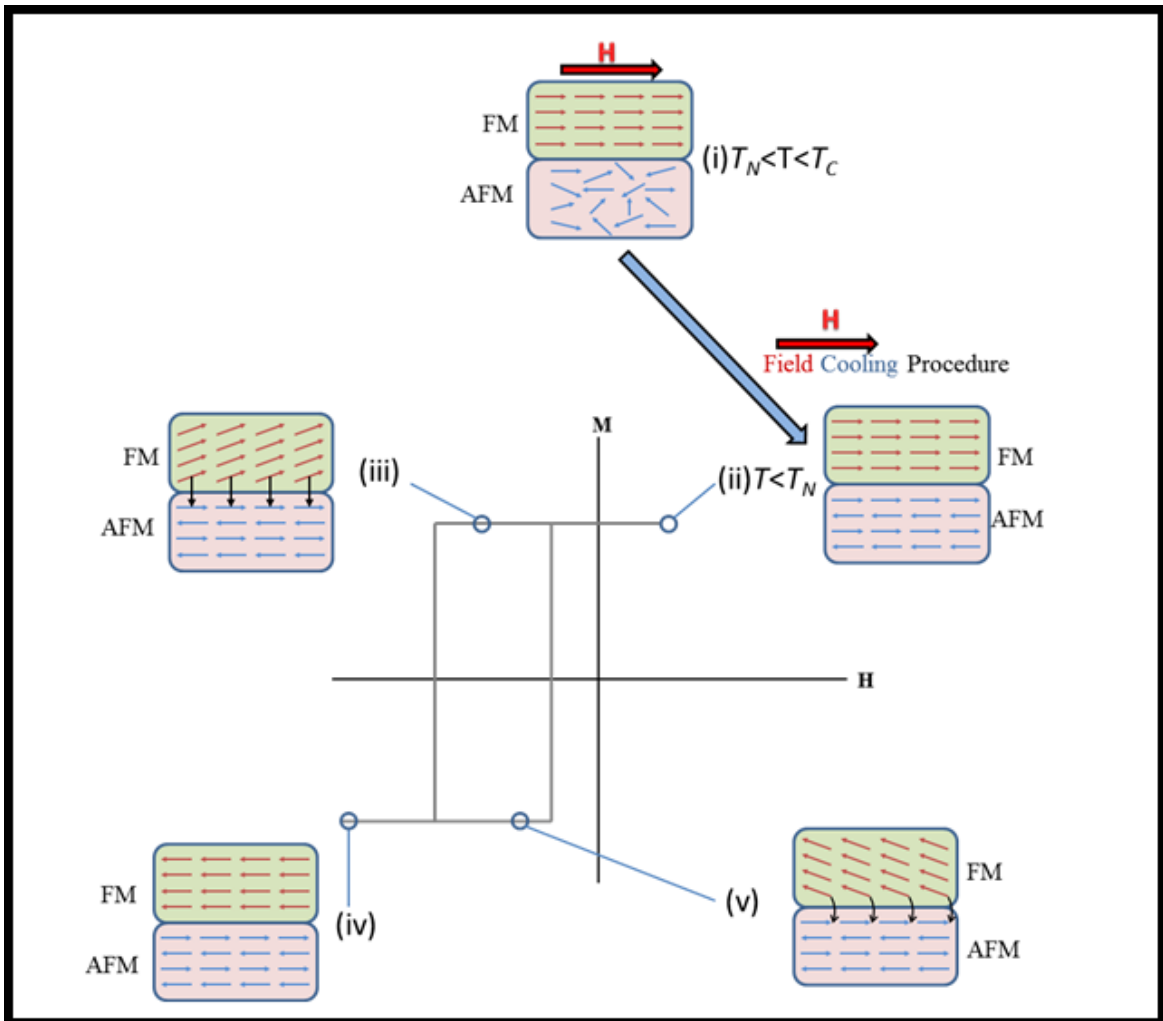


Figure 3.2. Spin configurations of FM and AFM spins at different stages of the hysteresis loop of an FM material in contact with an AFM material when the system is subjected to field cooling procedure.

3.3. IDEAL EXCHANGE BIAS MODEL

The first theoretical approach to exchange bias came from Meiklejohn and Bean [2, 4] who discovered the phenomenon. Their approach assumed a coherent rotation of the magnetization and defined an areal energy density (energy per unit area) given by

$$\begin{aligned} \mathcal{E} = & -HM_{FM}t_{FM} \cos(\theta - \beta) + K_{FM}t_{FM} \sin^2(\beta) + K_{AFM}t_{AFM} \sin^2(\alpha) \\ & - J_{INT} \cos(\beta - \alpha) \end{aligned} \quad (3.1)$$

where H is the applied field, M_{FM} the saturation magnetization of FM, t_{FM-AFM} the thicknesses, K_{FM-AFM} the anisotropy constants of the respective FM – AFM layers and J_{INT} the interfacial interaction constant.

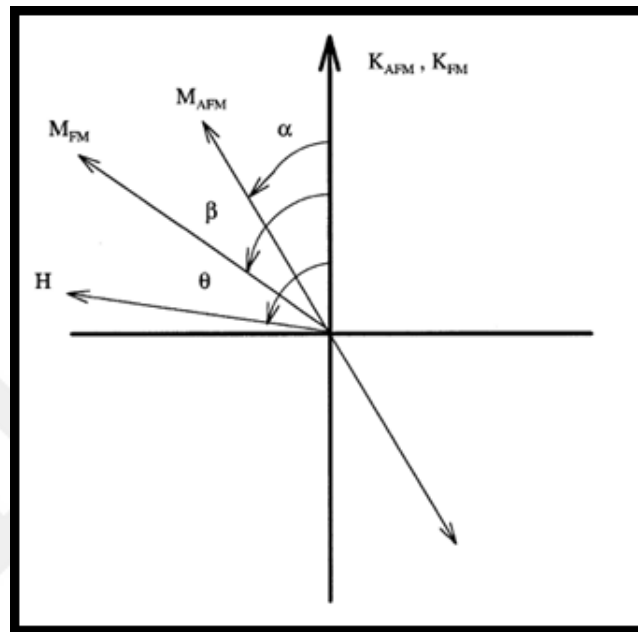


Figure 3.3. Geometry for the ideal exchange bias model [5].

The respective angles α , β , and θ between the AFM sublattice magnetization and anisotropy direction, FM layer magnetization and anisotropy direction, magnetic field and anisotropy directions are shown in Figure 3.3 with the assumption that FM and AFM layer anisotropies are collinear.

The terms in Equation (3.1) are as follows:

- First term for the interaction (Zeeman) between H and M_{FM}
- Second term for FM anisotropy
- Third term for AFM anisotropy
- Fourth term for coupling between M_{FM} and M_{AFM} at the interface

In this ideal Meiklejohn Bean (MB) model, magnetic field is applied along the the easy axis (anisotropy axis shown with K_{AFM}) which sets $\theta = 0$ and for strong AFM anisotropy $\alpha = 0$ condition is also met. Then, equation (3.1) becomes

$$\mathcal{E} = -HM_{FM}t_{FM} \cos(\beta) + K_{FM}t_{FM} \sin^2(\beta) - J_{INT} \cos(\beta) \quad (3.2)$$

by remembering that $\cos(-\beta) = \cos(\beta)$ and $\sin^2(\alpha = 0) = 0$. If the $\cos(\beta)$ terms are grouped together, one obtains

$$\mathcal{E} = -\left(H - \frac{J_{INT}}{M_{FM}t_{FM}}\right) M_{FM}t_{FM} \cos(\beta) + K_{FM}t_{FM} \sin^2(\beta) \quad (3.3)$$

which dictates that the system behaves as if the hysteresis loop is shifted by an amount

$$H_{EB} = \frac{J_{INT}}{M_{FM}t_{FM}} \quad (3.4)$$

along the magnetic field axis if we look at the term in parentheses in equation (3.3). equation (3.4) gives the exchange bias magnitude as predicted by the ideal MB model. Another prediction of the model is that, for low AFM anisotropy, that is $K_{AFM}t_{AFM} < J_{INT}$, the FM and AFM magnetizations will rotate together leading to $\beta - \alpha \approx 0$. In this case, there is only a coercivity increase without a loop shift and the condition for the observation of exchange bias then becomes

$$K_{AFM}t_{AFM} \geq J_{INT} \quad (3.5)$$

The ideal EB model by MB is capable of predicting some experimental observations like the loop shift, the dependence of EB on FM layer thickness (equation (3.4) and section 3.4.1), AFM layer thickness (equation (3.5) and section 3.4.2). In reality, however, the observed loop shifts are orders of magnitude smaller than what the theory can predict. We will not be giving an account of other models for EB but interested reader is referred to the publications [5-15, 65] and references therein for the main theoretical and experimental efforts.

3.4. GENERAL PROPERTIES OF EXCHANGE BIASED SYSTEMS

The material systems subjected to investigation for exchange bias properties can be collected under the umbrella of three main classes [5, 65]: a) small particle systems in core/shell form as in Co/CoO [1, 2, 66-75], Ni/NiO [69, 76-82], Fe/Fe Oxides [83-86] and ZnO-Fe/Fe Oxides [87], Fe/Fe₂N [88], Co/CoN [70], Fe/FeS [69]; b) inhomogeneous materials [89-93] and c) thin film structures discussed in [94-103] and references therein. Main properties that affect the exchange bias coupling and are commonly observed in exchange bias systems are thicknesses of ferromagnetic and antiferromagnetic layers, interface roughness, blocking temperature, cooling field and training effect.

3.4.1. Ferromagnetic Layer Thickness

The general trend in exchange biased systems indicates that the exchange bias is inversely proportional to the ferromagnetic layer thickness t_{FM} [5, 6, 104, 105]

$$H_{EB} \propto \frac{1}{t_{FM}} \quad (3.6)$$

which supports that EB is indeed an interfacial phenomenon [94, 95, 106-109]. The relation given in equation (3.6), which is also consistent with equation (3.4)) remains valid for increasing thicknesses up until it approaches the domain wall size of the ferromagnet [5]. There is also another power law $H_{EB} \propto 1/(t_{FM})^n$ observed and based on theoretical predictions with cases of $n = 1$ and $n = 1.5$ [14, 97, 110-112]. At the opposite extreme, the given relation does not hold for ultrathin ferromagnetic layers [5] probably due to the discontinuities and the tension at the interface.

3.4.2. Antiferromagnetic Layer Thickness

The dependency of the exchange bias strength on the antiferromagnetic layer thickness is less intuitive compared to that of ferromagnetic layer [113]. For the thin films, the exchange bias scales with the thickness of AFM (as also required by equation (3.5)), however below a certain range this is no longer true depending on the material,

microstructure and temperature [114]. Above a certain range of thickness, the exchange bias becomes independent of the antiferromagnetic layer thickness which is generally around 20 nm [5]. This behaviour, however, may not be applicable to some systems like NiFe/CoO system with $t_{AFM} > 10 \text{ nm}$ [115] and the exchange bias field H_{EB} (defined as the shift of the centre of the hysteresis curve from the $H = 0$ axis) may even scale inversely with t_{AFM} as $H_{EB} \propto 1/t_{AFM}$ [65].

3.4.3. Interface Roughness

Roughness of the interface between FM – AFM is observed to be detrimental for EB systems as increasing roughness decreases EB magnitude H_{EB} for most of the studied systems [116-120]. Rough surfaces may form arcs-steps along the interface, therefore leading to a reduced sum of spins pinning the ferromagnet in one direction (parallel to the ferromagnet-antiferromagnet interface). It should be mentioned that there are also studies showing the opposite behaviour [53, 121] or less sensitivity to roughness [122, 123].

3.4.4. Blocking Temperature

Exchange coupling between FM and AFM at the interface requires that antiferromagnetic order is set up in the AFM material which requires the temperature to be less than the ordering temperature of the AFM called the Néel temperature T_N . In exchange biased systems, however, the unidirectional anisotropy in some cases starts manifesting itself at temperatures much lower than the Néel temperature T_N . Therefore, the temperature at and above which exchange coupling vanishes is called the Blocking Temperature $T_B \leq T_N$. Thickness [5, 124-128] and chemical stoichiometry [129-132] have influences on the blocking temperature and will be elaborated more in Discussion in Section 6.

3.4.5. Cooling Field

There is no significant relationship between the magnitude of the cooling field and the exchange bias field H_{EB} in general. There are material systems like FeF₂/Fe and MnF₂/Fe however, that manifest unusual properties [133, 134] such that the hysteresis loop shift is generated in the same direction of the cooling field, a result called positive exchange bias

thought to be caused by the changes in the interface spin structure and antiferromagnetic coupling between FM – AFM layers instead of ferromagnetic exchange [135].

3.4.6. Training Effect

Successive hysteresis loops performed on an EB system diminishes the exchange bias field H_{EB} at each cycle and the decrease is a function of the number of cyclic repetitions [5]. This property is known as Training Effect and the functional relationship [136],

$$(H_{EB}^n - H_{EB}^\infty) \propto 1/\sqrt{n} \quad (3.7)$$

holds true if the cycle number satisfies $n \geq 2$. For a better fit consistent with the experimental values Binek approached the problem with a recursive formula [137]

$$H_{EB}^{n+1} - H_{EB}^n = -\Gamma(H_{EB}^{n+1} - H_{EB}^\infty) \quad (3.8)$$

where Γ is the fitting parameter and then Radu proposed [138] the following relationship

$$H_{EB}^n = H_{EB}^\infty + A_f e^{-\frac{n}{P_f}} + A_i e^{-\frac{n}{P_i}} \quad (3.9)$$

where A_f and P_f are related to frozen spins and A_i and P_i are related to interfacial disorder.

4. THEORETICAL WORK ON FERROMAGNETIC RESONANCE

Ferromagnetic resonance (FMR) is a powerful and nondestructive spectroscopic technique that can be applied to ferromagnetic materials to gather information on the magnetic anisotropies, anisotropy constants, effective g-factors, damping-relaxation processes and associated constants, interlayer exchange coupling etc. It is the resonant absorption of electromagnetic radiation by a ferromagnetic material when the frequency of the incident radiation matches the Larmor frequency of the magnetic moments under the influence of a static magnetic field. The effect can also be anticipated from the viewpoint of energy such that the external static magnetic field creates Zeeman-split energy levels and as static magnetic field strength is swept, there comes a point such that the energy difference becomes equal to the photon energy and the electromagnetic wave is absorbed.

Griffiths was the first to experimentally observe FMR in 1946 [139] when he was measuring the permeability of FM materials at wavelengths of 1-3 cm [140]. The phenomenon was further confirmed by the work of Yager and Bozorth [141]. The first theoretical attempt to explain FMR was made by Kittel in 1947 [142] who extended the initial theory to include the shape effects in 1948 [143]. Together with Van Vleck's work on the quantum mechanical treatment [144], these initial studies generalized the calculations of Landau and Lifshitz [145] whose damping mechanism was further developed by the work of Gilbert [146] that lead to the famous Landau-Lifshitz-Gilbert (LLG) equation in addition to the Bloch-Bloembergen type damping terms [147, 148]. Since the time of these initial studies, a great amount of data have been published [149-195] and within the references therein concerning theories, different geometries, applications and material classes.

In this part of the study, we wanted to make a theoretical account of the Ferromagnetic Resonance (FMR). The main goal was determined to be a basic theoretical understanding of FMR theory by studying a model of one of many for the simulations of FMR. The mathematical and numerical approaches vary from one model to another even if the starting equation of motion is the same which makes it harder for a quick and general level of understanding of the theory due to the immense number of contributions to the

literature. Therefore, it was the aim of the author to follow the basic steps first and try to analyse the equations from the perspective of filling in all the intermediate steps which we recognized to be missing in most of the published work that lead to the final forms of equations by stating that such an effort is neither complete nor free of mistakes. The main objective in Section 4.1 was then to derive the equations to obtain the fundamental resonance condition in FMR. In Section 4.2, the equations of ferromagnetic resonance are further analyzed, but this time effort is devoted to systems composed of many ferromagnetic (FM) layers (a multilayer structure), generally separated by nonmagnetic spacer layers.

4.1. FUNDAMENTAL THEORY OF FERROMAGNETIC RESONANCE

4.1.1. Magnetic Moment and Angular Momentum

The general theory of angular momenta and associated magnetic moments is already examined in more detail in Section 2. Here we shall continue with the main results. Throughout the remaining sections magnetic induction \vec{B} and magnetic field \vec{H} will be related by $\vec{B} = \vec{H} + 4\pi\vec{M}$ and the externally applied field will be given by $\vec{B} = \vec{H}$ without the effect of magnetization.

The magnetic moment $\vec{\mu}$ of an electron (or more precisely the net magnetic moment of all the electrons in an atom for our purposes) and the total angular momentum \vec{J} ($= \vec{L} + \vec{S}$ for light atoms and $= \sum(\vec{l}_i + \vec{s}_i)$ for heavy ones) are related to each other by

$$\vec{\mu} = -\gamma\vec{J} \quad (4.1)$$

where γ is the gyromagnetic (or magnetogyric) ratio given by $\gamma = g \frac{|e|\hbar}{2m_e c} = g \frac{|e|\hbar}{2m_e c} \frac{1}{\hbar} = g \frac{\mu_B}{\hbar}$ in CGS units. Here “ $|e|$ ” is the magnitude of the fundamental unit of charge (charge of a proton or electron), “ m_e ” is the electron mass, “ c ” is the speed of light in vacuum and “ μ_B ” is the Bohr Magneton. The term “ g ” is the Landé- g factor (or the spectroscopic splitting factor) given by

$$g = 1 + \frac{J(J + 1) + S(S + 1) - L(L + 1)}{2J(J + 1)} \quad (4.2)$$

with S , L and J representing the spin, orbital and total angular momentum quantum numbers respectively.

4.1.2. Equation of Motion and Damping

A magnetic moment $\vec{\mu}$ in a magnetic field \vec{H} experiences a torque given by

$$\vec{\tau} = \vec{\mu} \times \vec{H} \quad (4.3)$$

The torque is the time rate of change of angular momentum: $\vec{\tau} = d\vec{J}/dt$. Taking $\vec{J} = -\vec{\mu}/\gamma$ from (4.1) we get

$$\vec{\tau} = \frac{d\vec{J}}{dt} = \frac{d}{dt} \left(-\frac{\vec{\mu}}{\gamma} \right) = \vec{\mu} \times \vec{H} \quad (4.4)$$

from which we get the equation of motion of magnetic moment $\vec{\mu}$ as

$$\frac{d\vec{\mu}}{dt} = -\gamma \vec{\mu} \times \vec{H} \quad (4.5)$$

The macroscopic magnetization \vec{M} in a magnetized sample is the vectorial sum of all the magnetic moments in unit volume, i.e. $\vec{M} = \sum_i \vec{\mu}_i / V$. For identical magnetic moments we have the same gyromagnetic ratio for all spins, so the equation of motion of magnetization becomes

$$\frac{d\vec{M}}{dt} = -\gamma \vec{M} \times \vec{H} \quad (4.6)$$

Since the time rate of change of magnetization is a vector given by the cross product of \vec{M} and \vec{H} , it must be perpendicular to both \vec{M} and \vec{H} resulting in the precession of the

magnetization \vec{M} around the effective magnetic field \vec{H} with no alignment of \vec{M} along \vec{H} , contrary to the experimental facts. However, in a material media different types of damping processes also take place which transfer energy to the microscopic thermal motion in the form of spin waves, lattice vibrations (phonons) and thermal excitation of conduction electrons [146] that align magnetization with the magnetic field. Details of these damping mechanisms for the energy losses can be too complex to take into account in the equations explicitly. However, a phenomenological damping term that includes damping parameters corresponding to the rate of energy transfer can be added into the equation of motion.

$$\text{Landau-Lifshitz type damping} \quad : -\frac{\lambda}{M_0} \vec{M} \times (\vec{M} \times \vec{H}_{eff})$$

$$\text{Gilbert type damping} \quad : \frac{\alpha}{M_0} \vec{M} \times \frac{d\vec{M}}{dt}$$

$$\text{Bloch-Bloembergen type damping} \quad : -\frac{M_x}{T_2} \hat{i} - \frac{M_y}{T_2} \hat{j} - \frac{(M_z - M_0)}{T_1} \hat{k}$$

Bloembergen type damping term is the easiest to deal with mathematically. In this type of damping term T_1 is the spin-lattice relaxation time (longitudinal relaxation time) and T_2 is due to spin-spin interaction and corresponds to transverse relaxation time. The longitudinal relaxation time T_1 describes the direct path into the thermal bath and the so called transverse time T_2 is due to energy scattered into the transverse magnetization components M_x and M_y .

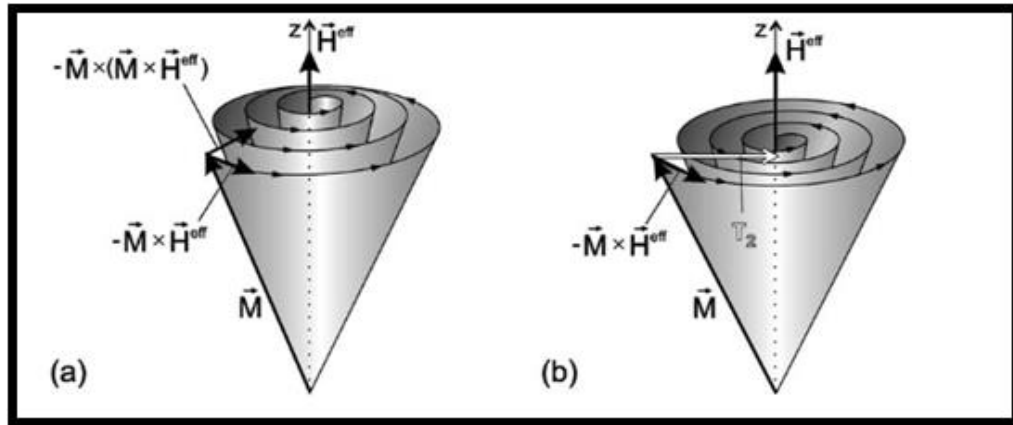


Figure 4.1. (a) Landau-Lifshitz-Gilbert and (b) Bloch-Bloembergen damping paths [196].

Figure 4.1 (a) depicts the LLG (Landau-Lifshitz-Gilbert) scenario. The Larmor precession is damped by viscosity and the magnetization spirals towards the z -axis (taken as the direction of the effective magnetic field). The magnitude of \vec{M} remains constant with an increased expectation value of M_z . Figure 4.1 (b) shows the Bloch-Bloembergen (BB) spin-spin relaxation. The z -projection of \vec{M} stays constant if $T_1 \gg T_2$ with the precessional energy scattered into the transverse components M_x and M_y [196].

4.1.3. Effective Magnetic Field Derived From Energy Density

The \vec{H} term in the equation of motion is the effective magnetic field \vec{H}_{eff} which is due not only to the externally applied magnetic field but also to all other internal interactions such as anisotropies, demagnetizing fields etc. able to apply a torque on the magnetization vector. Thus if we define $E(\vec{M})$ as the free energy (energy “density” to be precise) of the system with respect to the work done by rotating the moment against whatever forces are present, the effective magnetic field can be given by

$$\vec{H}_{eff} = -\frac{\partial E(\vec{M})}{\partial \vec{M}} \quad (4.7)$$

which reads in Cartesian geometry as

$$\vec{H}_{eff} = - \left[\hat{i} \frac{\partial E(\vec{M})}{\partial M_x} + \hat{j} \frac{\partial E(\vec{M})}{\partial M_y} + \hat{k} \frac{\partial E(\vec{M})}{\partial M_z} \right] = -\vec{\nabla}_{\vec{M}} E(\vec{M}) \quad (4.8)$$

This equation makes sense if one recalls the Zeeman energy density ($E_z = -\vec{M} \cdot \vec{H}$), for the derivative of E with respect to \vec{M} gives a magnetic field. In this sense, the effective field is defined as the gradient (with respect to \vec{M}) of the energy density. In FMR experiments, angular dependences of resonance fields are studied, so angle dependent terms in the expressions of the free energy density will appear in the equations. Then it is possible to derive effective magnetic field from the free energy density by taking the gradient with respect to the spherical components of \vec{M} . In general, the gradient of a scalar field E in spherical coordinates reads as

$$\vec{\nabla} E = \hat{r} \frac{\partial E}{\partial r} + \hat{\theta} \frac{1}{r} \frac{\partial E}{\partial \theta} + \hat{\phi} \frac{1}{r \sin \theta} \frac{\partial E}{\partial \phi} \quad (4.9)$$

Assuming the magnitude of the magnetization fixed at its saturation value M_0 , we will then be dealing with the dynamics of the magnetization as the dynamics of a point on an M-sphere, the only variables being the azimuthal (ϕ) and polar (θ) angles of the magnetization vector. Working on such an M-sphere allows one to replace the “ r ” term in equation (4.9) by M_0 , i.e. the radius of the M-sphere. Then we can define the effective magnetic field as

$$\vec{H}_{eff} = -\vec{\nabla}_{\vec{M}} E = - \left(\hat{r} \frac{\partial E}{\partial M} + \hat{\theta} \frac{1}{M_0} \frac{\partial E}{\partial \theta} + \hat{\phi} \frac{1}{M_0 \sin \theta} \frac{\partial E}{\partial \phi} \right) \quad (4.10)$$

\vec{H}_{eff} enters the equation of motion of \vec{M} only in the cross product $\vec{M} \times \vec{H}_{eff}$, so the only important components of \vec{H}_{eff} are the ones perpendicular to \vec{M} , i.e. components in the $\theta - \phi$ plane [182].

This will lead us to the act of dropping the first term from the expression of \vec{H}_{eff} , regarding the above gradient as a 2-D gradient on the surface of M-sphere so that it is automatically normal to the \vec{M} [197]. This means that we will be dealing with the

components of the effective magnetic field given by equation (4.10) perpendicular (normal) to \vec{M} which in turn yields a volume torque given by [198, 199]

$$\vec{\tau} = \vec{M} \times \vec{H}_{eff} = -\hat{\phi} \frac{\partial E}{\partial \theta} + \hat{\theta} \frac{1}{\sin \theta} \frac{\partial E}{\partial \phi} \quad (4.11)$$

However, it is still instructive to calculate the torque due to the effective magnetic field to see that the only remaining terms will be in the $\theta - \phi$ plane

$$\begin{aligned} \vec{\tau} &= \vec{M} \times \vec{H}_{eff} = M_o \hat{r} \times \left[-\left(\hat{r} \frac{\partial E}{\partial M} + \hat{\theta} \frac{1}{M_o} \frac{\partial E}{\partial \theta} + \hat{\phi} \frac{1}{M_o \sin \theta} \frac{\partial E}{\partial \phi} \right) \right] \\ &= -(\hat{r} \times \hat{r}) M_o \frac{\partial E}{\partial M} - (\hat{r} \times \hat{\theta}) M_o \frac{1}{M_o} \frac{\partial E}{\partial \theta} - (\hat{r} \times \hat{\phi}) M_o \frac{1}{M_o \sin \theta} \frac{\partial E}{\partial \phi} \\ &= 0 - \hat{\phi} \frac{\partial E}{\partial \theta} - (-\hat{\theta}) \frac{1}{\sin \theta} \frac{\partial E}{\partial \phi} \\ \Rightarrow \vec{\tau} &= -\hat{\phi} \frac{\partial E}{\partial \theta} + \hat{\theta} \frac{1}{\sin \theta} \frac{\partial E}{\partial \phi} \end{aligned}$$

which reads exactly as equation (4.11). In the intermediate steps use is made of the cyclic permutations of the spherical unit vectors in the cross products, i.e. $(\hat{r} \times \hat{r} = 0)$, $(\hat{r} \times \hat{\theta} = \hat{\phi})$ and $(\hat{r} \times \hat{\phi} = -\hat{\theta})$. In the calculations above $\vec{M} = M_o \hat{r}$ is taken as the magnetization vector in the spherical geometry. Azimuthal and polar angle dependences of the magnetization vector \vec{M} is already embedded in the definition of \hat{r} as $\hat{r} = \sin \theta \cos \phi \hat{i} + \sin \theta \sin \phi \hat{j} + \cos \theta \hat{k}$ with respect to Cartesian unit vectors.

4.1.4. The Geometry and Energy Terms

The Figure 4.2 shows the geometry under consideration for FMR measurements. The z -axis is taken along the direction normal to the film of thickness L . The film itself then lies in the $x - y$ plane. Here \vec{M} is the macroscopic magnetization, \vec{H} is the static magnetic field applied externally to the sample (which should not be confused with \vec{H}_{eff} representing the effect of not only \vec{H} but also all other torque applying internal interactions such as

anisotropies, demagnetizing fields etc.) and \vec{K}_g represents the direction of the geometric (oblique) anisotropy due to the film growth.

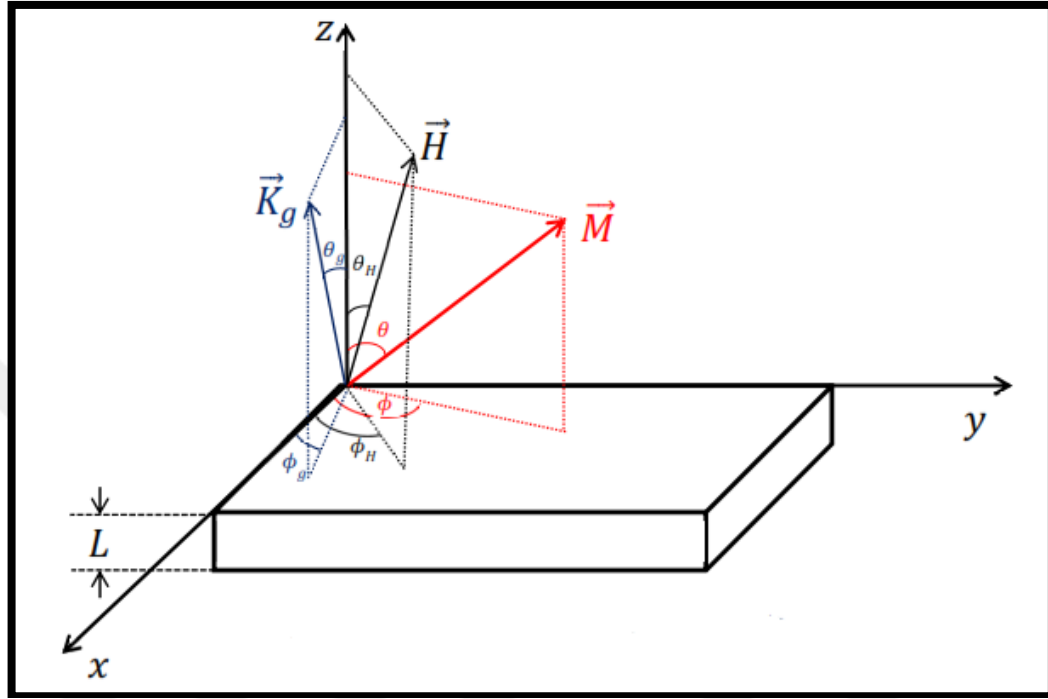


Figure 4.2. Geometry for the FMR calculations.

The angles $\theta_H-\phi_H$, $\theta-\phi$ and $\theta_g-\phi_g$ represent polar-azimuthal angles of static external magnetic field \vec{H} , the macroscopic magnetization \vec{M} and the geometric (oblique) anisotropy \vec{K}_g respectively.

Ferromagnetic (FM) samples can be modelled by the following energy density expression

$$E = E_Z + E_d + E_{ani} + E_g \quad (4.12)$$

where

E_Z : Zeeman energy density

E_d : Energy density due to the demagnetizing field (shape anisotropy)

E_{ani} : Bulk magnetocrystalline anisotropy energy density

E_g : Geometrical (oblique) anisotropy energy density

The contributing energy density terms to E will be calculated in Appendix A according to the geometry shown in Figure 4.2.

This energy density expression can be extended to include magneto-elastic, domain magnetostatic, field induced unidirectional exchange anisotropy and alike energy density terms depending upon the material and application.

Plugging in the torque $\vec{\tau}$ of equation (4.11) due to the total free energy density E defined in equation (4.12), expressing the effects of the rf-field and the exchange field separately and taking the Bloch-Bloembergen type damping term, the equation of motion given by equation (4.6) is modified to

$$\frac{d\vec{M}}{dt} = -\gamma \left[\vec{\tau} + \vec{M} \times \vec{h} + \vec{M} \times \frac{2A}{M_0^2} \nabla^2 \vec{M} \right] - \frac{\vec{M}_{x,y}}{T_2} \quad (4.13)$$

where $\vec{M} \times \vec{h}$ is the torque due to the rf-field and $\vec{M} \times \frac{2A}{M_0^2} \nabla^2 \vec{M}$ is the torque due to the exchange field $\vec{H}_{exc} = \frac{2A}{M_0^2} \nabla^2 \vec{M}$ [145].

Care must be taken when dealing with the Bloch-Bloembergen damping term $-\frac{\vec{M}_{x,y}}{T_2}$. The term in this original expression uses $\vec{M}_{x,y}$ to express the transverse components of the magnetization, transverse to the “equilibrium orientation of the magnetization vector” which is assumed to be the direction of the effective magnetic field. Since in the original expressions z-axis is assumed to be the direction of the effective field, then it is natural to think of $\vec{M}_{x,y}$ as the transverse components of the magnetization which dephase in a characteristic time T_2 . In our geometry, however, z-axis is not necessarily the direction of the effective field, so $\vec{M}_{x,y}$ will be replaced by a term more appropriate to the geometry that we use in our calculations.

4.1.5. Linearization of Equation of Motion

There will be no space and time variation of magnetization in the equilibrium orientation. Application of a small rf-field $\vec{h} = (h_\theta \hat{\theta} + h_\phi \hat{\phi})e^{i\omega t}$ will then induce little angular deflections $\delta\theta$ and $\delta\phi$ around the equilibrium orientation (θ_{eq}, ϕ_{eq}) of the magnetization. The angles (θ_{eq}, ϕ_{eq}) corresponding to the equilibrium orientation of magnetization are determined from free energy minimum conditions [200]

$$\frac{\partial E}{\partial \theta} = 0 \quad , \quad \frac{\partial E}{\partial \phi} = 0 \quad (4.14)$$

$$\frac{\partial^2 E}{\partial \theta^2} > 0, \quad \frac{\partial^2 E}{\partial \phi^2} > 0, \quad \frac{\partial^2 E}{\partial \theta \partial \phi} > 0 \quad (4.15)$$

Then the equation of motion of magnetization can be linearized about the equilibrium orientation by keeping only the first order terms in the deviation from equilibrium. The equilibrium orientation will then be \hat{r} direction and small deviations from the equilibrium will be in the $\hat{\theta}$ and $\hat{\phi}$ directions [158]. In this coordinate system the magnetization will have the form

$$\vec{M} = M_0 \hat{r} + m_\theta \hat{\theta} + m_\phi \hat{\phi} \quad (4.16)$$

where $m_\theta = M_0 \cdot \delta\theta$ and $m_\phi = M_0 \cdot \sin\theta \cdot \delta\phi$ (refer to Figure 4.3) represent dynamical small deviations of magnetization from the equilibrium direction. To linearize the equation of motion, we have to take first order deviations of both sides of equation (4.13) from equilibrium

$$\delta \left[\frac{d\vec{M}}{dt} \right] = \delta \left\{ -\gamma \left[\vec{\tau} + \vec{M} \times \vec{h} + \vec{M} \times \frac{2A}{M_0^2} \nabla^2 \vec{M} \right] - \frac{\vec{M}_{x,y}}{T_2} \right\} \quad (4.17)$$

for which

$$\delta \left[\frac{d\vec{M}}{dt} \right] = \frac{dm_\theta}{dt} \hat{\theta} + \frac{dm_\phi}{dt} \hat{\phi} \quad (4.18)$$

and

$$\begin{aligned} \delta \left(\vec{M} \times \frac{2A}{M_0^2} \nabla^2 \vec{M} \right) &\cong M_0 \hat{r} \times \frac{2A}{M_0^2} (\hat{\theta} \nabla^2 m_\theta + \hat{\phi} \nabla^2 m_\phi) \\ &= \frac{2A}{M_0} (\hat{\phi} \nabla^2 m_\theta - \hat{\theta} \nabla^2 m_\phi) \end{aligned} \quad (4.19)$$

where again we used $\hat{r} \times \hat{\theta} = \hat{\phi}$ and $\hat{r} \times \hat{\phi} = -\hat{\theta}$. The transverse components $\vec{M}_{x,y}$ will be replaced by

$$\vec{M}_{\theta,\phi} = m_\theta \hat{\theta} + m_\phi \hat{\phi} \quad (4.20)$$

making it more appropriate to our geometry as promised. The torque due to the rf-field:

$$\begin{aligned} \vec{M} \times \vec{h} &= (M_0 \hat{r} + m_\theta \hat{\theta} + m_\phi \hat{\phi}) \times (h_\theta \hat{\theta} + h_\phi \hat{\phi}) e^{i\omega t} \\ &= [M_0 h_\theta \hat{\phi} - M_0 h_\phi \hat{\theta} + (m_\theta h_\phi - m_\phi h_\theta) \hat{r}] e^{i\omega t} \end{aligned} \quad (4.21)$$

For the $\vec{\tau}$ term we can utilize a Taylor expansion around the equilibrium orientation of \vec{M} , i.e. around (θ_{eq}, ϕ_{eq}) . The Taylor expansion of a function $f(x)$ of a single variable x around $x = x_0$ was given by

$$f(x) \cong f(x_0) + \left. \frac{df}{dx} \right|_{x=x_0} (x - x_0) + \frac{1}{2!} \left. \frac{d^2 f}{dx^2} \right|_{x=x_0} (x - x_0)^2 \dots$$

We will only be using first order terms, i.e. $f(x) \cong f(x_0) + \left. \frac{df}{dx} \right|_{x=x_0} (x - x_0)$ which reads for a multivariable function $f(x, y)$ as

$$f(x, y) \cong f(x_0, y_0) + \left. \frac{\partial f}{\partial x} \right|_{x_0, y_0} (x - x_0) + \left. \frac{\partial f}{\partial y} \right|_{x_0, y_0} (y - y_0) \quad (4.22)$$

Remember from equation (4.11) that $\vec{\tau} = -\hat{\phi} \frac{\partial E}{\partial \theta} + \hat{\theta} \frac{1}{\sin \theta} \frac{\partial E}{\partial \phi}$, so we have to Taylor expand both $\frac{\partial E}{\partial \theta}$ and $\frac{\partial E}{\partial \phi}$ terms around (θ_{eq}, ϕ_{eq}) but we have to keep in mind that $\vec{\tau}$ is not a function of a single variable but a function of both θ and ϕ .

Taylor expansion of $f(\theta, \phi) = \frac{\partial E}{\partial \theta}$ around (θ_{eq}, ϕ_{eq}) by the use of equation (4.22):

$$\begin{aligned} \frac{\partial E}{\partial \theta} \cong \frac{\partial E}{\partial \theta} \Big|_{\theta_{eq}, \phi_{eq}} + \frac{\partial}{\partial \theta} \left(\frac{\partial E}{\partial \theta} \right) \Big|_{\theta_{eq}, \phi_{eq}} (\theta - \theta_{eq}) \\ + \frac{\partial}{\partial \phi} \left(\frac{\partial E}{\partial \theta} \right) \Big|_{\theta_{eq}, \phi_{eq}} (\phi - \phi_{eq}) \end{aligned} \quad (4.23)$$

The first term $\frac{\partial E}{\partial \theta} \Big|_{\theta_{eq}, \phi_{eq}}$ on the right hand side of equation (4.23) is zero because at equilibrium energy is minimized and the first derivative is zero. Realizing that $\theta - \theta_{eq} = \delta\theta$ and $\phi - \phi_{eq} = \delta\phi$, equation (4.23) becomes

$$\frac{\partial E}{\partial \theta} \cong \frac{\partial^2 E}{\partial \theta^2} \Big|_{\theta_{eq}, \phi_{eq}} \delta\theta + \frac{\partial^2 E}{\partial \phi \partial \theta} \Big|_{\theta_{eq}, \phi_{eq}} \delta\phi \quad (4.24)$$

Following the same arguments for Taylor expansion of $f(\theta, \phi) = \frac{\partial E}{\partial \phi}$ around (θ_{eq}, ϕ_{eq}) we get

$$\frac{\partial E}{\partial \phi} \cong \frac{\partial^2 E}{\partial \theta \partial \phi} \Big|_{\theta_{eq}, \phi_{eq}} \delta\theta + \frac{\partial^2 E}{\partial \phi^2} \Big|_{\theta_{eq}, \phi_{eq}} \delta\phi \quad (4.25)$$

Then by the use of equations (4.24) and (4.25), the first order approximation for the torque $\vec{\tau} = -\hat{\phi} \frac{\partial E}{\partial \theta} + \hat{\theta} \frac{1}{\sin \theta} \frac{\partial E}{\partial \phi}$ of equation (4.11) will be

$$\vec{\tau} \cong -\hat{\phi} \left(\frac{\partial^2 E}{\partial \theta^2} \delta\theta + \frac{\partial^2 E}{\partial \phi \partial \theta} \delta\phi \right) + \hat{\theta} \frac{1}{\sin \theta} \left(\frac{\partial^2 E}{\partial \theta \partial \phi} \delta\theta + \frac{\partial^2 E}{\partial \phi^2} \delta\phi \right) \quad (4.26)$$

in which we dropped θ_{eq}, ϕ_{eq} symbols below each partial derivative to avoid a formidable looking expression. We should, however, always keep in mind that all the partial derivatives expressed in $\vec{\tau}$ are calculated at $\theta = \theta_{eq}$ and $\phi = \phi_{eq}$ (after performing the derivatives of course), so they in fact represent scalar linear expansion coefficients rather than functions. Making the replacements $\delta\theta = m_\theta/M_0$ and $\delta\phi = m_\phi/M_0\sin\theta$ in equation (4.26) we get

$$\vec{\tau} \cong -\hat{\phi} \left(\frac{\partial^2 E}{\partial \theta^2} \frac{m_\theta}{M_0} + \frac{\partial^2 E}{\partial \phi \partial \theta} \frac{m_\phi}{M_0 \sin \theta} \right) + \hat{\theta} \frac{1}{\sin \theta} \left(\frac{\partial^2 E}{\partial \theta \partial \phi} \frac{m_\theta}{M_0} + \frac{\partial^2 E}{\partial \phi^2} \frac{m_\phi}{M_0 \sin \theta} \right)$$

which finally becomes

$$\begin{aligned} \vec{\tau} \cong & -\hat{\phi} \left(\frac{m_\theta}{M_0} \frac{\partial^2 E}{\partial \theta^2} + \frac{m_\phi}{M_0 \sin \theta} \frac{\partial^2 E}{\partial \phi \partial \theta} \right) \\ & + \hat{\theta} \left(\frac{m_\theta}{M_0 \sin \theta} \frac{\partial^2 E}{\partial \theta \partial \phi} + \frac{m_\phi}{M_0 \sin^2 \theta} \frac{\partial^2 E}{\partial \phi^2} \right) \end{aligned} \quad (4.27)$$

Inserting equations (4.18), (4.19), (4.20), (4.21) and (4.27) into equation (4.17) we get

$$\begin{aligned} & \frac{dm_\theta}{dt} \hat{\theta} + \frac{dm_\phi}{dt} \hat{\phi} = \\ & -\gamma \left\{ \begin{aligned} & -\hat{\phi} \left(\frac{m_\theta}{M_0} \frac{\partial^2 E}{\partial \theta^2} + \frac{m_\phi}{M_0 \sin \theta} \frac{\partial^2 E}{\partial \phi \partial \theta} \right) + \hat{\theta} \left(\frac{m_\theta}{M_0 \sin \theta} \frac{\partial^2 E}{\partial \theta \partial \phi} + \frac{m_\phi}{M_0 \sin^2 \theta} \frac{\partial^2 E}{\partial \phi^2} \right) \\ & + [M_0 h_\theta \hat{\phi} - M_0 h_\phi \hat{\theta} + (m_\theta h_\phi - m_\phi h_\theta) \hat{r}] e^{i\omega t} \\ & + \frac{2A}{M_0} (\hat{\phi} \nabla^2 m_\theta - \hat{\theta} \nabla^2 m_\phi) \\ & - \frac{m_\theta}{T_2} \hat{\theta} - \frac{m_\phi}{T_2} \hat{\phi} \end{aligned} \right\} \end{aligned} \quad (4.28)$$

Resolving \hat{r} , $\hat{\theta}$ and $\hat{\phi}$ components of the left and right hand sides of equation (4.28)

$$\hat{r}: \quad 0 = (m_\theta h_\phi - m_\phi h_\theta) e^{i\omega t} \quad (4.29)$$

$$\hat{\theta}: \quad \frac{dm_\theta}{dt} = -\gamma \frac{m_\theta}{M_0 \sin\theta} \frac{\partial^2 E}{\partial\theta\partial\phi} - \gamma \frac{m_\phi}{M_0 \sin^2\theta} \frac{\partial^2 E}{\partial\phi^2} + \gamma M_0 h_\phi e^{i\omega t} + \gamma \frac{2A}{M_0} \nabla^2 m_\phi - \frac{m_\theta}{T_2} \quad (4.30)$$

$$\hat{\phi}: \quad \frac{dm_\phi}{dt} = \gamma \frac{m_\theta}{M_0} \frac{\partial^2 E}{\partial\theta^2} + \gamma \frac{m_\phi}{M_0 \sin\theta} \frac{\partial^2 E}{\partial\phi\partial\theta} - \gamma M_0 h_\theta e^{i\omega t} - \gamma \frac{2A}{M_0} \nabla^2 m_\theta - \frac{m_\phi}{T_2} \quad (4.31)$$

Equation (4.29) for the \hat{r} component yields $m_\theta h_\phi - m_\phi h_\theta = 0$ which in turn implies

$$\frac{m_\theta}{h_\theta} = \frac{m_\phi}{h_\phi} = \chi_{\theta\theta} = \chi_{\phi\phi} = \text{transverse susceptibility} \quad (4.32)$$

4.1.6. Proposed Solutions

Because of the form of the magnetic component $\vec{h} = (h_\theta \hat{\theta} + h_\phi \hat{\phi})e^{i\omega t}$ of the driving rf-field, we can propose plane wave solutions to equations (4.30) and (4.31) in the form [198]

$$m_\theta^n(z, t) = m_\theta^{0,n} \sin(k_n z + \varphi_n) e^{i\omega t} \quad (4.33)$$

$$m_\phi^n(z, t) = m_\phi^{0,n} \sin(k_n z + \varphi_n) e^{i\omega t} \quad (4.34)$$

along the thickness (z -direction) of the thin film (of thickness L) where n and k_n represent the mode number and the wave number of mode n respectively. We need to calculate $\frac{dm_\theta^n}{dt}$, $\frac{dm_\phi^n}{dt}$, $\nabla^2 m_\theta^n$ and $\nabla^2 m_\phi^n$ from equations (4.33) and (4.34) to place into equations (4.30) and (4.31).

$$\frac{dm_\theta^n}{dt} = \frac{d}{dt} [m_\theta^{0,n} \sin(k_n z + \varphi_n) e^{i\omega t}] = i\omega m_\theta^{0,n} \sin(k_n z + \varphi_n) e^{i\omega t} \quad (4.35)$$

$$\frac{dm_\phi^n}{dt} = \frac{d}{dt} [m_\phi^{0,n} \sin(k_n z + \varphi_n) e^{i\omega t}] = i\omega m_\phi^{0,n} \sin(k_n z + \varphi_n) e^{i\omega t} \quad (4.36)$$

$$\begin{aligned} \nabla^2 m_\theta^n &= \left(\frac{\partial^2}{\partial x^2} + \frac{\partial^2}{\partial y^2} + \frac{\partial^2}{\partial z^2} \right) [m_\theta^{0,n} \sin(k_n z + \varphi_n) e^{i\omega t}] \\ &= -k_n^2 m_\theta^{0,n} \sin(k_n z + \varphi_n) e^{i\omega t} \end{aligned} \quad (4.37)$$

$$\begin{aligned} \nabla^2 m_\phi^n &= \left(\frac{\partial^2}{\partial x^2} + \frac{\partial^2}{\partial y^2} + \frac{\partial^2}{\partial z^2} \right) [m_\phi^{0,n} \sin(k_n z + \varphi_n) e^{i\omega t}] \\ &= -k_n^2 m_\phi^{0,n} \sin(k_n z + \varphi_n) e^{i\omega t} \end{aligned} \quad (4.38)$$

Putting equations (4.33) for m_θ^n , (4.34) for m_ϕ^n , (4.35) for $\frac{dm_\theta^n}{dt}$ and (4.38) for $\nabla^2 m_\phi^n$ into equation (4.30), one gets

$$\begin{aligned} &i\omega m_\theta^{0,n} \sin(k_n z + \varphi_n) e^{i\omega t} = \\ &- \gamma \frac{1}{M_0 \sin \theta} \frac{\partial^2 E}{\partial \theta \partial \phi} m_\theta^{0,n} \sin(k_n z + \varphi_n) e^{i\omega t} \\ &- \gamma \frac{1}{M_0 \sin^2 \theta} \frac{\partial^2 E}{\partial \phi^2} m_\phi^{0,n} \sin(k_n z + \varphi_n) e^{i\omega t} \\ &\quad + \gamma M_0 h_\phi e^{i\omega t} \\ &\quad + \gamma \frac{2A}{M_0} (-k_n^2) m_\phi^{0,n} \sin(k_n z + \varphi_n) e^{i\omega t} \\ &\quad - \frac{m_\theta^{0,n} \sin(k_n z + \varphi_n) e^{i\omega t}}{T_2} \end{aligned} \quad (4.39)$$

Putting now equations (4.33) for m_θ^n , (4.34) for m_ϕ^n , (4.36) for $\frac{dm_\phi^n}{dt}$ and (4.37) for $\nabla^2 m_\theta^n$ into equation (4.31), one gets

$$i\omega m_\phi^{0,n} \sin(k_n z + \varphi_n) e^{i\omega t} = \quad (4.40)$$

$$\begin{aligned}
& \gamma \frac{1}{M_0} \frac{\partial^2 E}{\partial \theta^2} m_\theta^{0,n} \sin(k_n z + \varphi_n) e^{i\omega t} \\
& + \gamma \frac{1}{M_0 \sin \theta} \frac{\partial^2 E}{\partial \phi \partial \theta} m_\phi^{0,n} \sin(k_n z + \varphi_n) e^{i\omega t} \\
& \quad - \gamma M_0 h_\theta e^{i\omega t} \\
& - \gamma \frac{2A}{M_0} (-k_n^2) m_\theta^{0,n} \sin(k_n z + \varphi_n) e^{i\omega t} \\
& \quad - \frac{m_\phi^{0,n} \sin(k_n z + \varphi_n) e^{i\omega t}}{T_2}
\end{aligned}$$

Cancelling out the common $e^{i\omega t}$ term from both sides, dividing through by γ and leaving $M_0 h_\phi$ alone on one side of the equation, equation (4.39) yields (where $D = 2A/M_0$)

$$\begin{aligned}
M_0 h_\phi = & \left[\frac{i\omega}{\gamma} + \frac{1}{M_0 \sin \theta} \frac{\partial^2 E}{\partial \theta \partial \phi} + \frac{1}{\gamma T_2} \right] m_\theta^{0,n} \sin(k_n z + \varphi_n) \\
& + \left[Dk_n^2 + \frac{1}{M_0 \sin^2 \theta} \frac{\partial^2 E}{\partial \phi^2} \right] m_\phi^{0,n} \sin(k_n z + \varphi_n)
\end{aligned} \tag{4.41}$$

Applying the same judgement of cancelling out the common $e^{i\omega t}$ term from both sides, dividing through by γ and leaving this time $M_0 h_\theta$ alone on one side of the equation, equation (4.40) yields

$$\begin{aligned}
M_0 h_\theta = & \left[Dk_n^2 + \frac{1}{M_0} \frac{\partial^2 E}{\partial \theta^2} \right] m_\theta^{0,n} \sin(k_n z + \varphi_n) \\
& + \left[-\frac{i\omega}{\gamma} + \frac{1}{M_0 \sin \theta} \frac{\partial^2 E}{\partial \phi \partial \theta} - \frac{1}{\gamma T_2} \right] m_\phi^{0,n} \sin(k_n z + \varphi_n)
\end{aligned} \tag{4.42}$$

Equations (4.41) and (4.42) constitute a set of linear equations in unknowns $m_\theta^{0,n} \sin(k_n z + \varphi_n)$ and $m_\phi^{0,n} \sin(k_n z + \varphi_n)$ in the following form

$$c = ax + by \tag{4.43}$$

$$f = dx + ey \tag{4.44}$$

with

$$x = m_{\theta}^{0,n} \sin(k_n z + \varphi_n)$$

$$y = m_{\phi}^{0,n} \sin(k_n z + \varphi_n)$$

$$a = \frac{i\omega}{\gamma} + \frac{1}{M_0 \sin\theta} \frac{\partial^2 E}{\partial\theta\partial\phi} + \frac{1}{\gamma T_2} \quad b = Dk_n^2 + \frac{1}{M_0 \sin^2\theta} \frac{\partial^2 E}{\partial\phi^2} \quad c = M_0 h_{\phi}$$

$$d = Dk_n^2 + \frac{1}{M_0} \frac{\partial^2 E}{\partial\theta^2} \quad e = -\frac{i\omega}{\gamma} + \frac{1}{M_0 \sin\theta} \frac{\partial^2 E}{\partial\phi\partial\theta} - \frac{1}{\gamma T_2} \quad f = M_0 h_{\theta}$$

The solutions for equations (4.43) and (4.44) are

$$x = \frac{ec - bf}{ae - db}$$

$$y = \frac{af - dc}{ae - db}$$

which then yields solutions to the equations (4.41) and (4.42) as

$$m_{\theta}^{0,n} \sin(k_n z + \varphi_n) =$$

$$\frac{\left[-\frac{i\omega}{\gamma} + \frac{1}{M_0 \sin\theta} \frac{\partial^2 E}{\partial\phi\partial\theta} - \frac{1}{\gamma T_2} \right] M_0 h_{\phi} - \left[Dk_n^2 + \frac{1}{M_0 \sin^2\theta} \frac{\partial^2 E}{\partial\phi^2} \right] M_0 h_{\theta}}{\Delta} \quad (4.45)$$

and

$$m_{\phi}^{0,n} \sin(k_n z + \varphi_n) =$$

$$\frac{\left[\frac{i\omega}{\gamma} + \frac{1}{M_0 \sin\theta} \frac{\partial^2 E}{\partial\theta\partial\phi} + \frac{1}{\gamma T_2} \right] M_0 h_{\theta} - \left[Dk_n^2 + \frac{1}{M_0} \frac{\partial^2 E}{\partial\theta^2} \right] M_0 h_{\phi}}{\Delta} \quad (4.46)$$

where

$$\begin{aligned}
\Delta &= \left[\frac{i\omega}{\gamma} + \frac{1}{M_0 \sin\theta} \frac{\partial^2 E}{\partial\theta\partial\phi} + \frac{1}{\gamma T_2} \right] \left[-\frac{i\omega}{\gamma} + \frac{1}{M_0 \sin\theta} \frac{\partial^2 E}{\partial\phi\partial\theta} - \frac{1}{\gamma T_2} \right] \\
&\quad - \left[Dk_n^2 + \frac{1}{M_0} \frac{\partial^2 E}{\partial\theta^2} \right] \left[Dk_n^2 + \frac{1}{M_0 \sin^2\theta} \frac{\partial^2 E}{\partial\phi^2} \right] \\
&= \left[\left(\frac{1}{M_0 \sin\theta} \frac{\partial^2 E}{\partial\theta\partial\phi} \right) + \left(\frac{i\omega}{\gamma} + \frac{1}{\gamma T_2} \right) \right] \left[\left(\frac{1}{M_0 \sin\theta} \frac{\partial^2 E}{\partial\phi\partial\theta} \right) - \left(\frac{i\omega}{\gamma} + \frac{1}{\gamma T_2} \right) \right] \\
&\quad - \left[Dk_n^2 + \frac{1}{M_0} \frac{\partial^2 E}{\partial\theta^2} \right] \left[Dk_n^2 + \frac{1}{M_0 \sin^2\theta} \frac{\partial^2 E}{\partial\phi^2} \right] \\
&= \left(\frac{1}{M_0 \sin\theta} \frac{\partial^2 E}{\partial\theta\partial\phi} \right)^2 - \left(\frac{i\omega}{\gamma} + \frac{1}{\gamma T_2} \right)^2 - \left[Dk_n^2 + \frac{1}{M_0} \frac{\partial^2 E}{\partial\theta^2} \right] \left[Dk_n^2 + \frac{1}{M_0 \sin^2\theta} \frac{\partial^2 E}{\partial\phi^2} \right] \\
&= \left(\frac{1}{M_0 \sin\theta} \frac{\partial^2 E}{\partial\theta\partial\phi} \right)^2 - \left(-\frac{\omega^2}{\gamma^2} + \frac{1}{\gamma^2 T_2^2} + 2 \frac{i\omega}{\gamma} \frac{1}{\gamma T_2} \right) \\
&\quad - \left[Dk_n^2 + \frac{1}{M_0} \frac{\partial^2 E}{\partial\theta^2} \right] \left[Dk_n^2 + \frac{1}{M_0 \sin^2\theta} \frac{\partial^2 E}{\partial\phi^2} \right] \\
&\Rightarrow \Delta = \left(\frac{1}{M_0 \sin\theta} \frac{\partial^2 E}{\partial\theta\partial\phi} \right)^2 + \frac{\omega^2}{\gamma^2} - \frac{1}{\gamma^2 T_2^2} - \frac{2i\omega}{\gamma^2 T_2} \\
&\quad - \left[Dk_n^2 + \frac{1}{M_0} \frac{\partial^2 E}{\partial\theta^2} \right] \left[Dk_n^2 + \frac{1}{M_0 \sin^2\theta} \frac{\partial^2 E}{\partial\phi^2} \right] \\
&\Rightarrow \Delta = \frac{\omega^2}{\gamma^2} - \left\{ \left[Dk_n^2 + \frac{1}{M_0} \frac{\partial^2 E}{\partial\theta^2} \right] \left[Dk_n^2 + \frac{1}{M_0 \sin^2\theta} \frac{\partial^2 E}{\partial\phi^2} \right] - \left(\frac{1}{M_0 \sin\theta} \frac{\partial^2 E}{\partial\theta\partial\phi} \right)^2 + \frac{1}{\gamma^2 T_2^2} \right\} \\
&\quad - \frac{2i\omega}{\gamma^2 T_2}
\end{aligned}$$

Calling the term in { } parenthesis as $\frac{\omega_0^2}{\gamma^2}$ we get

$$\begin{aligned} & \left[Dk_n^2 + \frac{1}{M_0} \frac{\partial^2 E}{\partial \theta^2} \right] \left[Dk_n^2 + \frac{1}{M_0 \sin^2 \theta} \frac{\partial^2 E}{\partial \phi^2} \right] - \left(\frac{1}{M_0 \sin \theta} \frac{\partial^2 E}{\partial \theta \partial \phi} \right)^2 + \frac{1}{\gamma^2 T_2^2} \\ & = \frac{\omega_0^2}{\gamma^2} \end{aligned} \quad (4.47)$$

and the Δ term becomes

$$\Delta = \frac{\omega^2}{\gamma^2} - \frac{\omega_0^2}{\gamma^2} - \frac{2i\omega}{\gamma^2 T_2} \quad (4.48)$$

Then equations (4.45) and (4.46) become (4.49) and (4.50) respectively

$$\begin{aligned} & m_\theta^{0,n} \sin(k_n z + \varphi_n) = \\ & \frac{\left[-\frac{i\omega}{\gamma} + \frac{1}{M_0 \sin \theta} \frac{\partial^2 E}{\partial \phi \partial \theta} - \frac{1}{\gamma T_2} \right] M_0 h_\phi - \left[Dk_n^2 + \frac{1}{M_0 \sin^2 \theta} \frac{\partial^2 E}{\partial \phi^2} \right] M_0 h_\theta}{\frac{\omega^2}{\gamma^2} - \frac{\omega_0^2}{\gamma^2} - \frac{2i\omega}{\gamma^2 T_2}} \end{aligned} \quad (4.49)$$

and

$$\begin{aligned} & m_\phi^{0,n} \sin(k_n z + \varphi_n) = \\ & \frac{\left[\frac{i\omega}{\gamma} + \frac{1}{M_0 \sin \theta} \frac{\partial^2 E}{\partial \theta \partial \phi} + \frac{1}{\gamma T_2} \right] M_0 h_\theta - \left[Dk_n^2 + \frac{1}{M_0} \frac{\partial^2 E}{\partial \theta^2} \right] M_0 h_\phi}{\frac{\omega^2}{\gamma^2} - \frac{\omega_0^2}{\gamma^2} - \frac{2i\omega}{\gamma^2 T_2}} \end{aligned} \quad (4.50)$$

4.1.7. Dynamic Susceptibility and Resonance Condition

The power absorbed by the unit volume of the sample from an rf-field of frequency ω is given as [169, 201]

$$P = \frac{1}{2} \omega \chi_2 h^2 \quad (4.51)$$

where χ_2 is the imaginary part of the susceptibility and h is the magnitude of the magnetic component of the rf field. The dynamic susceptibility is defined as [173, 198]

$$\chi = \frac{\vec{m} \cdot \vec{h}}{h^2} = \frac{m_\theta h_\theta + m_\phi h_\phi}{h_\theta^2 + h_\phi^2} = \frac{m_x}{h_x} = \left(\frac{m_\phi}{h_\phi} \right)_{\phi=\frac{\pi}{2}} = \chi_1 - i\chi_2 \quad (4.52)$$

Now, for the sake of simplicity we rewrite equations (4.49)-(4.50) as

$$m_\theta^{0,n} \sin(k_n z + \varphi_n) = \frac{A \cdot h_\phi - B \cdot h_\theta}{\Delta} \quad (4.53)$$

$$m_\phi^{0,n} \sin(k_n z + \varphi_n) = \frac{C \cdot h_\theta - D \cdot h_\phi}{\Delta} \quad (4.54)$$

where

$$A = \left[-\frac{i\omega}{\gamma} + \frac{1}{M_0 \sin\theta} \frac{\partial^2 E}{\partial \phi \partial \theta} - \frac{1}{\gamma T_2} \right] M_0 \quad B = \left[D k_n^2 + \frac{1}{M_0 \sin^2 \theta} \frac{\partial^2 E}{\partial \phi^2} \right] M_0$$

$$C = \left[\frac{i\omega}{\gamma} + \frac{1}{M_0 \sin\theta} \frac{\partial^2 E}{\partial \theta \partial \phi} + \frac{1}{\gamma T_2} \right] M_0 \quad D = \left[D k_n^2 + \frac{1}{M_0} \frac{\partial^2 E}{\partial \theta^2} \right] M_0$$

$$\Delta = \frac{\omega^2}{\gamma^2} - \frac{\omega_0^2}{\gamma^2} - \frac{2i\omega}{\gamma^2 T_2}$$

If we now multiply both sides of equations (4.53)-(4.54) with $\sin(k_m z + \varphi_m)$ and integrate with respect to "z" along the thickness L of the film we get

$$\begin{aligned} & \int_{z=0}^{z=L} m_\theta^{0,n} \sin(k_n z + \varphi_n) \sin(k_m z + \varphi_m) dz \\ & = \frac{A \cdot h_\phi - B \cdot h_\theta}{\Delta} \int_{z=0}^{z=L} \sin(k_m z + \varphi_m) dz \end{aligned} \quad (4.55)$$

and

$$\begin{aligned}
& \int_{z=0}^{z=L} m_{\phi}^{0,n} \sin(k_n z + \varphi_n) \sin(k_m z + \varphi_m) dz \\
&= \frac{C \cdot h_{\theta} - D \cdot h_{\phi}}{\Delta} \int_{z=0}^{z=L} \sin(k_m z + \varphi_m) dz
\end{aligned} \tag{4.56}$$

If we now leave $m_{\theta}^{0,n}$ and $m_{\phi}^{0,n}$ alone on the left hand sides by taking them outside the integrals (they have no z -dependence) and putting the remaining integral terms to the denominators of the right hand sides

$$m_{\theta}^{0,n} = \frac{A \cdot h_{\phi} - B \cdot h_{\theta}}{\Delta} \cdot \frac{\int_{z=0}^{z=L} \sin(k_m z + \varphi_m) dz}{\int_{z=0}^{z=L} \sin(k_n z + \varphi_n) \sin(k_m z + \varphi_m) dz} \tag{4.57}$$

$$m_{\phi}^{0,n} = \frac{C \cdot h_{\theta} - D \cdot h_{\phi}}{\Delta} \cdot \frac{\int_{z=0}^{z=L} \sin(k_m z + \varphi_m) dz}{\int_{z=0}^{z=L} \sin(k_n z + \varphi_n) \sin(k_m z + \varphi_m) dz} \tag{4.58}$$

Calling the terms related to integrals at the rights hand sights of (4.57)-(4.58) as I_n known as amplitude factor [198] or mode intensity [154] and remembering that $\Delta = \frac{\omega^2}{\gamma^2} - \frac{\omega_0^2}{\gamma^2} - i \frac{2\omega}{\gamma^2 T_2}$, we multiply and divide the right hand sides of (4.57)-(4.58) by the complex conjugate of Δ which is $\Delta^* = \frac{\omega^2}{\gamma^2} - \frac{\omega_0^2}{\gamma^2} + i \frac{2\omega}{\gamma^2 T_2}$ to make the denominators real, we get

$$m_{\theta}^{0,n} = \frac{(A \cdot h_{\phi} - B \cdot h_{\theta}) \cdot \Delta^*}{\Delta \cdot \Delta^*} \cdot I_n \tag{4.59}$$

$$m_{\phi}^{0,n} = \frac{(C \cdot h_{\theta} - D \cdot h_{\phi}) \cdot \Delta^*}{\Delta \cdot \Delta^*} \cdot I_n \tag{4.60}$$

where

$$\Delta \cdot \Delta^* = \left(\frac{\omega^2}{\gamma^2} - \frac{\omega_0^2}{\gamma^2} - i \frac{2\omega}{\gamma^2 T_2} \right) \cdot \left(\frac{\omega^2}{\gamma^2} - \frac{\omega_0^2}{\gamma^2} + i \frac{2\omega}{\gamma^2 T_2} \right) = \left(\frac{\omega^2}{\gamma^2} - \frac{\omega_0^2}{\gamma^2} \right)^2 + \frac{4\omega^2}{\gamma^4 T_2^2} \tag{4.61}$$

The dynamic susceptibility connects the dynamic magnetization and the excitation magnetic field. In most of the cases the susceptibility is given by a tensor. If we write down equations (4.59)-(4.60) in matrix form we get

$$\begin{pmatrix} m_{\theta}^{0,n} \\ m_{\phi}^{0,n} \end{pmatrix} = I_n \begin{pmatrix} \frac{-B \cdot \Delta^*}{\Delta \cdot \Delta^*} & \frac{A \cdot \Delta^*}{\Delta \cdot \Delta^*} \\ \frac{C \cdot \Delta^*}{\Delta \cdot \Delta^*} & \frac{-D \cdot \Delta^*}{\Delta \cdot \Delta^*} \end{pmatrix} \begin{pmatrix} h_{\theta} \\ h_{\phi} \end{pmatrix} \quad (4.62)$$

which resembles

$$\begin{pmatrix} m_{\theta}^{0,n} \\ m_{\phi}^{0,n} \end{pmatrix} = \begin{pmatrix} \chi_{\theta\theta} & \chi_{\theta\phi} \\ \chi_{\phi\theta} & \chi_{\phi\phi} \end{pmatrix} \begin{pmatrix} h_{\theta} \\ h_{\phi} \end{pmatrix} \quad (4.63)$$

Off diagonal components refer to the gyration which is related to the optical activity-scattering in the sample material and the diagonal components $\chi_{\theta\theta} = \chi_{\phi\phi}$ (equation (4.32)) are related to power absorption. By comparing (4.62) and (4.63), the important component of the susceptibility tensor becomes

$$\chi^n = \frac{m_x}{h_x} = \left. \left(\frac{m_{\phi}}{h_{\phi}} \right) \right|_{\phi=\frac{\pi}{2}} = \chi_{\phi\phi} = I_n \cdot \frac{-D \cdot \Delta^*}{\Delta \cdot \Delta^*} \quad (4.64)$$

Then by inserting

$$\begin{aligned} -D &= - \left[Dk_n^2 + \frac{1}{M_0} \frac{\partial^2 E}{\partial \theta^2} \right] M_0 \quad \text{and} \quad \Delta^* = \left(\frac{\omega^2}{\gamma^2} - \frac{\omega_0^2}{\gamma^2} + i \frac{2\omega}{\gamma^2 T_2} \right) \\ \Rightarrow -D \cdot \Delta^* &= M_0 \left[Dk_n^2 + \frac{1}{M_0} \frac{\partial^2 E}{\partial \theta^2} \right] \left(\frac{\omega_0^2}{\gamma^2} - \frac{\omega^2}{\gamma^2} - i \frac{2\omega}{\gamma^2 T_2} \right) \\ \Delta \cdot \Delta^* &= \left(\frac{\omega^2}{\gamma^2} - \frac{\omega_0^2}{\gamma^2} \right)^2 + \frac{4\omega^2}{\gamma^4 T_2^2} \end{aligned}$$

we get from (4.64)

$$\chi^n = \chi_{\phi\phi} = I_n \cdot \frac{M_0 \left[Dk_n^2 + \frac{1}{M_0} \frac{\partial^2 E}{\partial \theta^2} \right] \left(\frac{\omega_0^2}{\gamma^2} - \frac{\omega^2}{\gamma^2} - i \frac{2\omega}{\gamma^2 T_2} \right)}{\left(\frac{\omega^2}{\gamma^2} - \frac{\omega_0^2}{\gamma^2} \right)^2 + \frac{4\omega^2}{\gamma^4 T_2^2}} \quad (4.65)$$

By comparing equation (4.65) with $\chi^n = \chi_1^n - i\chi_2^n$ and remembering the fact that the absorbed power per unit volume is dependent upon the imaginary part χ_2^n , we extract from (4.65) that

$$\chi_2^n(\omega) = I_n \cdot \frac{M_0 \left[Dk_n^2 + \frac{1}{M_0} \frac{\partial^2 E}{\partial \theta^2} \right] \frac{2\omega}{\gamma^2 T_2}}{\left(\frac{\omega^2}{\gamma^2} - \frac{\omega_0^2}{\gamma^2} \right)^2 + \frac{4\omega^2}{\gamma^4 T_2^2}} \quad (4.66)$$

It is seen in equation (4.66) that susceptibility responsible for the absorbed power acquires a maximum when the term with the driving field frequency, the term $\frac{\omega^2}{\gamma^2}$, is equal to $\frac{\omega_0^2}{\gamma^2}$. In actual experiment, the frequency ω of the rf-field is fixed but the magnitude of the DC magnetic field is swept. During the magnetic field sweep, for a given orientation of the DC field with respect to the magnetic object, the magnitude of the DC field reaches a value such that the term $\frac{\omega_0^2}{\gamma^2}$ given by (equation (4.47))

$$\frac{\omega_0^2}{\gamma^2} = \left[Dk_n^2 + \frac{1}{M_0} \frac{\partial^2 E}{\partial \theta^2} \right] \left[Dk_n^2 + \frac{1}{M_0 \sin^2 \theta} \frac{\partial^2 E}{\partial \phi^2} \right] - \left(\frac{1}{M_0 \sin \theta} \frac{\partial^2 E}{\partial \theta \partial \phi} \right)^2 + \frac{1}{\gamma^2 T_2^2}$$

becomes equal to $\frac{\omega^2}{\gamma^2}$ where ω is the angular frequency of the rf-field. Therefore, ω_0 can be called the resonance frequency of the magnetic object with that particular orientation of the object and the DC field, DC field value, magnetic anisotropies, etc. One can then conclude that for every single orientation and DC field value, the system gains a particular value of ω_0 and for a specific set of parameters it is equal to ω of the driving field, so what we call a resonance phenomenon occurs.

Equation (4.47) rewritten above gives us the most general condition for both FMR and SWR (spin wave resonance). In the case of zero wavevector ($k = 0$) and neglecting the

damping term $\frac{1}{\gamma^2 T_2^2}$ we obtain the uniform precession mode (i.e. the FMR limit):

$$\begin{aligned} \frac{\omega_0^2}{\gamma^2} &= \left[\frac{1}{M_0} \frac{\partial^2 E}{\partial \theta^2} \right] \left[\frac{1}{M_0 \sin^2 \theta} \frac{\partial^2 E}{\partial \phi^2} \right] - \left(\frac{1}{M_0 \sin \theta} \frac{\partial^2 E}{\partial \theta \partial \phi} \right)^2 \\ \Rightarrow \left(\frac{\omega_0}{\gamma} \right)^2 &= \frac{1}{M_0^2 \sin^2 \theta} \left[\frac{\partial^2 E}{\partial \phi^2} \frac{\partial^2 E}{\partial \theta^2} - \left(\frac{\partial^2 E}{\partial \theta \partial \phi} \right)^2 \right] \end{aligned} \quad (4.67)$$

which is very well known as Smit–Beljers equation [202] and which is exactly the same as equation (2) of [203] and it yields the same condition with equation (2) of [175] to name a few correspondences from the literature.

4.2. FERROMAGNETIC RESONANCE IN MULTILAYER STRUCTURES

The form of the solution to the Landau-Lifshitz-Gilbert (LLG) equation for the multilayer structure is to linearize the equations of motions of magnetizations of each layer in the multilayer of N -FM layers and to write down a $2N \times 2N$ coefficient matrix multiplying the $2N \times 1$ dimensional dynamical magnetization vector (composed of azimuthal and polar components of all layers). Once the generalized form of the components of the coefficient matrix for a system of any number N of FM layers is found, the dynamical magnetizations in each layer can be solved at once by linear algebra which in turn can be used to calculate the dynamical susceptibility.

4.2.1. Equation of Motion

The equation of motion of magnetization for a ferromagnetic (FM) layer in a Ferromagnetic Resonance (FMR) experiment can be given in a most general form by

$$\frac{d\vec{M}}{dt} = -\gamma \vec{M} \times \vec{H}_{eff} + \vec{R} \quad (4.68)$$

where the first term on the right hand side is the torque due to and creating a precession around the effective magnetic field and the second is the damping term responsible for the relaxation of magnetization towards the equilibrium orientation close to the effective magnetic field. The damping term, for our purposes, can be of

- i. Gilbert Type $:\frac{\alpha}{M}\vec{M}\times\frac{d\vec{M}}{dt},$
- or
- ii. Bloch-Bloembergen Type: $-\frac{\vec{M}_{x,y}}{T_2}-\frac{\vec{M}_z-\vec{M}_0}{T_1}$

where α is the Gilbert Damping Parameter, T_1 is the longitudinal relaxation time responsible for spin-lattice interactions and T_2 is the transverse relaxation time corresponding to the spin-spin interactions. The term with T_1 can be neglected in our calculations because in FM samples spin-spin interactions are dominant [129] $\vec{M}_{x,y}$ is the transverse component of the magnetization (transverse to the equilibrium orientation of magnetization). Since we will be using spherical geometry to obtain resonance spectra as a function of orientation of \vec{M} , we will replace $\vec{M}_{x,y}$ by $\vec{M}_{\theta,\phi}$ which is transverse to the radially oriented magnetization vector (θ and ϕ directions are perpendicular and therefore transverse to the radial direction). Then, (4.68) can be rewritten as

$$\frac{d\vec{M}}{dt} = -\gamma\vec{M}\times\vec{H}_{eff} + \frac{\alpha}{M}\vec{M}\times\frac{d\vec{M}}{dt} - \frac{\vec{M}_{\theta,\phi}}{T_2} \quad (4.69)$$

The magnetization in the above representation then has the form:

$$\vec{M} = M\hat{r} + \vec{M}_{\theta,\phi} = M\hat{r} + m_\theta\hat{\theta} + m_\phi\hat{\phi} \quad (4.70)$$

in which $M\hat{r}$ is the radially directed equilibrium magnetization vector and $\vec{M}_{\theta,\phi} = m_\theta\hat{\theta} + m_\phi\hat{\phi}$ is the dynamical component of the magnetization transverse to the equilibrium orientation and is negligible compared to $M\hat{r}$ term.

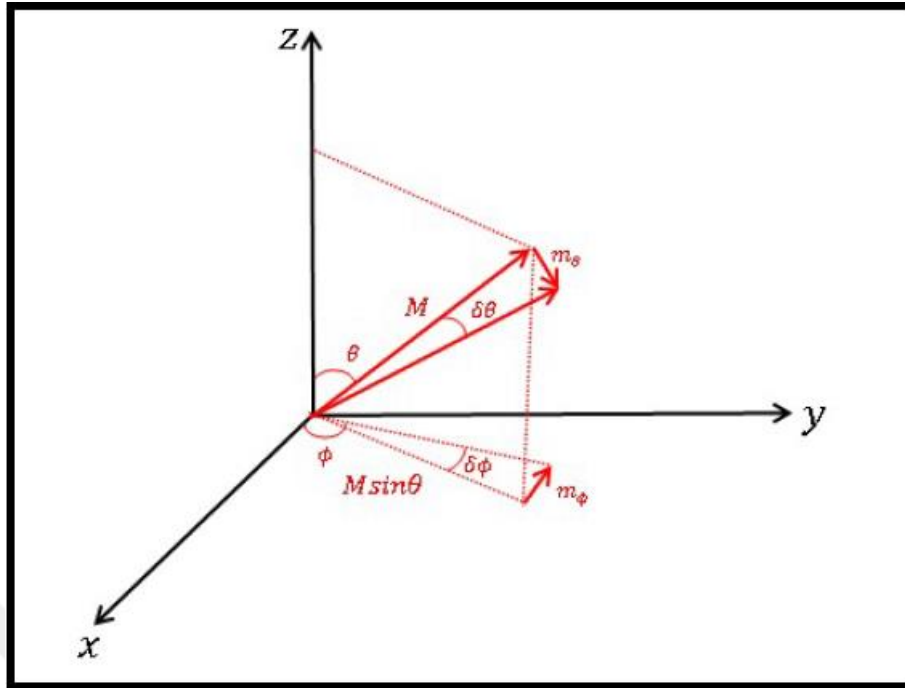


Figure 4.3. Components of the magnetization vector.

It is evident from Figure 4.3 that dynamical small deviations of magnetization from the equilibrium direction can be given by

$$m_{\theta} = M \cdot \delta\theta \quad (4.71)$$

$$m_{\phi} = M \cdot \sin\theta \cdot \delta\phi \quad (4.72)$$

4.2.2. Effective Field and Its Torque

The effective magnetic field in equation (4.69) can be given by the gradient of the volume energy density E of the system with respect to the magnetization as

$$\vec{H}_{eff} = -\vec{\nabla}_{\vec{M}} E \quad (4.73)$$

In dealing with a system composed of N ferromagnetic layers coupled by an exchange interaction and separated by nonmagnetic layers, areal energy density (energy per film area \mathcal{E}) can be used instead of volume energy density E [204]:

$$\mathcal{E} = \sum_{i=1}^N t_i E_i - \sum_{i=1}^{N-1} A_{i,i+1} \frac{\vec{M}_i \cdot \vec{M}_{i+1}}{M_i M_{i+1}} \quad (4.74)$$

where t_i is the thickness and E_i is the volume energy density of the i -th layer and $A_{i,i+1}$ is the bilinear energy density (energy per unit surface area) coupling constant responsible for interlayer exchange coupling between layers i and $i + 1$. The negative sign in front of $A_{i,i+1}$ is chosen so that a positive $A_{i,i+1}$ corresponds to parallel (ferromagnetic) coupling between neighbouring layers whereas a negative $A_{i,i+1}$ gives antiparallel (antiferromagnetic) coupling.

With the choice of an areal energy density \mathcal{E} , equation (4.73) turns into

$$\vec{H}_{eff}^i = -\frac{1}{t_i} \vec{\nabla}_{\vec{M}_i} \mathcal{E} \quad (4.75)$$

for the effective magnetic field acting within the i -th layer. Therefore, the equation of motion of magnetization of the i -th layer without damping can be given by

$$\frac{d\vec{M}_i}{dt} = -\gamma_i \vec{M}_i \times \vec{H}_{eff}^i = -\gamma_i \vec{M}_i \times \left(-\frac{1}{t_i} \vec{\nabla}_{\vec{M}_i} \mathcal{E} \right) = -\gamma_i \vec{\tau}_i \quad (4.76)$$

where $\vec{\tau}_i = \vec{M}_i \times \vec{H}_{eff}^i$ is the torque term which can be expanded as

$$\begin{aligned} \vec{\tau}_i &= \vec{M}_i \times \left(-\frac{1}{t_i} \vec{\nabla}_{\vec{M}_i} \mathcal{E} \right) \\ &= M_i \hat{r}_i \times \left[-\frac{1}{t_i} \left(\hat{r}_i \frac{\partial \mathcal{E}}{\partial M_i} + \hat{\theta}_i \frac{1}{M_i} \frac{\partial \mathcal{E}}{\partial \theta_i} + \hat{\phi}_i \frac{1}{M_i \sin \theta_i} \frac{\partial \mathcal{E}}{\partial \phi_i} \right) \right] \end{aligned} \quad (4.77)$$

which yields

$$\vec{\tau}_i = -\hat{\phi}_i \frac{1}{t_i} \frac{\partial \mathcal{E}}{\partial \theta_i} + \hat{\theta}_i \frac{1}{t_i \sin \theta_i} \frac{\partial \mathcal{E}}{\partial \phi_i} \quad (4.78)$$

In obtaining (4.78) from (4.77), use is made of the cyclic permutations of spherical unit vectors \hat{r} , $\hat{\theta}$ and $\hat{\phi}$ (i.e. $\hat{r} \times \hat{r} = 0$, $\hat{r} \times \hat{\theta} = \hat{\phi}$ and $\hat{r} \times \hat{\phi} = -\hat{\theta}$). In order to linearize the equation of motion, we expand the energy density around the equilibrium orientation of the magnetization

$$\mathcal{E} = \mathcal{E}_0 + \frac{\partial \mathcal{E}}{\partial \theta_k} \delta \theta_k + \frac{\partial \mathcal{E}}{\partial \phi_k} \delta \phi_k \quad (4.79)$$

where \mathcal{E}_0 is the energy minimum, $\delta \theta_k$ and $\delta \phi_k$ are small angular deviations of magnetization from the equilibrium direction and the partial derivatives are understood to be calculated at the equilibrium angles (so they represent merely scalar linear expansion coefficients rather than functions once the derivative of the E function is calculated at the equilibrium angles). Equation (4.78) then becomes

$$\begin{aligned} \vec{\tau}_i = & -\hat{\phi}_i \frac{1}{t_i} \frac{\partial}{\partial \theta_i} \left(\mathcal{E}_0 + \frac{\partial \mathcal{E}}{\partial \theta_k} \delta \theta_k + \frac{\partial \mathcal{E}}{\partial \phi_k} \delta \phi_k \right) \\ & + \hat{\theta}_i \frac{1}{t_i \sin \theta_i} \frac{\partial}{\partial \phi_i} \left(\mathcal{E}_0 + \frac{\partial \mathcal{E}}{\partial \theta_k} \delta \theta_k + \frac{\partial \mathcal{E}}{\partial \phi_k} \delta \phi_k \right) \end{aligned} \quad (4.80)$$

which results in

$$\vec{\tau}_i = -\hat{\phi}_i \frac{1}{t_i} (\mathcal{E}_{\theta_i \theta_k} \delta \theta_k + \mathcal{E}_{\theta_i \phi_k} \delta \phi_k) + \hat{\theta}_i \frac{1}{t_i \sin \theta_i} (\mathcal{E}_{\phi_i \theta_k} \delta \theta_k + \mathcal{E}_{\phi_i \phi_k} \delta \phi_k) \quad (4.81)$$

In expressing (4.81), use is made of

$$\frac{\partial \mathcal{E}_0}{\partial \theta_i} = \frac{\partial \mathcal{E}_0}{\partial \phi_i} = 0, \quad \frac{\partial^2 \mathcal{E}}{\partial \theta_i \partial \theta_k} = \mathcal{E}_{\theta_i \theta_k}, \quad \frac{\partial^2 \mathcal{E}}{\partial \theta_i \partial \phi_k} = \mathcal{E}_{\theta_i \phi_k}, \quad \frac{\partial^2 \mathcal{E}}{\partial \phi_i \partial \theta_k} = \mathcal{E}_{\phi_i \theta_k} \quad \text{and} \quad \frac{\partial^2 \mathcal{E}}{\partial \phi_i \partial \phi_k} = \mathcal{E}_{\phi_i \phi_k}$$

By utilizing equations (4.71) and (4.72), we now make the replacements $\delta \theta_k = m_{\theta_k} / M_k$ and $\delta \phi_k = m_{\phi_k} / M_k \sin \theta_k$, where m_{θ_k} and m_{ϕ_k} are the dynamical components of the magnetization of layer k with saturation value of M_k to get

$$\begin{aligned}\vec{\tau}_i = & -\hat{\phi}_i \frac{1}{t_i} \left(\varepsilon_{\theta_i \theta_k} \frac{m_{\theta_k}}{M_k} + \varepsilon_{\theta_i \phi_k} \frac{m_{\phi_k}}{M_k \sin \theta_k} \right) \\ & + \hat{\theta}_i \frac{1}{t_i \sin \theta_i} \left(\varepsilon_{\phi_i \theta_k} \frac{m_{\theta_k}}{M_k} + \varepsilon_{\phi_i \phi_k} \frac{m_{\phi_k}}{M_k \sin \theta_k} \right)\end{aligned}\quad (4.82)$$

If we now replace $\vec{\tau}_i$ in equation (4.76) with the right hand side of equation (4.82), we get

$$\begin{aligned}\frac{d\vec{M}_i}{dt} = & -\gamma_i \left[-\hat{\phi}_i \frac{1}{t_i} \left(\varepsilon_{\theta_i \theta_k} \frac{m_{\theta_k}}{M_k} + \varepsilon_{\theta_i \phi_k} \frac{m_{\phi_k}}{M_k \sin \theta_k} \right) \right. \\ & \left. + \hat{\theta}_i \frac{1}{t_i \sin \theta_i} \left(\varepsilon_{\phi_i \theta_k} \frac{m_{\theta_k}}{M_k} + \varepsilon_{\phi_i \phi_k} \frac{m_{\phi_k}}{M_k \sin \theta_k} \right) \right]\end{aligned}\quad (4.83)$$

The perturbation on the magnetization is due to the magnetic field component of the rf-field which creates small deviations of magnetization such that the magnetization can be expressed as (as given by (4.70))

$$\vec{M}_i = M_i \hat{r}_i + m_{\theta_i} \hat{\theta}_i + m_{\phi_i} \hat{\phi}_i \quad (4.84)$$

Using equation (4.84) and assuming that the magnitude of the magnetization is kept at its saturation value M_i (that is $dM_i/dt = 0$), equation (4.83) becomes

$$\begin{aligned}\frac{dm_{\theta_i}}{dt} \hat{\theta}_i + \frac{dm_{\phi_i}}{dt} \hat{\phi}_i \\ = & -\gamma_i \left[-\hat{\phi}_i \frac{1}{t_i} \left(\varepsilon_{\theta_i \theta_k} \frac{m_{\theta_k}}{M_k} + \varepsilon_{\theta_i \phi_k} \frac{m_{\phi_k}}{M_k \sin \theta_k} \right) \right. \\ & \left. + \hat{\theta}_i \frac{1}{t_i \sin \theta_i} \left(\varepsilon_{\phi_i \theta_k} \frac{m_{\theta_k}}{M_k} + \varepsilon_{\phi_i \phi_k} \frac{m_{\phi_k}}{M_k \sin \theta_k} \right) \right]\end{aligned}\quad (4.85)$$

By resolving $\hat{\theta}_i$ and $\hat{\phi}_i$ components of (4.85) and rearranging, we respectively get

$$\frac{1}{\gamma_i} \frac{dm_{\theta_i}}{dt} = -\frac{1}{t_i \sin \theta_i M_k} \left(\varepsilon_{\phi_i \theta_k} m_{\theta_k} + \frac{\varepsilon_{\phi_i \phi_k}}{\sin \theta_k} m_{\phi_k} \right) \quad (4.86)$$

$$\frac{1}{\gamma_i} \frac{dm_{\phi_i}}{dt} = \frac{1}{t_i M_k} \left(\mathcal{E}_{\theta_i \theta_k} m_{\theta_k} + \frac{\mathcal{E}_{\theta_i \phi_k}}{\sin \theta_k} m_{\phi_k} \right) \quad (4.87)$$

It must be realized at this stage that the left hand sides of (4.86)-(4.87) are due to layer i but right hand sides contain an additional index k . This has to do with the fact that our equations must allow for interactions between neighbouring ferromagnetic (FM) layers through interlayer exchange coupling. Therefore,

- for $i = 1$, k must run from 1 to 2
- for $2 \leq i \leq N - 1$, k must run from $i - 1$ to $i + 1$
- for $i = N$, k must run from $N - 1$ to N

where N is the number of FM layers. This means that the right hand sides of the equations (4.86) and (4.87) written for m_{θ_i} and m_{ϕ_i} are actually to be summed up over the allowed k -indices:

$$\frac{1}{\gamma_i} \frac{dm_{\theta_i}}{dt} = -\frac{1}{t_i \sin \theta_i} \sum_{k=i-1, k \neq 0}^{k=i+1, k \neq N+1} \left(\frac{\mathcal{E}_{\phi_i \theta_k}}{M_k} m_{\theta_k} + \frac{\mathcal{E}_{\phi_i \phi_k}}{M_k \sin \theta_k} m_{\phi_k} \right) \quad (4.88)$$

$$\frac{1}{\gamma_i} \frac{dm_{\phi_i}}{dt} = \frac{1}{t_i} \sum_{k=i-1, k \neq 0}^{k=i+1, k \neq N+1} \left(\frac{\mathcal{E}_{\theta_i \theta_k}}{M_k} m_{\theta_k} + \frac{\mathcal{E}_{\theta_i \phi_k}}{M_k \sin \theta_k} m_{\phi_k} \right) \quad (4.89)$$

which conform to equations (8) and (9) of reference [186] for a correspondence from the literature. Then from (4.88) and (4.89) and considering nearest neighbour interactions

- For $i = 1$ (k runs from 1 to 2)

$$\begin{aligned} \frac{1}{\gamma_1} \frac{dm_{\theta_1}}{dt} = & -\frac{1}{t_1 M_1 \sin \theta_1} \left(\varepsilon_{\phi_1 \theta_1} m_{\theta_1} + \frac{\varepsilon_{\phi_1 \phi_1}}{\sin \theta_1} m_{\phi_1} \right) \\ & - \frac{1}{t_1 M_2 \sin \theta_1} \left(\varepsilon_{\phi_1 \theta_2} m_{\theta_2} + \frac{\varepsilon_{\phi_1 \phi_2}}{\sin \theta_2} m_{\phi_2} \right) \end{aligned} \quad (4.90)$$

$$\begin{aligned} \frac{1}{\gamma_1} \frac{dm_{\phi_1}}{dt} = & \frac{1}{t_1 M_1} \left(\varepsilon_{\theta_1 \theta_1} m_{\theta_1} + \frac{\varepsilon_{\theta_1 \phi_1}}{\sin \theta_1} m_{\phi_1} \right) \\ & + \frac{1}{t_1 M_2} \left(\varepsilon_{\theta_1 \theta_2} m_{\theta_2} + \frac{\varepsilon_{\theta_1 \phi_2}}{\sin \theta_2} m_{\phi_2} \right) \end{aligned} \quad (4.91)$$

- for $2 \leq i \leq N - 1$ (k runs from $i - 1$ to $i + 1$)

$$\begin{aligned} \frac{1}{\gamma_i} \frac{dm_{\theta_i}}{dt} = & -\frac{1}{t_i M_{i-1} \sin \theta_i} \left(\varepsilon_{\phi_i \theta_{i-1}} m_{\theta_{i-1}} + \frac{\varepsilon_{\phi_i \phi_{i-1}}}{\sin \theta_{i-1}} m_{\phi_{i-1}} \right) \\ & - \frac{1}{t_i M_i \sin \theta_i} \left(\varepsilon_{\phi_i \theta_i} m_{\theta_i} + \frac{\varepsilon_{\phi_i \phi_i}}{\sin \theta_i} m_{\phi_i} \right) \\ & - \frac{1}{t_i M_{i+1} \sin \theta_i} \left(\varepsilon_{\phi_i \theta_{i+1}} m_{\theta_{i+1}} + \frac{\varepsilon_{\phi_i \phi_{i+1}}}{\sin \theta_{i+1}} m_{\phi_{i+1}} \right) \end{aligned} \quad (4.92)$$

$$\begin{aligned} \frac{1}{\gamma_i} \frac{dm_{\phi_i}}{dt} = & \frac{1}{t_i M_{i-1}} \left(\varepsilon_{\theta_i \theta_{i-1}} m_{\theta_{i-1}} + \frac{\varepsilon_{\theta_i \phi_{i-1}}}{\sin \theta_{i-1}} m_{\phi_{i-1}} \right) \\ & + \frac{1}{t_i M_i} \left(\varepsilon_{\theta_i \theta_i} m_{\theta_i} + \frac{\varepsilon_{\theta_i \phi_i}}{\sin \theta_i} m_{\phi_i} \right) \\ & + \frac{1}{t_i M_{i+1}} \left(\varepsilon_{\theta_i \theta_{i+1}} m_{\theta_{i+1}} + \frac{\varepsilon_{\theta_i \phi_{i+1}}}{\sin \theta_{i+1}} m_{\phi_{i+1}} \right) \end{aligned} \quad (4.93)$$

- and for $i = N$ (k runs from $N - 1$ to N)

$$\begin{aligned} \frac{1}{\gamma_N} \frac{dm_{\theta_N}}{dt} = & -\frac{1}{t_N M_{N-1} \sin \theta_N} \left(\varepsilon_{\phi_N \theta_{N-1}} m_{\theta_{N-1}} + \frac{\varepsilon_{\phi_N \phi_{N-1}}}{\sin \theta_{N-1}} m_{\phi_{N-1}} \right) \\ & - \frac{1}{t_N M_N \sin \theta_N} \left(\varepsilon_{\phi_N \theta_N} m_{\theta_N} + \frac{\varepsilon_{\phi_N \phi_N}}{\sin \theta_N} m_{\phi_N} \right) \end{aligned} \quad (4.94)$$

$$\begin{aligned} \frac{1}{\gamma_N} \frac{dm_{\phi_N}}{dt} = & \frac{1}{t_N M_{N-1}} \left(\mathcal{E}_{\theta_N \theta_{N-1}} m_{\theta_{N-1}} + \frac{\mathcal{E}_{\theta_N \phi_{N-1}}}{\sin \theta_{N-1}} m_{\phi_{N-1}} \right) \\ & + \frac{1}{t_N M_N} \left(\mathcal{E}_{\theta_N \theta_N} m_{\theta_N} + \frac{\mathcal{E}_{\theta_N \phi_N}}{\sin \theta_N} m_{\phi_N} \right) \end{aligned} \quad (4.95)$$

The expressions from (4.90) to (4.95) thus obtained by running equations (4.88) and (4.89) over the allowed values of k are in conformity with the set of expressions given in equation (6) of reference [204].

4.2.3. Effects of RF Field and Damping

Equations from (4.90) to (4.95) are just linearized outcomes of equation (4.68) without damping (without \vec{R} term) to the first order of m_{θ_i} and m_{ϕ_i} in terms of the gradients of the surface energy density \mathcal{E} of the system of N coupled ferromagnetic layers. We now include the damping terms and express the effect of the rf-field separately in equation (4.68) for the i -th layer.

$$\frac{d\vec{M}_i}{dt} = -\gamma_i \vec{M}_i \times \vec{H}_{eff}^i - \gamma_i \vec{M}_i \times \vec{h} + \frac{\alpha_i}{M_i} \vec{M}_i \times \frac{d\vec{M}_i}{dt} - \frac{\vec{M}_{\theta_i \phi_i}}{T_2} \quad (4.96)$$

where the second term on the right is the effect of the rf-field, the third is the Gilbert Type damping with damping parameter α and the fourth term is the Bloch-Bloembergen type damping term with the transverse magnetization $\vec{M}_{\theta_i \phi_i} = m_{\theta_i} \hat{\theta}_i + m_{\phi_i} \hat{\phi}_i$ with T_2 as the transverse relaxation time due to the spin-spin interactions. We now calculate the first order contributions of these terms.

- RF torque:

$$\vec{M}_i \times \vec{h}_i = M_i \hat{r}_i \times (h_{\theta_i} \hat{\theta}_i + h_{\phi_i} \hat{\phi}_i) = -M_i h_{\phi_i} \hat{\theta}_i + M_i h_{\theta_i} \hat{\phi}_i \quad (4.97)$$

Any magnetic component of the driving rf-field along the radial direction will have zero net contribution to the torque, due to the cross product nature of the torque term which

favours the perpendicular terms. Therefore, \vec{h}_i is explicitly given by $h_{\theta_i}\hat{\theta}_i + h_{\phi_i}\hat{\phi}_i$ because any possible radial term will disappear in the final form.

- Gilbert damping

$$\frac{\alpha_i}{M_i} \vec{M}_i \times \frac{d\vec{M}_i}{dt} = \frac{\alpha_i}{M_i} M_i \hat{r}_i \times \left(\frac{dm_{\theta_i}}{dt} \hat{\theta}_i + \frac{dm_{\phi_i}}{dt} \hat{\phi}_i \right) \quad (4.98)$$

Due to the rf excitation, time dependence of the transverse magnetization components can be assumed as

$$m_{\theta_i} = m_{\theta_i}^0 e^{-j\omega t}$$

$$m_{\phi_i} = m_{\phi_i}^0 e^{-j\omega t}$$

so that $\frac{dm_{\theta_i}}{dt} = -j\omega m_{\theta_i}^0 e^{-j\omega t} = -j\omega m_{\theta_i}$ and $\frac{dm_{\phi_i}}{dt} = -j\omega m_{\phi_i}^0 e^{-j\omega t} = -j\omega m_{\phi_i}$.

Therefore the Gilbert damping term becomes

$$\begin{aligned} \frac{\alpha_i}{M_i} \vec{M}_i \times \frac{d\vec{M}_i}{dt} &= \frac{\alpha_i}{M_i} M_i \hat{r}_i \times (-j\omega) (m_{\theta_i} \hat{\theta}_i + m_{\phi_i} \hat{\phi}_i) \\ &= j\omega \alpha_i m_{\phi_i} \hat{\theta}_i - j\omega \alpha_i m_{\theta_i} \hat{\phi}_i \end{aligned} \quad (4.99)$$

where ω is the angular frequency of the rf field and $j = \sqrt{-1}$.

- Bloch-Bloembergen type damping

$$-\frac{\vec{M}_{\theta_i \phi_i}}{T_2} = -\frac{m_{\theta_i}}{T_2} \hat{\theta}_i - \frac{m_{\phi_i}}{T_2} \hat{\phi}_i \quad (4.100)$$

Putting (4.97), (4.99) and (4.100) into (4.96) and dividing through by γ_i , one gets

$$\begin{aligned}
\frac{1}{\gamma_i} \frac{d\vec{M}_i}{dt} &= \frac{1}{\gamma_i} \frac{dm_{\theta_i}}{dt} \hat{\theta}_i + \frac{1}{\gamma_i} \frac{dm_{\phi_i}}{dt} \hat{\phi}_i \\
&= -\vec{M}_i \times \vec{H}_{eff}^i - (-M_i h_{\phi_i} \hat{\theta}_i + M_i h_{\theta_i} \hat{\phi}_i) + \frac{j\omega}{\gamma_i} \alpha_i m_{\phi_i} \hat{\theta}_i \\
&\quad - \frac{j\omega}{\gamma_i} \alpha_i m_{\theta_i} \hat{\phi}_i - \frac{m_{\theta_i}}{\gamma_i T_2} \hat{\theta}_i - \frac{m_{\phi_i}}{\gamma_i T_2} \hat{\phi}_i
\end{aligned} \tag{4.101}$$

Resolving $\hat{\theta}_i$ and $\hat{\phi}_i$ components of (4.101):

$$\frac{1}{\gamma_i} \frac{dm_{\theta_i}}{dt} = (-\vec{M}_i \times \vec{H}_{eff}^i)_{\theta_i} + M_i h_{\phi_i} + \frac{j\omega}{\gamma_i} \alpha_i m_{\phi_i} - \frac{m_{\theta_i}}{\gamma_i T_2} \tag{4.102}$$

$$\frac{1}{\gamma_i} \frac{dm_{\phi_i}}{dt} = (-\vec{M}_i \times \vec{H}_{eff}^i)_{\phi_i} - M_i h_{\theta_i} - \frac{j\omega}{\gamma_i} \alpha_i m_{\theta_i} - \frac{m_{\phi_i}}{\gamma_i T_2} \tag{4.103}$$

In equations (4.102) and (4.103) $(-\vec{M}_i \times \vec{H}_{eff}^i)_{\theta_i}$ and $(-\vec{M}_i \times \vec{H}_{eff}^i)_{\phi_i}$ stand for the $\hat{\theta}_i$ and $\hat{\phi}_i$ components of the $-\vec{M}_i \times \vec{H}_{eff}^i$ term of (4.101). These components had already been given by the right hand sides of equations (4.88) and (4.89). Plugging those components into (4.102) and (4.103) yields

$$\begin{aligned}
\frac{1}{\gamma_i} \frac{dm_{\theta_i}}{dt} &= -\frac{1}{t_i \sin \theta_i} \sum_{k=i-1, k \neq 0}^{k=i+1, k \neq N+1} \left(\frac{\mathcal{E}_{\phi_i \theta_k}}{M_k} m_{\theta_k} + \frac{\mathcal{E}_{\phi_i \phi_k}}{M_k \sin \theta_k} m_{\phi_k} \right) + M_i h_{\phi_i} \\
&\quad + \frac{j\omega}{\gamma_i} \alpha_i m_{\phi_i} - \frac{m_{\theta_i}}{\gamma_i T_2}
\end{aligned} \tag{4.104}$$

and

$$\begin{aligned}
\frac{1}{\gamma_i} \frac{dm_{\phi_i}}{dt} &= \frac{1}{t_i} \sum_{k=i-1, k \neq 0}^{k=i+1, k \neq N+1} \left(\frac{\mathcal{E}_{\theta_i \theta_k}}{M_k} m_{\theta_k} + \frac{\mathcal{E}_{\theta_i \phi_k}}{M_k \sin \theta_k} m_{\phi_k} \right) \\
&\quad - M_i h_{\theta_i} - \frac{j\omega}{\gamma_i} \alpha_i m_{\theta_i} - \frac{m_{\phi_i}}{\gamma_i T_2}
\end{aligned} \tag{4.105}$$

The expressions thus obtained give us the equation of motion of the dynamical components of magnetization including the effects of the rf-field and damping terms. Once we run the summations over the allowed k -indices in (4.104) and (4.105) and recalling that

$$\frac{dm_{\theta_i}}{dt} = -j\omega m_{\theta_i}^0 e^{-j\omega t} = -j\omega m_{\theta_i} \quad \text{and} \quad \frac{dm_{\phi_i}}{dt} = -j\omega m_{\phi_i}^0 e^{-j\omega t} = -j\omega m_{\phi_i}$$

- For $i = 1$ (k runs from 1 to 2)

$$\begin{aligned} -\frac{j\omega}{\gamma_1} m_{\theta_1} = & -\frac{1}{t_1 M_1 \sin\theta_1} \left(\varepsilon_{\phi_1 \theta_1} m_{\theta_1} + \frac{\varepsilon_{\phi_1 \phi_1}}{\sin\theta_1} m_{\phi_1} \right) \\ & -\frac{1}{t_1 M_2 \sin\theta_1} \left(\varepsilon_{\phi_1 \theta_2} m_{\theta_2} + \frac{\varepsilon_{\phi_1 \phi_2}}{\sin\theta_2} m_{\phi_2} \right) \\ & + M_1 h_{\phi_1} + \frac{j\omega}{\gamma_1} \alpha_1 m_{\phi_1} - \frac{m_{\theta_1}}{\gamma_1 T_2} \end{aligned} \quad (4.106)$$

$$\begin{aligned} -\frac{j\omega}{\gamma_1} m_{\phi_1} = & \frac{1}{t_1 M_1} \left(\varepsilon_{\theta_1 \theta_1} m_{\theta_1} + \frac{\varepsilon_{\theta_1 \phi_1}}{\sin\theta_1} m_{\phi_1} \right) \\ & + \frac{1}{t_1 M_2} \left(\varepsilon_{\theta_1 \theta_2} m_{\theta_2} + \frac{\varepsilon_{\theta_1 \phi_2}}{\sin\theta_2} m_{\phi_2} \right) \\ & - M_1 h_{\theta_1} - \frac{j\omega}{\gamma_1} \alpha_1 m_{\theta_1} - \frac{m_{\phi_1}}{\gamma_1 T_2} \end{aligned} \quad (4.107)$$

- for $2 \leq i \leq N - 1$ (k runs from $i - 1$ to $i + 1$)

$$\begin{aligned} -\frac{j\omega}{\gamma_i} m_{\theta_i} = & -\frac{1}{t_i M_{i-1} \sin\theta_i} \left(\varepsilon_{\phi_i \theta_{i-1}} m_{\theta_{i-1}} + \frac{\varepsilon_{\phi_i \phi_{i-1}}}{\sin\theta_{i-1}} m_{\phi_{i-1}} \right) \\ & -\frac{1}{t_i M_i \sin\theta_i} \left(\varepsilon_{\phi_i \theta_i} m_{\theta_i} + \frac{\varepsilon_{\phi_i \phi_i}}{\sin\theta_i} m_{\phi_i} \right) \\ & -\frac{1}{t_i M_{i+1} \sin\theta_i} \left(\varepsilon_{\phi_i \theta_{i+1}} m_{\theta_{i+1}} + \frac{\varepsilon_{\phi_i \phi_{i+1}}}{\sin\theta_{i+1}} m_{\phi_{i+1}} \right) \\ & + M_i h_{\phi_i} + \frac{j\omega}{\gamma_i} \alpha_i m_{\phi_i} - \frac{m_{\theta_i}}{\gamma_i T_2} \end{aligned} \quad (4.108)$$

$$\begin{aligned}
-\frac{j\omega}{\gamma_i} m_{\phi_i} = & \frac{1}{t_i M_{i-1}} \left(\mathcal{E}_{\theta_i \theta_{i-1}} m_{\theta_{i-1}} + \frac{\mathcal{E}_{\theta_i \phi_{i-1}}}{\sin \theta_{i-1}} m_{\phi_{i-1}} \right) \\
& + \frac{1}{t_i M_i} \left(\mathcal{E}_{\theta_i \theta_i} m_{\theta_i} + \frac{\mathcal{E}_{\theta_i \phi_i}}{\sin \theta_i} m_{\phi_i} \right) \\
& + \frac{1}{t_i M_{i+1}} \left(\mathcal{E}_{\theta_i \theta_{i+1}} m_{\theta_{i+1}} + \frac{\mathcal{E}_{\theta_i \phi_{i+1}}}{\sin \theta_{i+1}} m_{\phi_{i+1}} \right) \\
& - M_i h_{\theta_i} - \frac{j\omega}{\gamma_i} \alpha_i m_{\theta_i} - \frac{m_{\phi_i}}{\gamma_i T_2}
\end{aligned} \tag{4.109}$$

- and for $i = N$ (k runs from $N - 1$ to N)

$$\begin{aligned}
-\frac{j\omega}{\gamma_N} m_{\theta_N} = & -\frac{1}{t_N M_{N-1} \sin \theta_N} \left(\mathcal{E}_{\phi_N \theta_{N-1}} m_{\theta_{N-1}} + \frac{\mathcal{E}_{\phi_N \phi_{N-1}}}{\sin \theta_{N-1}} m_{\phi_{N-1}} \right) \\
& - \frac{1}{t_N M_N \sin \theta_N} \left(\mathcal{E}_{\phi_N \theta_N} m_{\theta_N} + \frac{\mathcal{E}_{\phi_N \phi_N}}{\sin \theta_N} m_{\phi_N} \right) \\
& + M_N h_{\phi_N} + \frac{j\omega}{\gamma_N} \alpha_N m_{\phi_N} - \frac{m_{\theta_N}}{\gamma_N T_2}
\end{aligned} \tag{4.110}$$

$$\begin{aligned}
-\frac{j\omega}{\gamma_N} m_{\phi_N} = & \frac{1}{t_N M_{N-1}} \left(\mathcal{E}_{\theta_N \theta_{N-1}} m_{\theta_{N-1}} + \frac{\mathcal{E}_{\theta_N \phi_{N-1}}}{\sin \theta_{N-1}} m_{\phi_{N-1}} \right) \\
& + \frac{1}{t_N M_N} \left(\mathcal{E}_{\theta_N \theta_N} m_{\theta_N} + \frac{\mathcal{E}_{\theta_N \phi_N}}{\sin \theta_N} m_{\phi_N} \right) \\
& - M_N h_{\theta_N} - \frac{j\omega}{\gamma_N} \alpha_N m_{\theta_N} - \frac{m_{\phi_N}}{\gamma_N T_2}
\end{aligned} \tag{4.111}$$

4.2.4. Matrix Representation of the Magnetization Dynamics

The equations from (4.106) to (4.111) represent a set of coupled equations for the dynamical components of magnetization of layers from $i = 1$ to N under the influence of the torque due to the effective magnetic field derived from the surface energy density \mathcal{E} of the system of N coupled FM layers, microwave magnetic field and damping. All these coupled equations can now be put into a more compact matrix form

$$C \cdot \vec{m} = \overline{M} \vec{h} \tag{4.112}$$

where C is a $2N \times 2N$ dimensional coefficient matrix multiplying a column matrix \vec{m} of dimensions $2N \times 1$ composed of the dynamical magnetization components such that its transpose reads as

$$\vec{m}^T = (m_{\theta_1}, m_{\phi_1}, \dots, m_{\theta_i}, m_{\phi_i}, \dots, m_{\theta_N}, m_{\phi_N}) \quad (4.113)$$

The right hand side of (4.112) is the column matrix \overline{Mh} of dimensions $2N \times 1$ with elements obtained from the multiplication of the saturation magnetization M_i of each layer by the projection of external microwave field on polar unit vectors of each FM layer such that its transpose is given by

$$\overline{Mh}^T = (M_1 h_{\theta_1}, M_1 h_{\phi_1}, \dots, M_i h_{\theta_i}, M_i h_{\phi_i}, \dots, M_N h_{\theta_N}, M_N h_{\phi_N}) \quad (4.114)$$

In order to obtain the form given by equation (4.112), we reorganize equations (4.106) to (4.111) as follows:

From (4.107):

$$\begin{aligned} & \left(\frac{\mathcal{E}_{\theta_1 \theta_1}}{t_1 M_1} - \frac{j\omega}{\gamma_1} \alpha_1 \right) \cdot m_{\theta_1} + \left(\frac{\mathcal{E}_{\theta_1 \phi_1}}{t_1 M_1 \sin \theta_1} + \frac{j\omega}{\gamma_1} - \frac{1}{\gamma_1 T_2} \right) \cdot m_{\phi_1} \\ & + \left(\frac{\mathcal{E}_{\theta_1 \theta_2}}{t_1 M_2} \right) \cdot m_{\theta_2} + \left(\frac{\mathcal{E}_{\theta_1 \phi_2}}{t_1 M_2 \sin \theta_2} \right) \cdot m_{\phi_2} = M_1 h_{\theta_1} \end{aligned} \quad (4.115)$$

From (4.106):

$$\begin{aligned} & \left(\frac{\mathcal{E}_{\phi_1 \theta_1}}{t_1 M_1 \sin \theta_1} + \frac{1}{\gamma_1 T_2} - \frac{j\omega}{\gamma_1} \right) \cdot m_{\theta_1} + \left(\frac{\mathcal{E}_{\phi_1 \phi_1}}{t_1 M_1 \sin^2 \theta_1} - \frac{j\omega}{\gamma_1} \alpha_1 \right) \cdot m_{\phi_1} \\ & + \left(\frac{\mathcal{E}_{\phi_1 \theta_2}}{t_1 M_2 \sin \theta_1} \right) \cdot m_{\theta_2} + \left(\frac{\mathcal{E}_{\phi_1 \phi_2}}{t_1 M_2 \sin \theta_1 \sin \theta_2} \right) \cdot m_{\phi_2} \\ & = M_1 h_{\phi_1} \end{aligned} \quad (4.116)$$

From (4.109):

$$\begin{aligned}
& \left(\frac{\mathcal{E}_{\theta_i \theta_{i-1}}}{t_i M_{i-1}} \right) \cdot m_{\theta_{i-1}} + \left(\frac{\mathcal{E}_{\theta_i \phi_{i-1}}}{t_i M_{i-1} \sin \theta_{i-1}} \right) \cdot m_{\phi_{i-1}} \\
& + \left(\frac{\mathcal{E}_{\theta_i \theta_i} - \frac{j\omega}{\gamma_i} \alpha_i}{t_i M_i} \right) \cdot m_{\theta_i} + \left(\frac{\mathcal{E}_{\theta_i \phi_i}}{t_i M_i \sin \theta_i} + \frac{j\omega}{\gamma_i} - \frac{1}{\gamma_i T_2} \right) \cdot m_{\phi_i} \\
& + \left(\frac{\mathcal{E}_{\theta_i \theta_{i+1}}}{t_i M_{i+1}} \right) \cdot m_{\theta_{i+1}} + \left(\frac{\mathcal{E}_{\theta_i \phi_{i+1}}}{t_i M_{i+1} \sin \theta_{i+1}} \right) \cdot m_{\phi_{i+1}} \\
& = M_i h_{\theta_i}
\end{aligned} \tag{4.117}$$

From (4.108):

$$\begin{aligned}
& \left(\frac{\mathcal{E}_{\phi_i \theta_{i-1}}}{t_i M_{i-1} \sin \theta_i} \right) \cdot m_{\theta_{i-1}} + \left(\frac{\mathcal{E}_{\phi_i \phi_{i-1}}}{t_i M_{i-1} \sin \theta_i \sin \theta_{i-1}} \right) \cdot m_{\phi_{i-1}} \\
& + \left(\frac{\mathcal{E}_{\phi_i \theta_i} - \frac{j\omega}{\gamma_i} + \frac{1}{\gamma_i T_2}}{t_i M_i \sin \theta_i} \right) \cdot m_{\theta_i} + \left(\frac{\mathcal{E}_{\phi_i \phi_i}}{t_i M_i \sin^2 \theta_i} - \frac{j\omega}{\gamma_i} \alpha_i \right) \cdot m_{\phi_i} \\
& + \left(\frac{\mathcal{E}_{\phi_i \theta_{i+1}}}{t_i M_{i+1} \sin \theta_i} \right) \cdot m_{\theta_{i+1}} + \left(\frac{\mathcal{E}_{\phi_i \phi_{i+1}}}{t_i M_{i+1} \sin \theta_i \sin \theta_{i+1}} \right) \cdot m_{\phi_{i+1}} \\
& = M_i h_{\phi_i}
\end{aligned} \tag{4.118}$$

From (4.111):

$$\begin{aligned}
& \left(\frac{\mathcal{E}_{\theta_N \theta_{N-1}}}{t_N M_{N-1}} \right) \cdot m_{\theta_{N-1}} + \left(\frac{\mathcal{E}_{\theta_N \phi_{N-1}}}{t_N M_{N-1} \sin \theta_{N-1}} \right) \cdot m_{\phi_{N-1}} \\
& + \left(\frac{\mathcal{E}_{\theta_N \theta_N} - \frac{j\omega}{\gamma_N} \alpha_N}{t_N M_N} \right) \cdot m_{\theta_N} + \left(\frac{\mathcal{E}_{\theta_N \phi_N}}{t_N M_N \sin \theta_N} + \frac{j\omega}{\gamma_N} - \frac{1}{\gamma_N T_2} \right) \cdot m_{\phi_N} \\
& = M_N h_{\theta_N}
\end{aligned} \tag{4.119}$$

From (4.110):

$$\begin{aligned}
& \left(\frac{\mathcal{E}_{\phi_N \theta_{N-1}}}{t_N M_{N-1} \sin \theta_N} \right) \cdot m_{\theta_{N-1}} + \left(\frac{\mathcal{E}_{\phi_N \phi_{N-1}}}{t_N M_{N-1} \sin \theta_N \sin \theta_{N-1}} \right) \cdot m_{\phi_{N-1}} \\
& + \left(\frac{\mathcal{E}_{\phi_N \theta_N} - \frac{j\omega}{\gamma_N} + \frac{1}{\gamma_N T_2}}{t_N M_N \sin \theta_N} \right) \cdot m_{\theta_N} + \left(\frac{\mathcal{E}_{\phi_N \phi_N}}{t_N M_N \sin^2 \theta_N} - \frac{j\omega}{\gamma_N} \alpha_N \right) \cdot m_{\phi_N} \\
& = M_N h_{\phi_N}
\end{aligned} \tag{4.120}$$

Thus, the products $M_i h_{\theta_i}$ and $M_i h_{\phi_i}$ (elements of \overrightarrow{Mh} matrix given in equations (4.112) and (4.114)) are obtained

- for $i = 1$ by Equations (4.115) and (4.116)
- for $2 \leq i \leq N - 1$ by Equations (4.117) and (4.118)
- and for $i = N$ by Equations (4.119) and (4.120)

as a linear combination of $m_{\theta_1}, m_{\phi_1}, \dots, m_{\theta_i}, m_{\phi_i}, \dots, m_{\theta_N}, m_{\phi_N}$ which are the elements of \vec{m} matrix given in equations (4.112) and (4.113). Not all the elements of \vec{m} contribute to $M_i h_{\theta_i}$ and $M_i h_{\phi_i}$ for a given FM layer number i and this is due to the fact that the coefficients multiplying some m_{θ_k} and m_{ϕ_k} are zero (physically it is the result of the fact that $M_i h_{\theta_i}$ and $M_i h_{\phi_i}$ for a given i are dependent upon m_{θ_i} , m_{ϕ_i} and upon interactions with the nearest neighbours with index numbers " $i - 1$ " and " $i + 1$ ".

It is now instructive to create the matrix form of the dynamics of a multilayer system composed of $N = 3$ FM layers separated by nonmagnetic layers and interacting through interlayer exchange coupling to deduce the general matrix representation of a system composed of any number N of FM layers. For $N = 3$ one will calculate $M_1 h_{\theta_1}$, $M_1 h_{\phi_1}$, $M_2 h_{\theta_2}$, $M_2 h_{\phi_2}$, $M_3 h_{\theta_3}$ and $M_3 h_{\phi_3}$, therefore we will need 6 equations for $N = 3$ (that is why it is necessary to use a matrix form with dimensions $2N \times 2N$ for C and with dimensions $2N \times 1$ for \vec{m} and \overrightarrow{Mh} for a system of N coupled FM layers).

$M_1 h_{\theta_1}$ and $M_1 h_{\phi_1}$ are already obtained in (4.115) and (4.116) respectively. To get $M_2 h_{\theta_2}$ and $M_2 h_{\phi_2}$ we put $i = 2$ into equations (4.117) and (4.118):

From (4.117) with $i = 2$

$$\begin{aligned}
& \left(\frac{\mathcal{E}_{\theta_2\theta_1}}{t_2 M_1} \right) \cdot m_{\theta_1} + \left(\frac{\mathcal{E}_{\theta_2\phi_1}}{t_2 M_1 \sin\theta_1} \right) \cdot m_{\phi_1} \\
& + \left(\frac{\mathcal{E}_{\theta_2\theta_2}}{t_2 M_2} - \frac{j\omega}{\gamma_2} \alpha_2 \right) \cdot m_{\theta_2} + \left(\frac{\mathcal{E}_{\theta_2\phi_2}}{t_2 M_2 \sin\theta_2} + \frac{j\omega}{\gamma_2} - \frac{1}{\gamma_2 T_2} \right) \cdot m_{\phi_2} \\
& + \left(\frac{\mathcal{E}_{\theta_2\theta_3}}{t_2 M_3} \right) \cdot m_{\theta_3} + \left(\frac{\mathcal{E}_{\theta_2\phi_3}}{t_2 M_3 \sin\theta_3} \right) \cdot m_{\phi_3} \\
& = M_2 h_{\theta_2}
\end{aligned} \tag{4.121}$$

and from (4.118) with $i = 2$

$$\begin{aligned}
& \left(\frac{\mathcal{E}_{\phi_2\theta_1}}{t_2 M_1 \sin\theta_2} \right) \cdot m_{\theta_1} + \left(\frac{\mathcal{E}_{\phi_2\phi_1}}{t_2 M_1 \sin\theta_2 \sin\theta_1} \right) \cdot m_{\phi_1} \\
& + \left(\frac{\mathcal{E}_{\phi_2\theta_2}}{t_2 M_2 \sin\theta_2} - \frac{j\omega}{\gamma_2} + \frac{1}{\gamma_2 T_2} \right) \cdot m_{\theta_2} + \left(\frac{\mathcal{E}_{\phi_2\phi_2}}{t_2 M_2 \sin^2\theta_2} - \frac{j\omega}{\gamma_2} \alpha_2 \right) \cdot m_{\phi_2} \\
& + \left(\frac{\mathcal{E}_{\phi_2\theta_3}}{t_2 M_3 \sin\theta_2} \right) \cdot m_{\theta_3} + \left(\frac{\mathcal{E}_{\phi_2\phi_3}}{t_2 M_3 \sin\theta_2 \sin\theta_3} \right) \cdot m_{\phi_3} \\
& = M_2 h_{\phi_2}
\end{aligned} \tag{4.122}$$

To get $M_3 h_{\theta_3}$ and $M_3 h_{\phi_3}$, we put $N = 3$ into (4.119) and (4.120). From (4.119)

$$\begin{aligned}
& \left(\frac{\mathcal{E}_{\theta_3\theta_2}}{t_3 M_2} \right) \cdot m_{\theta_2} + \left(\frac{\mathcal{E}_{\theta_3\phi_2}}{t_3 M_2 \sin\theta_2} \right) \cdot m_{\phi_2} \\
& + \left(\frac{\mathcal{E}_{\theta_3\theta_3}}{t_3 M_3} - \frac{j\omega}{\gamma_3} \alpha_3 \right) \cdot m_{\theta_3} + \left(\frac{\mathcal{E}_{\theta_3\phi_3}}{t_3 M_3 \sin\theta_3} + \frac{j\omega}{\gamma_3} - \frac{1}{\gamma_3 T_2} \right) \cdot m_{\phi_3} \\
& = M_3 h_{\theta_3}
\end{aligned} \tag{4.123}$$

and from (4.120)

$$\begin{aligned}
& \left(\frac{\mathcal{E}_{\phi_3\theta_2}}{t_3 M_2 \sin\theta_3} \right) \cdot m_{\theta_2} + \left(\frac{\mathcal{E}_{\phi_3\phi_2}}{t_3 M_2 \sin\theta_3 \sin\theta_2} \right) \cdot m_{\phi_2} \\
& + \left(\frac{\mathcal{E}_{\phi_3\theta_3}}{t_3 M_3 \sin\theta_3} - \frac{j\omega}{\gamma_3} + \frac{1}{\gamma_3 T_2} \right) \cdot m_{\theta_3} + \left(\frac{\mathcal{E}_{\phi_3\phi_3}}{t_3 M_3 \sin^2\theta_3} - \frac{j\omega}{\gamma_3} \alpha_3 \right) \cdot m_{\phi_3} \\
& = M_3 h_{\phi_3}
\end{aligned} \tag{4.124}$$

Now, the dynamics of a multilayer system composed of $N = 3$ FM layers is represented by

$$\begin{pmatrix} c_{11} & c_{12} & c_{13} & c_{14} & c_{15} & c_{16} \\ c_{21} & c_{22} & c_{23} & c_{24} & c_{25} & c_{26} \\ c_{31} & c_{32} & c_{33} & c_{34} & c_{35} & c_{36} \\ c_{41} & c_{42} & c_{43} & c_{44} & c_{45} & c_{46} \\ c_{51} & c_{52} & c_{53} & c_{54} & c_{55} & c_{56} \\ c_{61} & c_{62} & c_{63} & c_{64} & c_{65} & c_{66} \end{pmatrix} \times \begin{pmatrix} m_{\theta_1} \\ m_{\phi_1} \\ m_{\theta_2} \\ m_{\phi_2} \\ m_{\theta_3} \\ m_{\phi_3} \end{pmatrix} = \begin{pmatrix} M_1 h_{\theta_1} \\ M_1 h_{\phi_1} \\ M_2 h_{\theta_2} \\ M_2 h_{\phi_2} \\ M_3 h_{\theta_3} \\ M_3 h_{\phi_3} \end{pmatrix} \quad (4.125)$$

which is the form promised in equation (4.112), that is $C \cdot \vec{m} = \vec{Mh}$. We see from (4.125) that

$$c_{11}m_{\theta_1} + c_{12}m_{\phi_1} + c_{13}m_{\theta_2} + c_{14}m_{\phi_2} + c_{15}m_{\theta_3} + c_{16}m_{\phi_3} = M_1 h_{\theta_1} \quad (4.126)$$

$$c_{21}m_{\theta_1} + c_{22}m_{\phi_1} + c_{23}m_{\theta_2} + c_{24}m_{\phi_2} + c_{25}m_{\theta_3} + c_{26}m_{\phi_3} = M_1 h_{\phi_1} \quad (4.127)$$

$$c_{31}m_{\theta_1} + c_{32}m_{\phi_1} + c_{33}m_{\theta_2} + c_{34}m_{\phi_2} + c_{35}m_{\theta_3} + c_{36}m_{\phi_3} = M_2 h_{\theta_2} \quad (4.128)$$

$$c_{41}m_{\theta_1} + c_{42}m_{\phi_1} + c_{43}m_{\theta_2} + c_{44}m_{\phi_2} + c_{45}m_{\theta_3} + c_{46}m_{\phi_3} = M_2 h_{\phi_2} \quad (4.129)$$

$$c_{51}m_{\theta_1} + c_{52}m_{\phi_1} + c_{53}m_{\theta_2} + c_{54}m_{\phi_2} + c_{55}m_{\theta_3} + c_{56}m_{\phi_3} = M_3 h_{\theta_3} \quad (4.130)$$

$$c_{61}m_{\theta_1} + c_{62}m_{\phi_1} + c_{63}m_{\theta_2} + c_{64}m_{\phi_2} + c_{65}m_{\theta_3} + c_{66}m_{\phi_3} = M_3 h_{\phi_3} \quad (4.131)$$

Comparison of (4.126) with (4.115) which was given by

$$\begin{aligned} & \left(\frac{\mathcal{E}_{\theta_1\theta_1}}{t_1 M_1} - \frac{j\omega}{\gamma_1} \alpha_1 \right) \cdot m_{\theta_1} + \left(\frac{\mathcal{E}_{\theta_1\phi_1}}{t_1 M_1 \sin\theta_1} + \frac{j\omega}{\gamma_1} - \frac{1}{\gamma_1 T_2} \right) \cdot m_{\phi_1} \\ & \quad + \left(\frac{\mathcal{E}_{\theta_1\theta_2}}{t_1 M_2} \right) \cdot m_{\theta_2} + \left(\frac{\mathcal{E}_{\theta_1\phi_2}}{t_1 M_2 \sin\theta_2} \right) \cdot m_{\phi_2} \\ & \quad = M_1 h_{\theta_1} \end{aligned}$$

reveals that

$$\begin{aligned}
c_{11} &= \frac{\mathcal{E}_{\theta_1\theta_1}}{t_1 M_1} - \frac{j\omega}{\gamma_1} \alpha_1 \\
c_{12} &= \frac{\mathcal{E}_{\theta_1\phi_1}}{t_1 M_1 \sin\theta_1} + \frac{j\omega}{\gamma_1} - \frac{1}{\gamma_1 T_2} \\
c_{13} &= \frac{\mathcal{E}_{\theta_1\theta_2}}{t_1 M_2} \\
c_{14} &= \frac{\mathcal{E}_{\theta_1\phi_2}}{t_1 M_2 \sin\theta_2} \\
c_{15} &= c_{16} = 0
\end{aligned} \tag{4.132}$$

If the same judgement is applied to the remaining rows of (4.125) expressed in equations (4.127) to (4.131) and they are respectively compared with equations (4.116) and (4.121) to (4.124), all the other matrix elements the coefficient matrix C can be obtained as follows

Comparison of (4.127) with (4.116) yields

$$\begin{aligned}
c_{21} &= \frac{\mathcal{E}_{\phi_1\theta_1}}{t_1 M_1 \sin\theta_1} + \frac{1}{\gamma_1 T_2} - \frac{j\omega}{\gamma_1} \\
c_{22} &= \frac{\mathcal{E}_{\phi_1\phi_1}}{t_1 M_1 \sin^2\theta_1} - \frac{j\omega}{\gamma_1} \alpha_1 ; c_{23} = \frac{\mathcal{E}_{\phi_1\theta_2}}{t_1 M_2 \sin\theta_1} \\
c_{24} &= \frac{\mathcal{E}_{\phi_1\phi_2}}{t_1 M_2 \sin\theta_1 \sin\theta_2} ; c_{25} = c_{26} = 0
\end{aligned} \tag{4.133}$$

From (4.128) and (4.121)

$$\begin{aligned}
c_{31} &= \frac{\mathcal{E}_{\theta_2\theta_1}}{t_2 M_1} ; c_{32} = \frac{\mathcal{E}_{\theta_2\phi_1}}{t_2 M_1 \sin\theta_1} ; c_{33} = \frac{\mathcal{E}_{\theta_2\theta_2}}{t_2 M_2} - \frac{j\omega}{\gamma_2} \alpha_2 \\
c_{34} &= \frac{\mathcal{E}_{\theta_2\phi_2}}{t_2 M_2 \sin\theta_2} + \frac{j\omega}{\gamma_2} - \frac{1}{\gamma_2 T_2} \\
c_{35} &= \frac{\mathcal{E}_{\theta_2\theta_3}}{t_2 M_3} ; c_{36} = \frac{\mathcal{E}_{\theta_2\phi_3}}{t_2 M_3 \sin\theta_3}
\end{aligned} \tag{4.134}$$

From (4.129) and (4.122)

$$\begin{aligned}
c_{41} &= \frac{\mathcal{E}_{\phi_2\theta_1}}{t_2 M_1 \sin\theta_2} ; c_{42} = \frac{\mathcal{E}_{\phi_2\phi_1}}{t_2 M_1 \sin\theta_2 \sin\theta_1} \\
c_{43} &= \frac{\mathcal{E}_{\phi_2\theta_2}}{t_2 M_2 \sin\theta_2} - \frac{j\omega}{\gamma_2} + \frac{1}{\gamma_2 T_2} ; c_{44} = \frac{\mathcal{E}_{\phi_2\phi_2}}{t_2 M_2 \sin^2\theta_2} - \frac{j\omega}{\gamma_2} \alpha_2 \\
c_{45} &= \frac{\mathcal{E}_{\phi_2\theta_3}}{t_2 M_3 \sin\theta_2} ; c_{46} = \frac{\mathcal{E}_{\phi_2\phi_3}}{t_2 M_3 \sin\theta_2 \sin\theta_3}
\end{aligned} \tag{4.135}$$

From (4.130) and (4.123)

$$\begin{aligned}
c_{51} &= c_{52} = 0 ; c_{53} = \frac{\mathcal{E}_{\theta_3\theta_2}}{t_3 M_2} \\
c_{54} &= \frac{\mathcal{E}_{\theta_3\phi_2}}{t_3 M_2 \sin\theta_2} ; c_{55} = \frac{\mathcal{E}_{\theta_3\theta_3}}{t_3 M_3} - \frac{j\omega}{\gamma_3} \alpha_3 \\
c_{56} &= \frac{\mathcal{E}_{\theta_3\phi_3}}{t_3 M_3 \sin\theta_3} + \frac{j\omega}{\gamma_3} - \frac{1}{\gamma_3 T_2}
\end{aligned} \tag{4.136}$$

From (4.131) and (4.124)

$$\begin{aligned}
c_{61} &= c_{62} = 0 ; c_{63} = \frac{\mathcal{E}_{\phi_3\theta_2}}{t_3 M_2 \sin\theta_3} \\
c_{64} &= \frac{\mathcal{E}_{\phi_3\phi_2}}{t_3 M_2 \sin\theta_3 \sin\theta_2} ; c_{65} = \frac{\mathcal{E}_{\phi_3\theta_3}}{t_3 M_3 \sin\theta_3} - \frac{j\omega}{\gamma_3} + \frac{1}{\gamma_3 T_2} \\
c_{66} &= \frac{\mathcal{E}_{\phi_3\phi_3}}{t_3 M_3 \sin^2\theta_3} - \frac{j\omega}{\gamma_3} \alpha_3
\end{aligned} \tag{4.137}$$

Expressions (4.132) to (4.137) give us the components of the C -matrix first introduced in equation (4.112) and exemplified in (4.125) for a system of $N = 3$ FM layers. Therefore, the system of $N = 3$ FM layers interacting via interlayer exchange coupling will be represented by the matrix (4.125) which now has the form given below with only its nonzero components.

$$\begin{pmatrix} c_{11} & c_{12} & c_{13} & c_{14} & 0 & 0 \\ c_{21} & c_{22} & c_{23} & c_{24} & 0 & 0 \\ c_{31} & c_{32} & c_{33} & c_{34} & c_{35} & c_{36} \\ c_{41} & c_{42} & c_{43} & c_{44} & c_{45} & c_{46} \\ 0 & 0 & c_{53} & c_{54} & c_{55} & c_{56} \\ 0 & 0 & c_{63} & c_{64} & c_{65} & c_{66} \end{pmatrix} \times \begin{pmatrix} m_{\theta_1} \\ m_{\phi_1} \\ m_{\theta_2} \\ m_{\phi_2} \\ m_{\theta_3} \\ m_{\phi_3} \end{pmatrix} = \begin{pmatrix} M_1 h_{\theta_1} \\ M_1 h_{\phi_1} \\ M_2 h_{\theta_2} \\ M_2 h_{\phi_2} \\ M_3 h_{\theta_3} \\ M_3 h_{\phi_3} \end{pmatrix} \quad (4.138)$$

If one were to compute the matrix representation of a multilayer system composed of, let's say, $N = 5$ FM layers separated by nonmagnetic layers and interacting through interlayer exchange coupling, the coefficient matrix would be as follows

$$\begin{pmatrix} c_{11} & c_{12} & c_{13} & c_{14} & 0 & 0 & 0 & 0 & 0 & 0 \\ c_{21} & c_{22} & c_{23} & c_{24} & 0 & 0 & 0 & 0 & 0 & 0 \\ c_{31} & c_{32} & c_{33} & c_{34} & c_{35} & c_{36} & 0 & 0 & 0 & 0 \\ c_{41} & c_{42} & c_{43} & c_{44} & c_{45} & c_{46} & 0 & 0 & 0 & 0 \\ 0 & 0 & c_{53} & c_{54} & c_{55} & c_{56} & c_{57} & c_{58} & 0 & 0 \\ 0 & 0 & c_{63} & c_{64} & c_{65} & c_{66} & c_{67} & c_{68} & 0 & 0 \\ 0 & 0 & 0 & 0 & c_{75} & c_{76} & c_{77} & c_{78} & c_{79} & c_{7,10} \\ 0 & 0 & 0 & 0 & c_{85} & c_{86} & c_{87} & c_{88} & c_{89} & c_{8,10} \\ 0 & 0 & 0 & 0 & 0 & 0 & c_{97} & c_{98} & c_{99} & c_{9,10} \\ 0 & 0 & 0 & 0 & 0 & 0 & c_{10,7} & c_{10,8} & c_{10,9} & c_{10,10} \end{pmatrix} \times \begin{pmatrix} m_{\theta_1} \\ m_{\phi_1} \\ m_{\theta_2} \\ m_{\phi_2} \\ m_{\theta_3} \\ m_{\phi_3} \\ m_{\theta_4} \\ m_{\phi_4} \\ m_{\theta_5} \\ m_{\phi_5} \end{pmatrix} = \begin{pmatrix} M_1 h_{\theta_1} \\ M_1 h_{\phi_1} \\ M_2 h_{\theta_2} \\ M_2 h_{\phi_2} \\ M_3 h_{\theta_3} \\ M_3 h_{\phi_3} \\ M_4 h_{\theta_4} \\ M_4 h_{\phi_4} \\ M_5 h_{\theta_5} \\ M_5 h_{\phi_5} \end{pmatrix} \quad (4.139)$$

We see from (4.139) that the first two rows of the C -matrix are responsible for connecting $M_1 h_{\theta_1}$ and $M_1 h_{\phi_1}$ to $m_{\theta_1}, m_{\phi_1}, m_{\theta_2}, m_{\phi_2}$. For the first two rows, therefore, only the first four components are non-zero because $M_1 h_{\theta_1}$ and $M_1 h_{\phi_1}$ are only coupled to dynamical magnetizations m_{θ_k}, m_{ϕ_k} with $k \leq 2$ explicitly, i.e. $m_{\theta_1}, m_{\phi_1}, m_{\theta_2}, m_{\phi_2}$. The same holds true for $M_5 h_{\theta_5}$ and $M_5 h_{\phi_5}$ that they are only coupled to those m_{θ_k}, m_{ϕ_k} with $k \geq N - 1$, i.e. $m_{\theta_4}, m_{\phi_4}, m_{\theta_5}, m_{\phi_5}$. Therefore, only the last four components of the last two rows are nonzero. For the $M_i h_{\theta_i}$ and $M_i h_{\phi_i}$ of the intermediate layers with $2 \leq i \leq N - 1$, they are coupled to those m_{θ_k}, m_{ϕ_k} with $i - 1 \leq k \leq i + 1$. For example, for $i = 2$ we have $M_2 h_{\theta_2}$ and $M_2 h_{\phi_2}$ coupled to m_{θ_k}, m_{ϕ_k} with $k = 1, 2$ and 3 , i.e. to $m_{\theta_1}, m_{\phi_1}, m_{\theta_2}, m_{\phi_2}, m_{\theta_3}, m_{\phi_3}$. Therefore, there are only six nonzero components in a given row of the C -matrix except the first two and the last two rows where there are only four. Starting with the third row, we have the initial six components in the row being non-zero which is also true for the fourth row. Then, this block of six nonzero components shift to the right by two columns for every two rows.

4.2.5. General Rules for Calculating the Nonzero Elements of the Matrix Representation

The aim of our analysis so far was to obtain the general form of the matrix representation of the magnetization dynamics of a multilayer system composed of FM layers interacting through interlayer exchange coupling mediated by spacer layers. Since this general outlook is obtained that shed light on where the nonzero components are located, we now turn our attention to finding out the general rules for calculating these non-zero components of the C -matrix for a multilayer system for any given number N of FM layers.

If examined carefully, it is seen from equations from (4.132) to (4.137) written for the elements of the C -matrix (which were only for a multilayer with $N = 3$ FM layers but which can be generalized as we are set out to do), one realizes that the mathematical expressions of the components can be grouped to only 12 number of distinct forms. Below are those distinct forms forming recursive relationships that can be utilized to calculate the matrix components of the C -matrix by examining what we found earlier:

$c_{11} = \frac{\mathcal{E}_{\theta_1\theta_1}}{t_1 M_1} - \frac{j\omega}{\gamma_1} \alpha_1$	$\Rightarrow c_{2i-1, 2i-1}$	(4.140)
$c_{33} = \frac{\mathcal{E}_{\theta_2\theta_2}}{t_2 M_2} - \frac{j\omega}{\gamma_2} \alpha_2$	$= \frac{\mathcal{E}_{\theta_i\theta_i}}{t_i M_i} - \frac{j\omega}{\gamma_i} \alpha_i$	
$c_{55} = \frac{\mathcal{E}_{\theta_3\theta_3}}{t_3 M_3} - \frac{j\omega}{\gamma_3} \alpha_3$	$1 \leq i \leq N, \text{ for any } N$ $j = \sqrt{-1}$	

$c_{12} = \frac{\mathcal{E}_{\theta_1\phi_1}}{t_1 M_1 \sin\theta_1} + \frac{j\omega}{\gamma_1} - \frac{1}{\gamma_1 T_2}$	$\Rightarrow c_{2i-1,2i}$
$c_{34} = \frac{\mathcal{E}_{\theta_2\phi_2}}{t_2 M_2 \sin\theta_2} + \frac{j\omega}{\gamma_2} - \frac{1}{\gamma_2 T_2}$	$= \frac{\mathcal{E}_{\theta_i\phi_i}}{t_i M_i \sin\theta_i} + \frac{j\omega}{\gamma_i} - \frac{1}{\gamma_i T_2}$
$c_{56} = \frac{\mathcal{E}_{\theta_3\phi_3}}{t_3 M_3 \sin\theta_3} + \frac{j\omega}{\gamma_3} - \frac{1}{\gamma_3 T_2}$	$j = \sqrt{-1}$

(4.141)

$1 \leq i \leq N$, for any N

$c_{21} = \frac{\mathcal{E}_{\phi_1\theta_1}}{t_1 M_1 \sin\theta_1} + \frac{1}{\gamma_1 T_2} - \frac{j\omega}{\gamma_1}$	$\Rightarrow c_{2i,2i-1}$
$c_{43} = \frac{\mathcal{E}_{\phi_2\theta_2}}{t_2 M_2 \sin\theta_2} + \frac{1}{\gamma_2 T_2} - \frac{j\omega}{\gamma_2}$	$= \frac{\mathcal{E}_{\phi_i\theta_i}}{t_i M_i \sin\theta_i} + \frac{1}{\gamma_i T_2} - \frac{j\omega}{\gamma_i}$
$c_{65} = \frac{\mathcal{E}_{\phi_3\theta_3}}{t_3 M_3 \sin\theta_3} + \frac{1}{\gamma_3 T_2} - \frac{j\omega}{\gamma_3}$	$j = \sqrt{-1}$

(4.142)

$1 \leq i \leq N$, for any N

$c_{22} = \frac{\mathcal{E}_{\phi_1\phi_1}}{t_1 M_1 \sin^2 \theta_1} - \frac{j\omega}{\gamma_1} \alpha_1$	$\Rightarrow c_{2i,2i}$
$c_{44} = \frac{\mathcal{E}_{\phi_2\phi_2}}{t_2 M_2 \sin^2 \theta_2} - \frac{j\omega}{\gamma_2} \alpha_2$	$= \frac{\mathcal{E}_{\phi_i\phi_i}}{t_i M_i \sin^2 \theta_i} - \frac{j\omega}{\gamma_i} \alpha_i$
$c_{66} = \frac{\mathcal{E}_{\phi_3\phi_3}}{t_3 M_3 \sin^2 \theta_3} - \frac{j\omega}{\gamma_3} \alpha_3$	$j = \sqrt{-1}$

(4.143)

$1 \leq i \leq N$, for any N

$c_{13} = \frac{\mathcal{E}_{\theta_1\theta_2}}{t_1 M_2}$	$\Rightarrow c_{2i-1,2i+1}$
$c_{35} = \frac{\mathcal{E}_{\theta_2\theta_3}}{t_2 M_3}$	$= \frac{\mathcal{E}_{\theta_i\theta_{i+1}}}{t_i M_{i+1}}$
$\dots c_{57} = \frac{\mathcal{E}_{\theta_3\theta_4}}{t_3 M_4}$	$j = \sqrt{-1}$

(4.144)

$1 \leq i \leq N - 1$, $N \geq 2$

$c_{31} = \frac{\mathcal{E}_{\theta_2\theta_1}}{t_2 M_1}$	$\Rightarrow c_{2i+1,2i-1}$	(4.145)
$c_{53} = \frac{\mathcal{E}_{\theta_3\theta_2}}{t_3 M_2}$	$= \frac{\mathcal{E}_{\theta_{i+1}\theta_i}}{t_{i+1} M_i}$	
$\dots c_{75} = \frac{\mathcal{E}_{\theta_4\theta_3}}{t_4 M_3}$	$1 \leq i \leq N - 1, N \geq 2$	
	$j = \sqrt{-1}$	

$c_{14} = \frac{\mathcal{E}_{\theta_1\phi_2}}{t_1 M_2 \sin\theta_2}$	$\Rightarrow c_{2i-1,2i+2}$	(4.146)
$c_{36} = \frac{\mathcal{E}_{\theta_2\phi_3}}{t_2 M_3 \sin\theta_3}$	$= \frac{\mathcal{E}_{\theta_i\phi_{i+1}}}{t_i M_{i+1} \sin\theta_{i+1}}$	
$\dots c_{58} = \frac{\mathcal{E}_{\theta_3\phi_4}}{t_3 M_4 \sin\theta_4}$	$1 \leq i \leq N - 1, N \geq 2$	
	$j = \sqrt{-1}$	

$c_{41} = \frac{\mathcal{E}_{\phi_2\theta_1}}{t_2 M_1 \sin\theta_2}$	$\Rightarrow c_{2i+2,2i-1}$
$c_{63} = \frac{\mathcal{E}_{\phi_3\theta_2}}{t_3 M_2 \sin\theta_3}$	$= \frac{\mathcal{E}_{\phi_{i+1}\theta_i}}{t_{i+1} M_i \sin\theta_{i+1}}$
$\dots c_{85} = \frac{\mathcal{E}_{\phi_4\theta_3}}{t_4 M_3 \sin\theta_4}$	$j = \sqrt{-1}$

(4.147)

$c_{23} = \frac{\mathcal{E}_{\phi_1\theta_2}}{t_1 M_2 \sin\theta_1}$	$\Rightarrow c_{2i,2i+1}$
$c_{45} = \frac{\mathcal{E}_{\phi_2\theta_3}}{t_2 M_3 \sin\theta_2}$	$= \frac{\mathcal{E}_{\phi_i\theta_{i+1}}}{t_i M_{i+1} \sin\theta_i}$
$\dots c_{67} = \frac{\mathcal{E}_{\phi_3\theta_4}}{t_3 M_4 \sin\theta_3}$	$j = \sqrt{-1}$

(4.148)

$c_{32} = \frac{\varepsilon_{\theta_2 \phi_1}}{t_2 M_1 \sin \theta_1}$	$\Rightarrow c_{2i+1, 2i}$	(4.149)
$c_{54} = \frac{\varepsilon_{\theta_3 \phi_2}}{t_3 M_2 \sin \theta_2}$	$= \frac{\varepsilon_{\theta_{i+1} \phi_i}}{t_{i+1} M_i \sin \theta_i}$	
$\dots c_{76} = \frac{\varepsilon_{\theta_4 \phi_3}}{t_4 M_3 \sin \theta_3}$	$j = \sqrt{-1}$	

$1 \leq i \leq N - 1, N \geq 2$

$c_{24} = \frac{\varepsilon_{\phi_1 \phi_2}}{t_1 M_2 \sin \theta_1 \sin \theta_2}$	$\Rightarrow c_{2i, 2i+2}$	(4.150)
$c_{46} = \frac{\varepsilon_{\phi_2 \phi_3}}{t_2 M_3 \sin \theta_2 \sin \theta_3}$	$= \frac{\varepsilon_{\phi_i \phi_{i+1}}}{t_i M_{i+1} \sin \theta_i \sin \theta_{i+1}}$	
$\dots c_{68} = \frac{\varepsilon_{\phi_3 \phi_4}}{t_3 M_4 \sin \theta_3 \sin \theta_4}$	$j = \sqrt{-1}$	

$1 \leq i \leq N - 1, N \geq 2$

$c_{42} = \frac{\mathcal{E}_{\phi_2\phi_1}}{t_2 M_1 \sin\theta_2 \sin\theta_1}$	$\Rightarrow c_{2i+2,2i}$	(4.151)
$c_{64} = \frac{\mathcal{E}_{\phi_3\phi_2}}{t_3 M_2 \sin\theta_3 \sin\theta_2}$	$= \frac{\mathcal{E}_{\phi_{i+1}\phi_i}}{t_{i+1} M_i \sin\theta_{i+1} \sin\theta_i}$	
$\dots c_{86} = \frac{\mathcal{E}_{\phi_4\phi_3}}{t_4 M_3 \sin\theta_4 \sin\theta_3}$	$1 \leq i \leq N - 1, N \geq 2$ $j = \sqrt{-1}$	

- Expressions from (4.140) to (4.151) give us the recursive formulae for the nonzero elements of the C -matrix along with their range of valid i and N values.
- The first four expressions, (4.140) to (4.143), are valid for a multilayer system of any number N of FM layers and the index i is to run in the range $1 \leq i \leq N$.
- However, the other eight expressions from (4.144) to (4.151) are only to be applied to multilayers consisting of at least $N = 2$ FM layers with the restriction on the index i as $1 \leq i \leq N - 1$.

To clear these restrictions consider the case where there is only one FM layer. This FM layer will have only two dynamical magnetization components and the matrix form of the dynamics of the system will be

$$\begin{pmatrix} c_{11} & c_{12} \\ c_{21} & c_{22} \end{pmatrix} \times \begin{pmatrix} m_{\theta_1} \\ m_{\phi_1} \end{pmatrix} = \begin{pmatrix} M_1 h_{\theta_1} \\ M_1 h_{\phi_1} \end{pmatrix}$$

The elements c_{11} , c_{12} , c_{21} and c_{22} are calculated by expressions written for $c_{2i-1,2i-1}$, $c_{2i-1,2i}$, $c_{2i,2i-1}$ and $c_{2i,2i}$ given respectively by (4.140), (4.141), (4.142) and (4.143). So,

for this system of $N = 1$ FM layer, we will only need expressions from (4.140) to (4.143) which are valid for any number N of FM layers and the condition $1 \leq i \leq N$ will guarantee that the only value to be assumed by i is 1 because $N = 1$ for this specific case. The expressions given by (4.144) to (4.151) are restricted to the cases for $N \geq 2$ and therefore they will not be calculated.

In the case of $N = 2$, the matrix representation will be

$$\begin{pmatrix} c_{11} & c_{12} & c_{13} & c_{14} \\ c_{21} & c_{22} & c_{23} & c_{24} \\ c_{31} & c_{32} & c_{33} & c_{34} \\ c_{41} & c_{42} & c_{43} & c_{44} \end{pmatrix} \times \begin{pmatrix} m_{\theta_1} \\ m_{\phi_1} \\ m_{\theta_2} \\ m_{\phi_2} \end{pmatrix} = \begin{pmatrix} M_1 h_{\theta_1} \\ M_1 h_{\phi_1} \\ M_2 h_{\theta_2} \\ M_2 h_{\phi_2} \end{pmatrix}$$

This time, expressions (4.140) to (4.143) will be used to calculate c_{11} , c_{12} , c_{21} and c_{22} with the index i set to 1 and c_{33} , c_{34} , c_{43} and c_{44} with the index i set to 2 because this time $N = 2$ and the condition $1 \leq i \leq N$ imposed on expressions (4.140) to (4.143) will allow i to run from 1 to 2. The remaining eight components of the C -matrix will be calculated by expressions (4.144) to (4.151) which were restricted to conditions i) $N \geq 2$ which is met because $N = 2$ in this case and ii) $1 \leq i \leq N - 1$ and this latter condition will only allow the index i to assume a single value, namely $i = 1$. Therefore, no unneeded matrix components will be calculated by expressions (4.144) to (4.151).

Once the nonzero matrix elements of the C -matrix defined in equation (4.112) by $C \cdot \vec{m} = \vec{Mh}$ are determined via running equations (4.140) to (4.151) with the appropriate range of i and N values, its inverse (C^{-1}) can be utilized such that

$$\vec{m} = C^{-1} \cdot \vec{Mh} \quad (4.152)$$

gives us the components of the dynamical magnetization, transpose of which was given by equation (4.113) as

$$\vec{m}^T = (m_{\theta_1}, m_{\phi_1}, \dots, m_{\theta_i}, m_{\phi_i}, \dots, m_{\theta_N}, m_{\phi_N})$$

where \overrightarrow{Mh} in (4.152) was defined in (4.114) as

$$\overrightarrow{Mh}^T = (M_1 h_{\theta_1}, M_1 h_{\phi_1}, \dots, M_i h_{\theta_i}, M_i h_{\phi_i}, \dots, M_N h_{\theta_N}, M_N h_{\phi_N})$$

4.2.6. Extracting Dynamical Magnetic Susceptibility

Microwave power absorption is proportional to average dynamical magnetization which is to be constructed from the contributions of all layers. Therefore, one can calculate the θ and ϕ components of the dynamical magnetization, namely m_θ and m_ϕ , of each layer by the steps given above and then these two components can be projected onto the x -axis on which the magnetic field component h_x^0 of the rf-field resides. After summing up all the contributions from all the layers, the resultant dynamical magnetization on x -axis (m_x) is divided by h_x^0 such that the average magnetic susceptibility becomes

$$\chi = \frac{m_x}{h_x^0} \quad (4.153)$$

This method is not restricted to those geometries where magnetic component of the microwave field is on the x -axis but can be applied to any polarization of the h -field by considering the projections of dynamical magnetizations on to the respective polarization axis of the h -field. In this example, we are considering a geometry where the microwave h -field is on the x -axis (this is known as the out of plane geometry).

In order to calculate χ , we need to write down h_{θ_i} and h_{ϕ_i} of any layer i in terms of h_x^0 . Therefore, we have to find out the projection of h_x^0 onto the $\hat{\theta}$ and $\hat{\phi}$ axes as follows

$$h_\theta = \overrightarrow{h_x^0} \cdot \hat{\theta} \quad (4.154)$$

and

$$h_\phi = \overrightarrow{h_x^0} \cdot \hat{\phi} \quad (4.155)$$

where

$$\vec{h}_x^0 = h_x^0 \hat{i} \quad (4.156)$$

in which \hat{i} is the Cartesian unit vector along the x -axis. To perform the inner products given (4.154) and (4.155), one needs to recall the transformation from Cartesian unit vectors to the ones in spherical geometry as given by

$$\begin{pmatrix} \hat{r} \\ \hat{\theta} \\ \hat{\phi} \end{pmatrix} = \begin{bmatrix} \sin\theta\cos\phi & \sin\theta\sin\phi & \cos\theta \\ \cos\theta\cos\phi & \cos\theta\sin\phi & -\sin\theta \\ -\sin\phi & \cos\phi & 0 \end{bmatrix} \cdot \begin{pmatrix} \hat{i} \\ \hat{j} \\ \hat{k} \end{pmatrix} \quad (4.157)$$

From (4.157) one can get

$$\hat{\theta} = \cos\theta\cos\phi \hat{i} + \cos\theta\sin\phi \hat{j} - \sin\theta \hat{k} \quad (4.158)$$

$$\hat{\phi} = -\sin\phi \hat{i} + \cos\phi \hat{j} \quad (4.159)$$

Using (4.156) for \vec{h}_x^0 and (4.158) for $\hat{\theta}$, h_θ in (4.154) becomes

$$h_\theta = \vec{h}_x^0 \cdot \hat{\theta} = h_x^0 \hat{i} \cdot (\cos\theta\cos\phi \hat{i} + \cos\theta\sin\phi \hat{j} - \sin\theta \hat{k}) = h_x^0 \cos\theta\cos\phi$$

which reads for a given layer number i as

$$h_{\theta_i} = h_x^0 \cos\theta_i \cos\phi_i \quad (4.160)$$

Following the same judgement and using (4.156) and (4.159) in (4.155) one gets

$$h_\phi = \vec{h}_x^0 \cdot \hat{\phi} = h_x^0 \hat{i} \cdot (-\sin\phi \hat{i} + \cos\phi \hat{j}) = -h_x^0 \sin\phi$$

which then yields for layer number i

$$h_{\phi_i} = -h_x^0 \sin \phi_i \quad (4.161)$$

We are now able to replace h_{θ_i} and h_{ϕ_i} in \overrightarrow{Mh}^T given by (4.114) as

$$\overrightarrow{Mh}^T = (M_1 h_{\theta_1}, M_1 h_{\phi_1}, \dots, M_i h_{\theta_i}, M_i h_{\phi_i}, \dots, M_N h_{\theta_N}, M_N h_{\phi_N})$$

by the expressions given in (4.160) and (4.161). However, $\chi = m_x/h_x^0$ implies that we also have to write down m_x in terms of m_{θ_i} 's and m_{ϕ_i} 's as pointed out early in this chapter. Therefore, we project each m_{θ_i} and m_{ϕ_i} onto the x -axis to find the contribution of each layer to m_x and then sum them up from $i = 1$ to $i = N$ where N is the number of FM layers.

The contribution of the dynamic magnetization of layer i to m_x is given by

$$m_x^i = m_{\theta_i}^x + m_{\phi_i}^x \quad (4.162)$$

where $m_{\theta_i}^x$ and $m_{\phi_i}^x$ are projections of m_{θ_i} and m_{ϕ_i} onto the x -axis. $m_{\theta_i}^x$ can be found by

$$\begin{aligned} m_{\theta_i}^x &= \overrightarrow{m}_{\theta_i} \cdot \hat{i} = m_{\theta_i} \hat{\theta}_i \cdot \hat{i} \\ \Rightarrow m_{\theta_i}^x &= m_{\theta_i} (\cos \theta_i \cos \phi_i \hat{i} + \cos \theta_i \sin \phi_i \hat{j} - \sin \theta_i \hat{k}) \cdot \hat{i} \end{aligned}$$

which gives us

$$m_{\theta_i}^x = m_{\theta_i} \cos \theta_i \cos \phi_i \quad (4.163)$$

where use is made of (4.158) for expanding $\hat{\theta}_i$. For $m_{\phi_i}^x$ we proceed as follows:

$$\begin{aligned} m_{\phi_i}^x &= \overrightarrow{m}_{\phi_i} \cdot \hat{i} = m_{\phi_i} \hat{\phi}_i \cdot \hat{i} \\ \Rightarrow m_{\phi_i}^x &= m_{\phi_i} (-\sin \phi_i \hat{i} + \cos \phi_i \hat{j}) \cdot \hat{i} \end{aligned}$$

which yields

$$m_{\phi_i}^x = -m_{\phi_i} \sin \phi_i \quad (4.164)$$

where in expanding $\hat{\phi}_i$, use is made of (4.159). If we now feed (4.163) and (4.164) into (4.162), we get

$$m_x^i = m_{\theta_i} \cos \theta_i \cos \phi_i - m_{\phi_i} \sin \phi_i \quad (4.165)$$

To find the total dynamical magnetization along x -axis, we sum (4.165) over all the FM layers within the system to get

$$m_x = \sum_{i=1}^N m_x^i = \sum_{i=1}^N (m_{\theta_i} \cos \theta_i \cos \phi_i - m_{\phi_i} \sin \phi_i) \quad (4.166)$$

Equation (4.166) gives us m_x in terms of m_{θ_i} and m_{ϕ_i} of all layers which were embedded in the term \vec{m} in equation (4.152) given by

$$\vec{m} = C^{-1} \cdot \overline{Mh}$$

in which C was the so-called coefficient matrix, elements of which were defined by expressions from (4.140) to (4.151) and \vec{m} was defined in (4.113) as

$$\vec{m}^T = (m_{\theta_1}, m_{\phi_1}, \dots, m_{\theta_i}, m_{\phi_i}, \dots, m_{\theta_N}, m_{\phi_N})$$

and \overline{Mh} was defined in (4.114) as

$$\overline{Mh}^T = (M_1 h_{\theta_1}, M_1 h_{\phi_1}, \dots, M_i h_{\theta_i}, M_i h_{\phi_i}, \dots, M_N h_{\theta_N}, M_N h_{\phi_N})$$

where h_{θ_i} and h_{ϕ_i} were calculated respectively by (4.160) and (4.161) as

$$h_{\theta_i} = h_x^0 \cos \theta_i \cos \phi_i \quad h_{\phi_i} = -h_x^0 \sin \phi_i$$

Therefore, (4.160) and (4.161) can be used to calculate h_{θ_i} and h_{ϕ_i} which were then inserted into \overline{Mh}^T in (4.114). Once the coefficient matrix C is calculated by expressions from (4.140) to (4.151), one can use the expression $\overline{m} = C^{-1} \cdot \overline{Mh}$ to calculate all m_{θ_i} and m_{ϕ_i} . These m_{θ_i} and m_{ϕ_i} are then fed into (4.166) written for m_x which then is finally inserted into (4.153) to find the susceptibility $\chi = m_x/h_x^0$. Since m_x includes h_x^0 as a common multiplicative term (starting from h_{θ_i} and h_{ϕ_i} , through \overline{Mh} and finally m_{θ_i} and m_{ϕ_i} in \overline{m}), $\chi = m_x/h_x^0$ will cancel out all h_x^0 dependence. This will give us a workflow as depicted in Figure 4.4 for the calculation of the dynamical susceptibility.

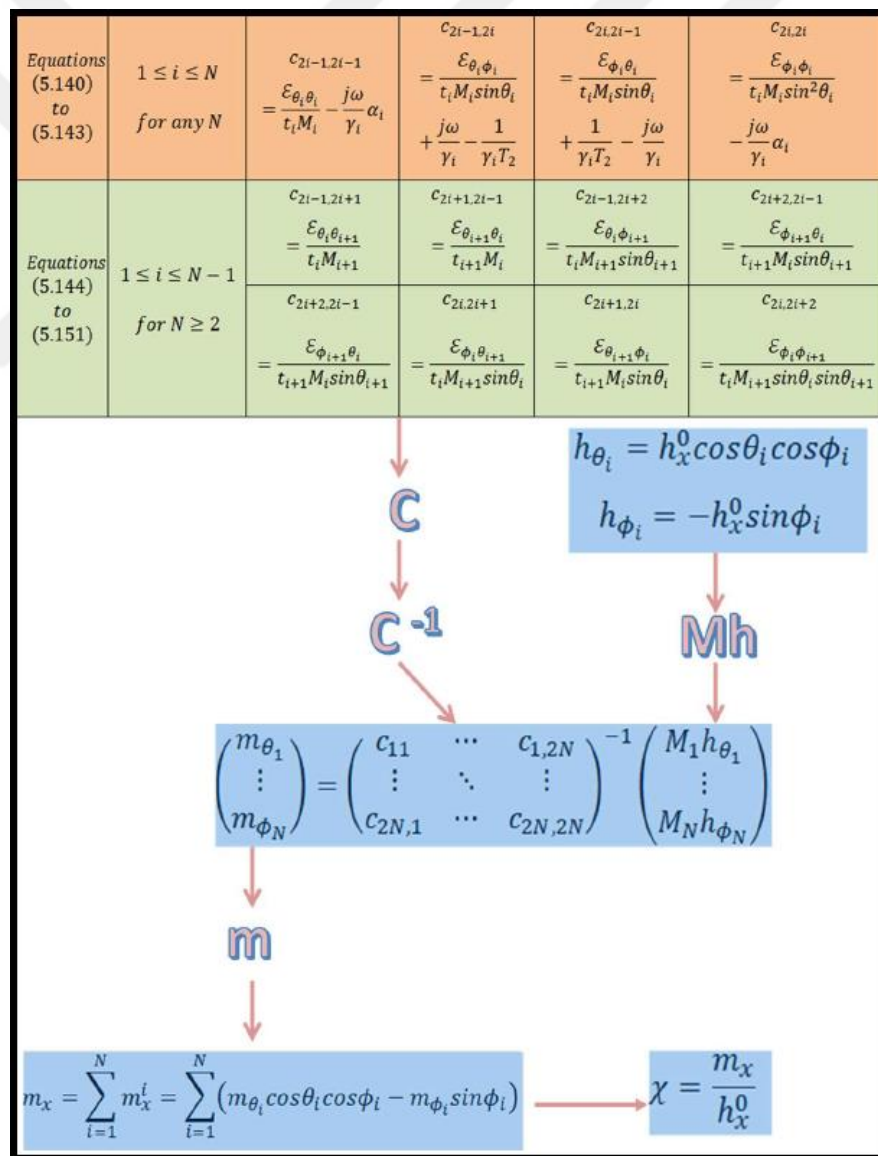


Figure 4.4. Workflow for the calculation of the dynamical susceptibility.

5. MATERIAL, EXPERIMENTAL WORK AND RESULTS

The material systems studied in this work are thin film structures composed of ferromagnetic (FM) Co and antiferromagnetic (AFM) CoO with nominal thicknesses of 10 nm and 15 nm. Four samples were produced on top of Si substrates. The first sample is composed only of a single bilayer structure of CoO/Co. In the other samples, this bilayer structure repeats itself for two, three and five times. We, therefore have produced samples of single, double, triple and quintuple bilayers of CoO/Co structure as shown in Figure 5.1 below.

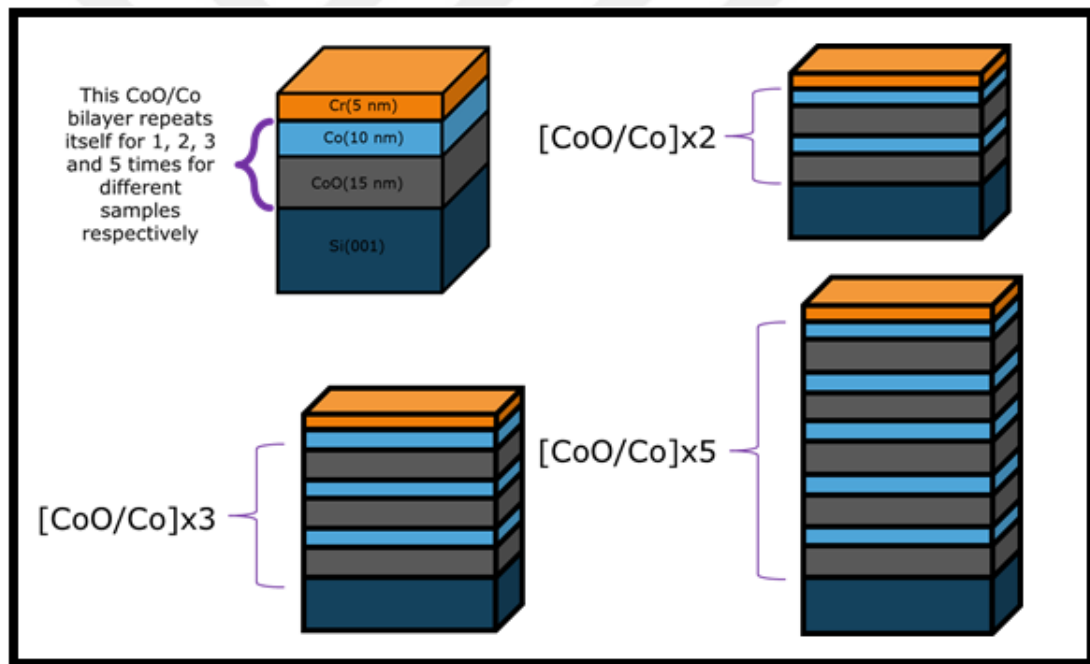


Figure 5.1. CoO/Co multilayer thin film structure.

The deposited Cr layer seen in the figures acts as a protective capping layer. The samples were produced by magnetron sputtering and structurally and magnetically characterized by XPS, TEM, VSM and FMR techniques as given in the following sections. Some parts of the following material are “reproduced from [205] [M. Öztürk, E. Sınır, E. Demirci, M. Erkovan, O. Öztürk and N. Akdoğan. Exchange bias properties of $[\text{Co/CoO}]_n$ multilayers. *Journal of Applied Physics*, 112(9):093911(1-7), 2012], with the permission of AIP Publishing”.

5.1. SAMPLE PREPARATION

The samples were prepared at Gebze Technical University Nanotechnology Center Surface Physics Laboratory in a cluster ultra high vacuum (UHV) chamber, depicted in Figure 5.2 combined with one preparation chamber and analytical chamber. The preparation chamber has 6 magnetron sputtering deposition guns (3 DC, 2 RF and one DC pulse) and one sample holder with quartz crystal microbalance. The analytical chamber is equipped with X-ray, UV photoelectron spectroscopy and low energy ion scattering systems with a hemispherical charged particles energy analyzer. The photoelectron spectroscopy was used to characterize the electronic structure and identify the chemical stoichiometry of samples. All processes were carried out on native-oxide p type Si (001) wafer. Before loading the sample into the chambers, the wafer substrate was cleaned by sonication in acetone and methanol, respectively. The wafers were further cleaned by several cycles of Ar⁺ sputtering for 10 min followed by annealing at 600 °C for 10 min. The cleanness of the surface was confirmed by XPS.



Figure 5.2. Cluster UHV chamber at Gebze Technical University for magnetron sputtering and surface characterization.

Reactive deposition was used to grow cobalt oxide films. The Co target (6N grade) attached to rf-sputter gun was operated with 40 W so that the deposition rate achieved 0.3 Å/s for pure Co growth. In order to grow the CoO film, the pure oxygen molecular gas (6N grade) was released (by mass flow meter fixed at 0.15 sccm) to the growth chamber. When the base pressure became stable at 5×10^{-5} mbar, the rf-sputter gun loaded by Co target was fired. During the reactive sputtering deposition, the chamber pressure was established in range of $(1.2 - 1.3) \times 10^{-3}$ mbar.

The thickness of CoO films was determined by Vecoo profilometer. The 300 Sec deposition succeeds the thickness of 15 nm. The samples and their nominal thicknesses are as follows: single bilayer [Co(10 nm)/CoO(15 nm)]₁, double bilayer [Co(10 nm)/CoO(15 nm)]₂, triple bilayer [Co(10 nm)/CoO(15 nm)]₃ and quintuple bilayer [Co(10 nm)/CoO(15 nm)]₅. Chromium cap layers were grown on top of all four samples against any environmental effect, especially against the oxidation of uppermost Co layer. Chromium target (6N grade) attached to DC sputter gun was fired for the deposition of the cap layer.

5.2. STRUCTURAL CHARACTERIZATION

In order to structurally characterize the samples, two techniques, X-Ray Photoelectron Spectroscopy (XPS) and Transmission Electron Microscopy (TEM) were employed. XPS provided information on the expected formation of the oxidized form of Co, cobalt-oxide, and also gave us the presence of different phases of cobalt-oxide: CoO and Co₃O₄. TEM images provided us with the thicknesses of individual layers.

5.2.1. X-Ray Photoelectron Spectroscopy (XPS) Measurements

The XPS data provided by Gebze Technical University Surface Physics Laboratory in Figure 5.3 are used to confirm the chemical stoichiometry with satellite peaks which indicate the successful CoO surface. The satellite peaks associated with Co2p peaks on XPS from the surface of CoO appear to be stronger rather than the other forms of Co-oxide due to the charge-transfer band structure characteristic of the late 3d transition metal oxide [206]. The lack of electron on the d bands causes the charge-transfer readily on XP spectra.

However, Co 2p peak is broader compared to the peak of a single oxide surface that proves the coexistence of different oxide forms such as CoO and Co₃O₄ (in spinel form CoO.Co₂O₃). Co₃O₄ is a mixed valence compound with Co²⁺ and Co³⁺ ions in tetrahedral and octahedral sites respectively of cubic close packed lattice of oxygen anions [207]. Different stoichiometries of cobalt oxide as CoO, Co₂O₃ and Co₃O₄ are expected because they can coexist below 900°C [208]. The width of the Co 2p photoemission peaks is consistent with the presence of both Co²⁺ and Co³⁺ as well as the Co²⁺ satellites. In the region of both Co 2p_{3/2} and Co 2p_{1/2} peak lines, two Voigt-peaks were fitted to calculate ratio of Co-oxide formation ratio. The result shows that Co²⁺ / Co³⁺ ratio is 2.6. This means that Co-oxide layer contains mostly CoO formation. The O1s XPS spectrum shows a main peak at 529.5 eV. This main peak indicates main CoO formation. The details of the CoO XPS analysis can be found in [103].

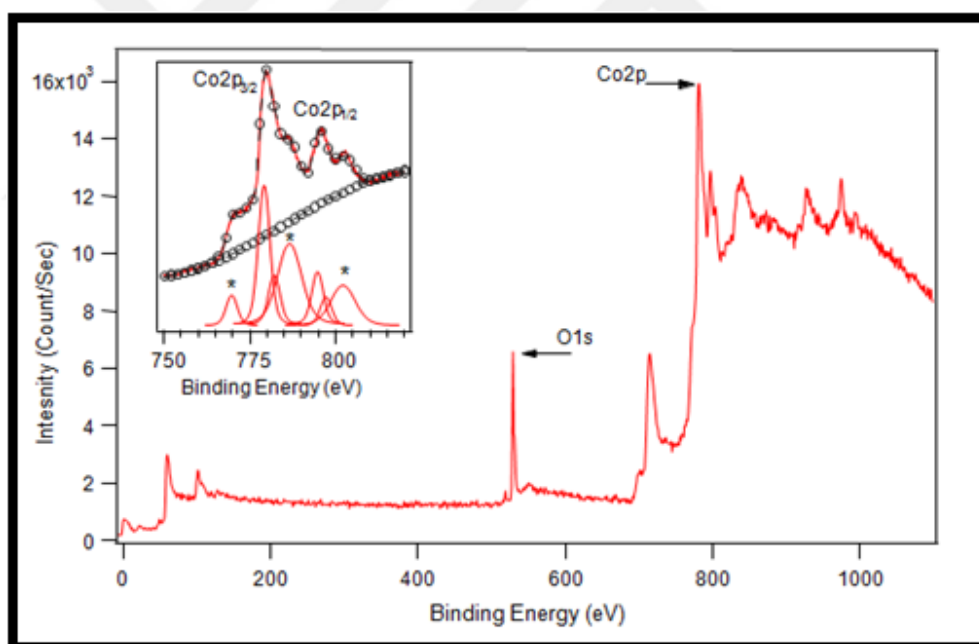


Figure 5.3. XPS survey spectra from the Co-oxide surface and the Co 2p spectral region showing the effects of oxidation. Inset data indicate the satellite peaks of CoO films.

Reproduced from [205] with the permission of AIP Publishing.

5.2.2. Transmission Electron Microscopy (TEM) Measurements

In order to determine the real thicknesses of the samples and to see the successful deposition of multilayers, we have used the advantage of transmission electron microscopy

technique (TEM) with Tecnai G2 F20 S-TWIN system at Gebze Technical University. This technique produces images via the interaction of electrons with samples, for this reason the samples are needed to be thin enough to become transparent for electrons. Focused ion beam (FIB) at national nanotechnology research centre (UNAM) is used to prepare very thin cross sectional samples out of multilayer samples for TEM imaging. During FIB, buildup of excess electrons on the surface of the sample can cause charging effects. To avoid the system from charging effects the top of the samples are covered with Pt layers before preparing thin cross-section with FIB for TEM measurements. The cross-sectional pieces from the samples are examined by TEM in detail as given in Figure 5.4. The thicknesses of each layer are tabulated in Table 5.1.

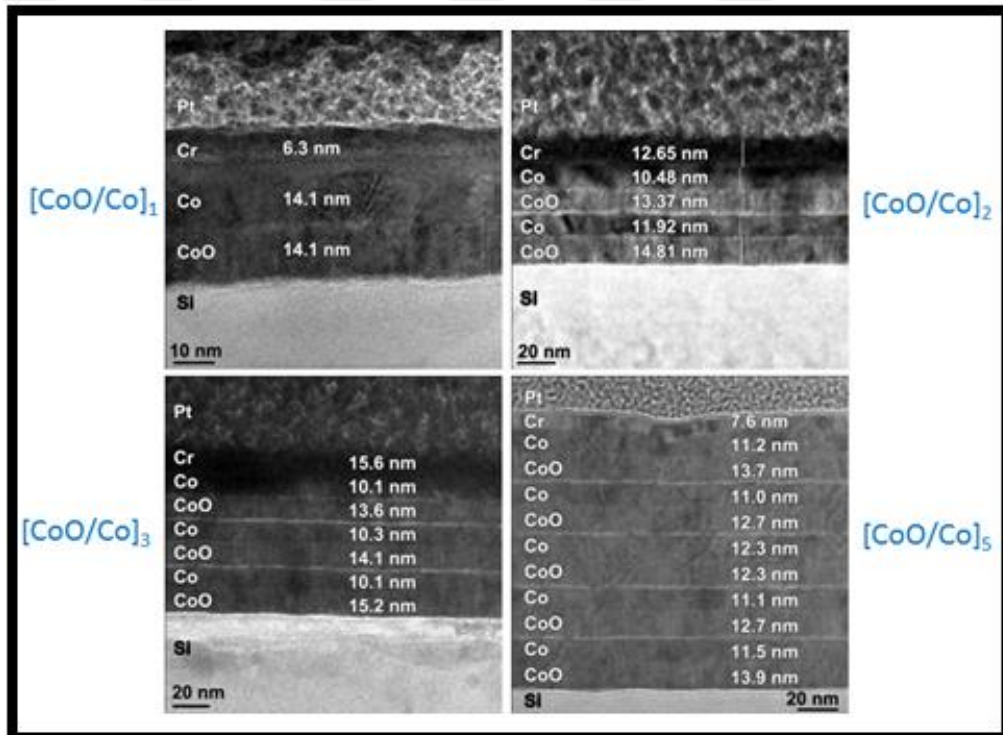


Figure 5.4. TEM images of $[\text{CoO/Co}]_n$ multilayers. Cr cap layers were grown on top of all four samples against the oxidation of uppermost Co layer. The Pt layers are due to FIB sample preparation for TEM imaging. Reproduced from [205] with the permission of AIP Publishing.

For the single bilayer sample, FM and AFM layers have nearly the same thicknesses around 14.1 nm. For the other samples, the FM layer thicknesses are lower than those of AFMs. It is important to note that although the layer thicknesses are very close to each

other, they have small differences to play a crucial role in exchange bias properties. Table 5.1 shows all measured thicknesses of the samples. The Pt layer is due to the Focused Ion Beam (FIB) sample extraction process for TEM imaging.

Table 5.1. The TEM measured thicknesses of $[\text{CoO}/\text{Co}]_n$ multilayers [205].

From bottom to top	Single Bilayer $[\text{CoO}/\text{Co}]_1$	Double Bilayer $[\text{CoO}/\text{Co}]_2$	Triple Bilayer $[\text{CoO}/\text{Co}]_3$	Quintuple Bilayer $[\text{CoO}/\text{Co}]_5$
CoO	14.1 nm	14.8 nm	15.2 nm	13.9 nm
Co	14.1 nm	11.9 nm	10.1 nm	11.5 nm
CoO	-	13.4 nm	14.1 nm	12.7 nm
Co	-	10.5 nm	10.3 nm	11.1 nm
CoO	-	-	13.6 nm	12.3 nm
Co	-	-	10.1 nm	12.3 nm
CoO	-	-	-	12.7 nm
Co	-	-	-	11.0 nm
CoO	-	-	-	13.7 nm
Co	-	-	-	11.2 nm
Cr	6.3 nm	12.7 nm	15.6 nm	7.6 nm

5.3. MAGNETIC CHARACTERIZATION

For the magnetic characterization of the samples, the techniques of Ferromagnetic Resonance (FMR) and Vibrational Sample Magnetometry (VSM) are employed. Magnetic anisotropies of the as-produced samples are examined in both in-plane and out-of-plane geometries by FMR. The exchange bias properties of the samples are determined by VSM.

Room temperature (RT) FMR measurements have been carried out by using a Bruker EMX spectrometer operating at X-band (9.8 GHz) frequency.

As the VSM tool, Quantum Design Physical Property Measurement System (PPMS) with 9 T magnetic field capability have been used.

5.3.1. Ferromagnetic Resonance (FMR) Measurements

The Electron Spin Resonance (ESR) also known as Electron Paramagnetic Resonance (EPR) spectrometer system at Gebze Technical University as shown in Figure 5.5 can be used for taking FMR measurements by operating at X-band frequency of 9.8 GHz.

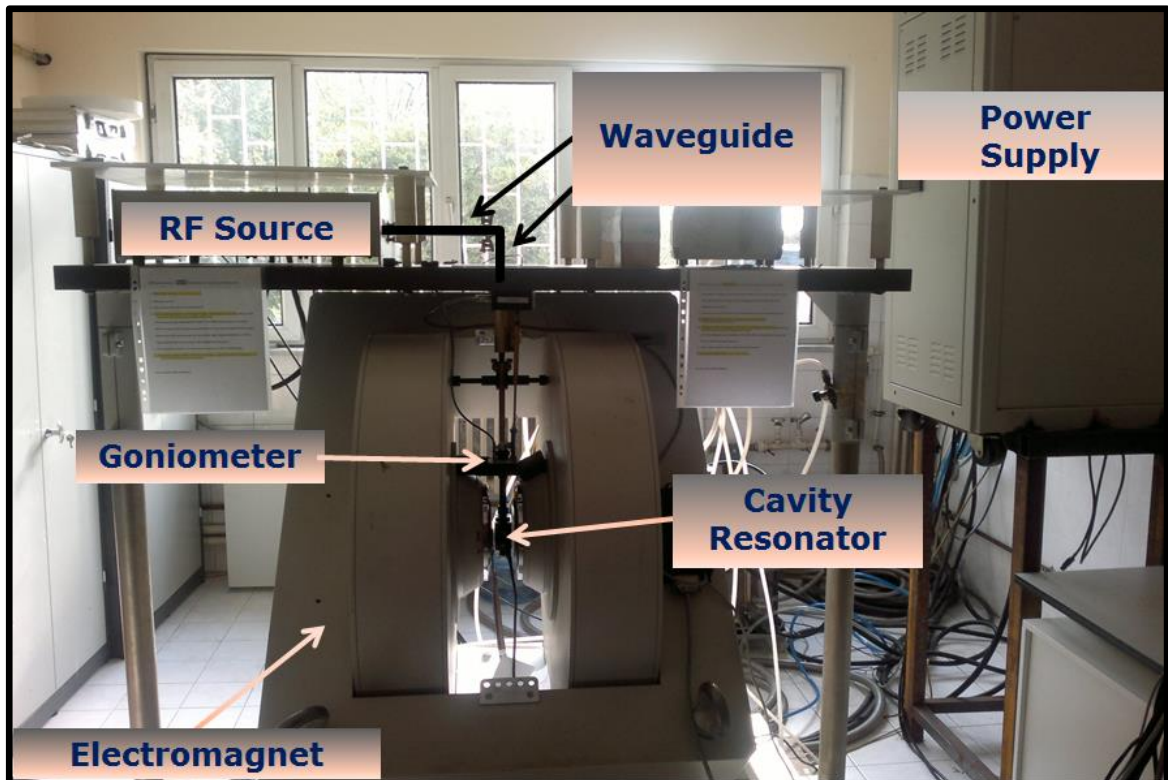


Figure 5.5. Bruker EMX EPR system at Gebze Technical University for FMR measurements.

The spectrometer is equipped by an electromagnet which provides a dc magnetic field up to 2.2 Tesla in the horizontal plane. A goniometer was used to rotate the vertical rod shaped sample holder which is parallel to the microwave magnetic field and perpendicular to the applied static magnetic field. Both in-plane (IP) and out-of-plane (OOP) measurements are performed with respect to the static magnetic field. For the in-plane geometry, samples are attached to the bottom of the holder to keep the static magnetic field parallel to the film surface during the 360° rotation. For the out-of plane geometry, the samples are attached to the side of the holder and rotated by 180° to convert the magnetic field from parallel to perpendicular and then parallel again to the film surface. Microwave

magnetic field is kept fixed perpendicular to the surface for the in-plane geometry and parallel to the surface for the out-of-plane measurements. In Figure 5.6 and Figure 5.7, one can see how the sample is placed in the sample holder and rotated in IP and OOP geometries.

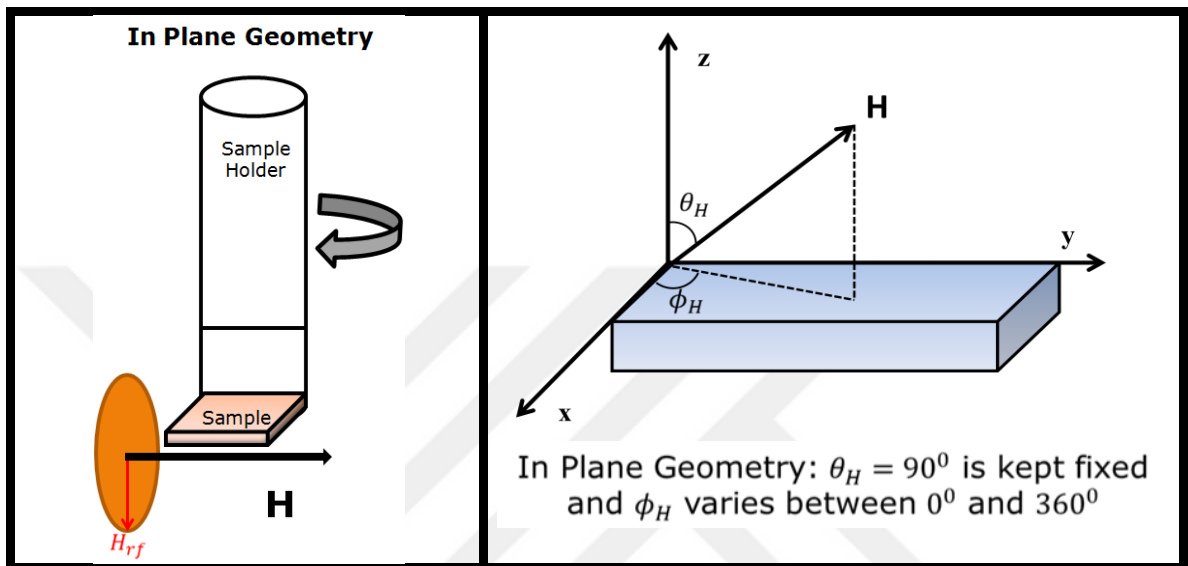


Figure 5.6. In-plane sample placement and angular sweep for FMR.

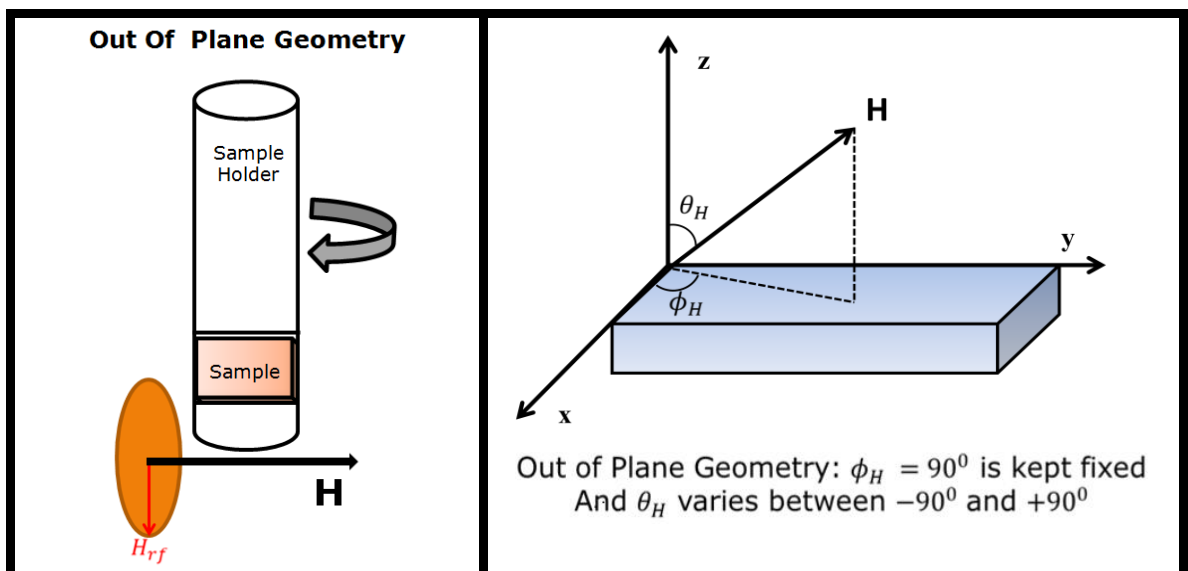


Figure 5.7. Out-of-plane sample placement and angular sweep for FMR.

Figure 5.8 shows the in-plane and out-of-plane geometries together without giving specifics of the angular sweeps and how the sample is located within the sample holder, but providing a much clearer picture.

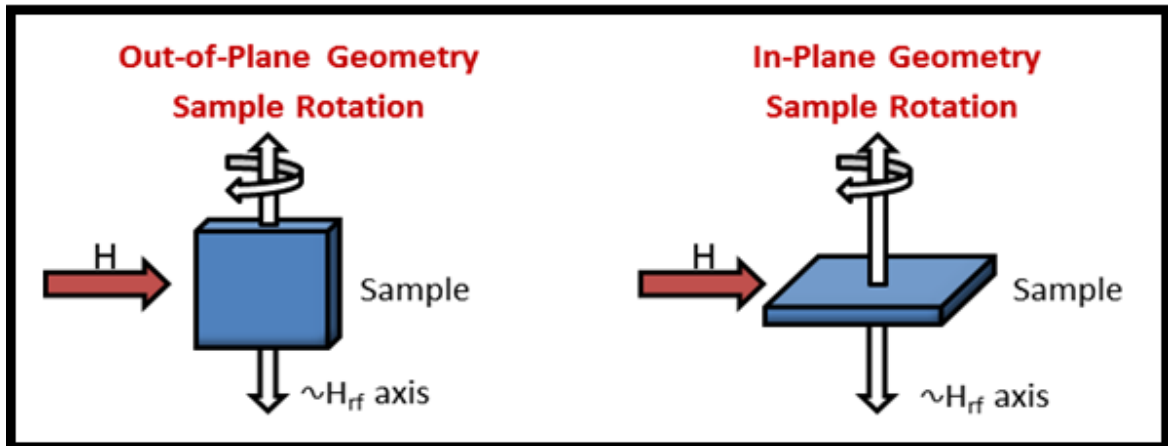


Figure 5.8. In-plane and out-of-plane geometries for FMR measurements [132].

We have not been able to observe in-plane FMR signal in single and double bilayer CoO/Co samples. Non-conventional structure of our FMR system does not allow for in-plane measurements for very thin films. The in-plane FMR spectra of triple bilayer [CoO/Co]₃ and quintuple bilayer [CoO/Co]₅ samples are shown in Figure 5.9. In order to check the presence of anisotropic behaviour, the samples were rotated by 360 degrees in the film plane. At zero degree, the applied field was chosen parallel to the geometric [100] edge direction of the sample. At the beginning, the resonance fields of the in-plane peaks are small but after rotating the sample to higher angles the required magnetic fields for resonance increase and the peaks possess the maximum field values at 90 and 270 degrees. Therefore, samples used in this study show two collinear easy directions and two collinear hard directions resulting in an in-plane uniaxial anisotropy. Since the samples are polycrystalline, the uniaxial anisotropic behaviour of the samples can be attributed to growth-induced geometric (or oblique) anisotropy [209-211] which will be detailed in Discussion part in Section 6.

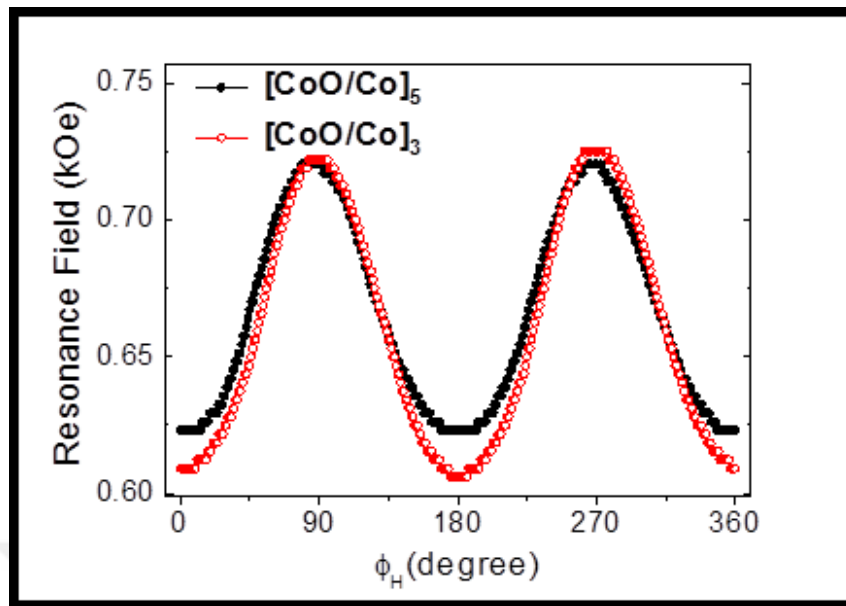


Figure 5.9. In-plane FMR data for the angular dependence of resonance fields from triple bilayer $[\text{CoO}/\text{Co}]_3$ and quintuple bilayer $[\text{CoO}/\text{Co}]_5$. 0° and 180° correspond to collinear easy directions while 90° and 270° are on hard directions [205].

For out-of-plane FMR spectra, easy axes of the samples which were determined by the in-plane measurements were parallel to the applied dc magnetic field at the beginning and the sample plane is in the vertical. The sample was then rotated around the vertical axis by 180 degrees from parallel position to the antiparallel position, reducing the angular step to even 0.125 degrees for those directions of dc magnetic field close to the film surface normal. Figure 5.10 reveals the resonance fields of FMR signal as a function of polar angle which represents the angle made by dc magnetic field with the surface normal. Well resolved FMR peaks were observed for this geometry.

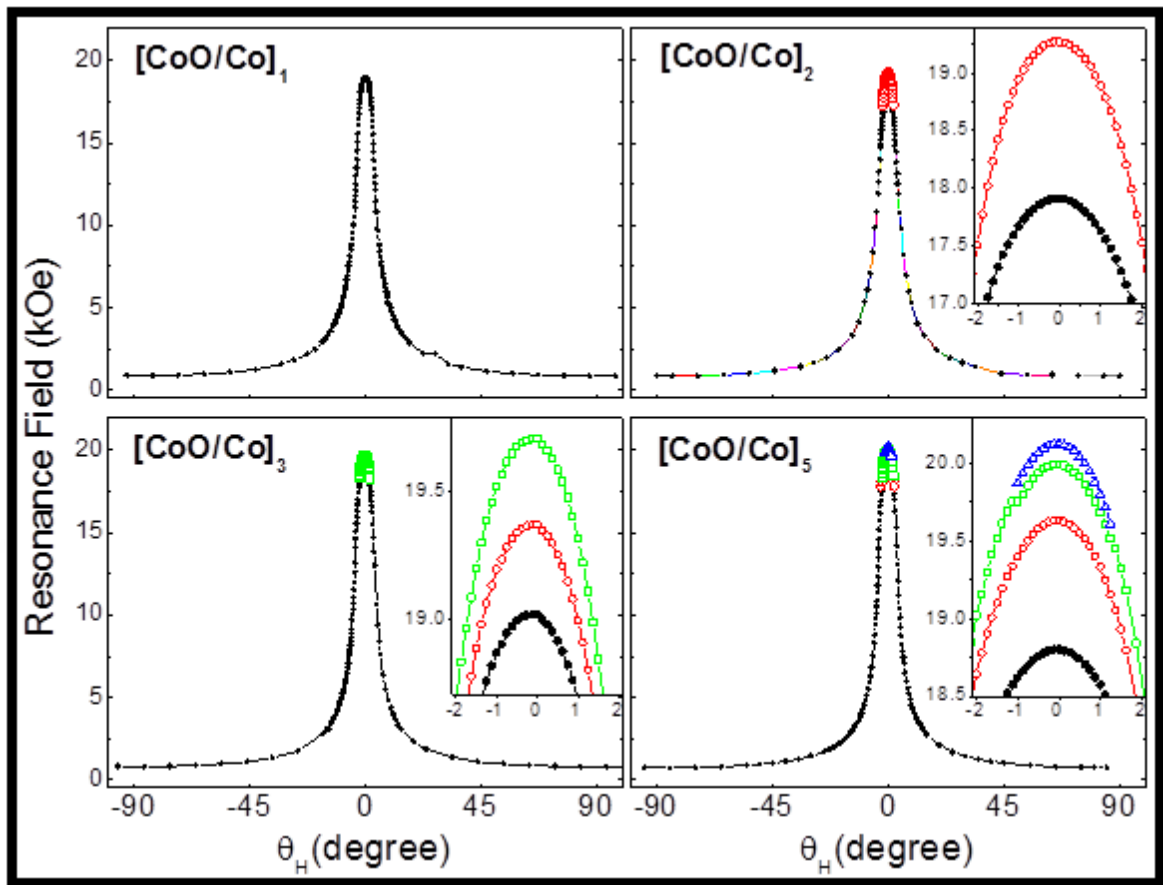


Figure 5.10. The angular dependence of resonance field from FMR data of single bilayer [CoO/Co], double bilayer [CoO/Co]₂, triple bilayer [CoO/Co]₃ and quintuple bilayer [CoO/Co]₅ for out-of-plane geometry [205]. $\theta_H = \pm 90^\circ$ corresponds to magnetic field parallel to easy magnetization axis of Co in the plane of the thin film. The insets show the details of resonance fields when the direction of the magnetic fields is close to the film normal for the related samples.

As can be seen in Figure 5.10, one, two, three and four peaks are observed for single, double, triple and quintuple bilayers, respectively. One peak was missing for quintuple sample. However, it can be said that the fifth peak was embedded in the fourth peak. The embedding behaviour is clear in the real spectra as shown in Figure 5.11 that the distance between the peaks getting closer for the deepest layer.

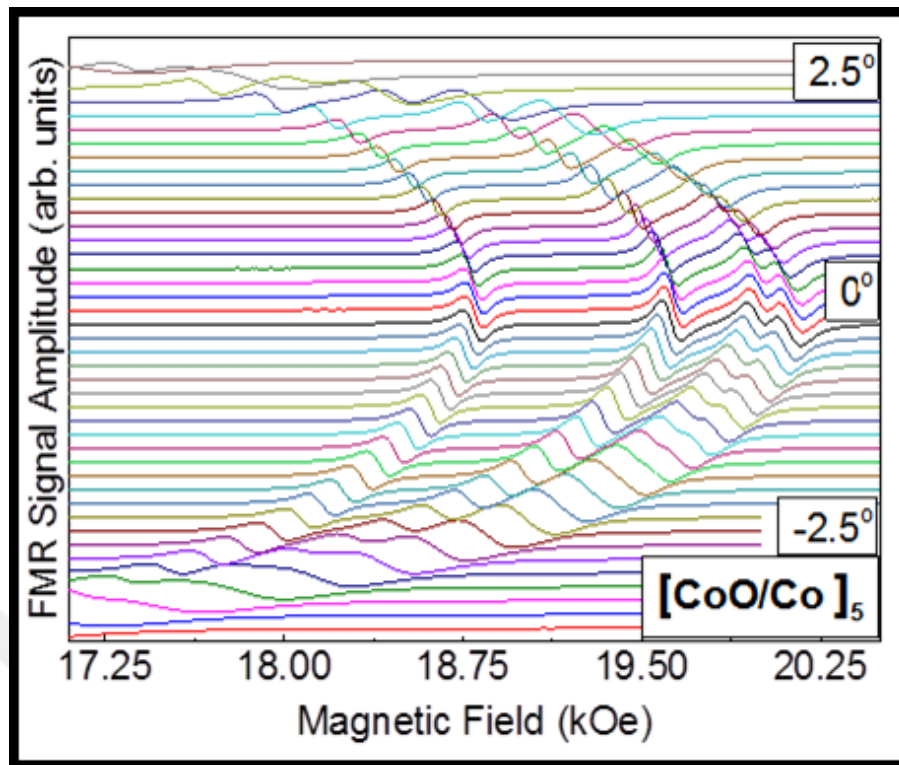


Figure 5.11. A part of out-of-plane collective FMR detailed real spectra of quintuple bilayer $[\text{CoO}/\text{Co}]_5$ taken at varying θ_H [205]. Four peaks can be seen clearly. The fifth peak is thought to be embedded in the fourth peak seen at the right.

5.3.2. Vibrational Sample Magnetometry (VSM) Measurements

In order to characterize the exchange bias (EB) properties of bilayers, a VSM magnetometer (Quantum Design PPMS 9T) was used as given in Figure 5.12. M versus H loops have been recorded at selected temperatures from 10 K to 320 K. Since the Néel temperature of CoO is about 290 K, the samples were heated up to 320 K to control the magnetic order of AFM layers before arriving at each target temperature. While field-cooling (FC) the samples from 320 K to the target temperatures, an in-plane magnetic field (H_{FC}) of 2 kOe was applied to set the unidirectional anisotropy.



Figure 5.12. Quantum Design PPMS (9 T) System at Gebze Technical University for VSM measurements.

It is well-known in exchange bias systems that performing successive hysteresis measurements at a given target temperature leads to a decrease in the exchange bias field which is defined as the training effect [5, 99]. After measuring a single hysteresis loop at the lowest target temperature of 10 K, we cannot directly heat the FM/AFM system to the next target temperature because the system is already at the verge of suffering from the training effect. Therefore, after taking a single hysteresis loop at a given target temperature the system is heated to above the bulk Néel temperature of the AFM material to bring it back to the paramagnetic state. The above mentioned FC procedure is then exactly repeated with the same H_{FC} to re-field-cool the system to the next target temperature to induce the unidirectional anisotropy in the same direction as in the previous target temperature. The measurement protocol is depicted in Figure 5.13.

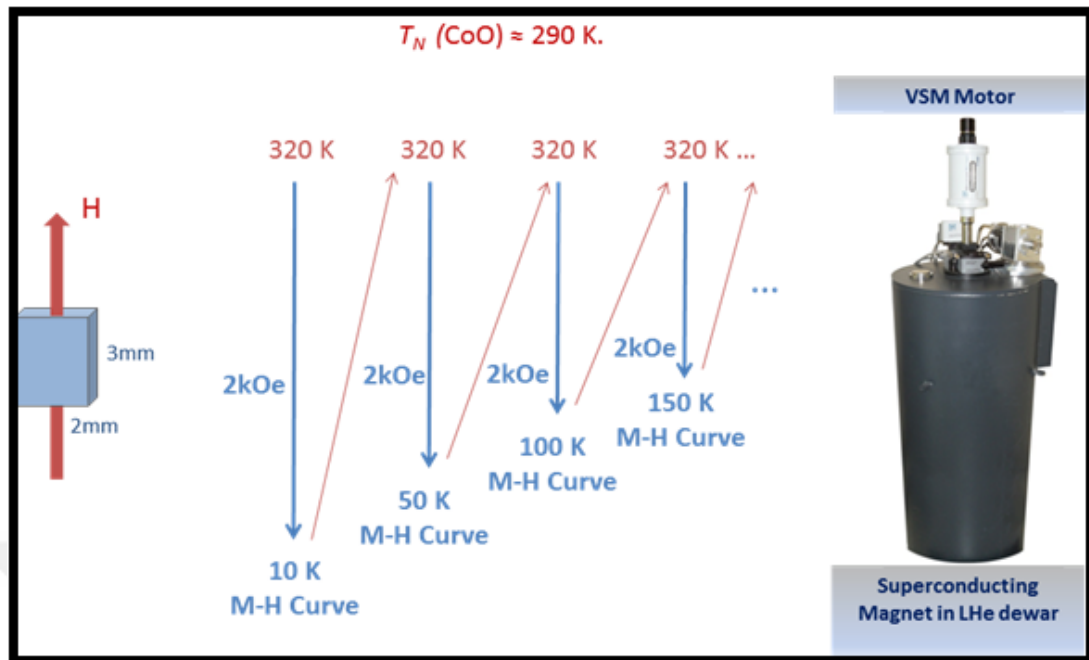


Figure 5.13. Measurement protocol for EB measurements with VSM [reproduced with appropriate changes from a drawing of Dr. Mustafa Öztürk from Gebze Technical University].

Figure 5.14 shows the easy axis hysteresis loops of the samples at 10 K and 300 K. The coercive fields are symmetric at 300 K, but after field cooling the coercive fields become asymmetric at 10 K and the sample has a negative exchange bias as expected. The dependency of coercive fields is strongly related with temperature. Single bilayer sample has a standard exchange bias behaviour. In the double bilayer system one more step observed for the 10 K exchange biased hysteresis loop. Double bilayer system has two Co and two CoO layers. The main step of the hysteresis loop which has a smaller shift is related to the upper Co and the second step which has a larger exchange bias is related to the inner Co. The easy axis hysteresis loops of triple bilayer sample revealed three steps. In the triple bilayer system, there are three Co and three CoO layers. It is thought that the first step is belonging to upper Co and the third (the largest) is belonging to the innermost Co layer. Two steps for double bilayer and three steps for triple bilayer were observed. The expectation that the number of steps is directly related to number of bilayers, however, is false because only two steps are observed for quintuple bilayer instead of five. The reason for the observation of additional steps and identification of these steps and the asymmetric

character of the hysteresis loops between ascending and descending branches will be addressed in the Discussion part in Section 6.

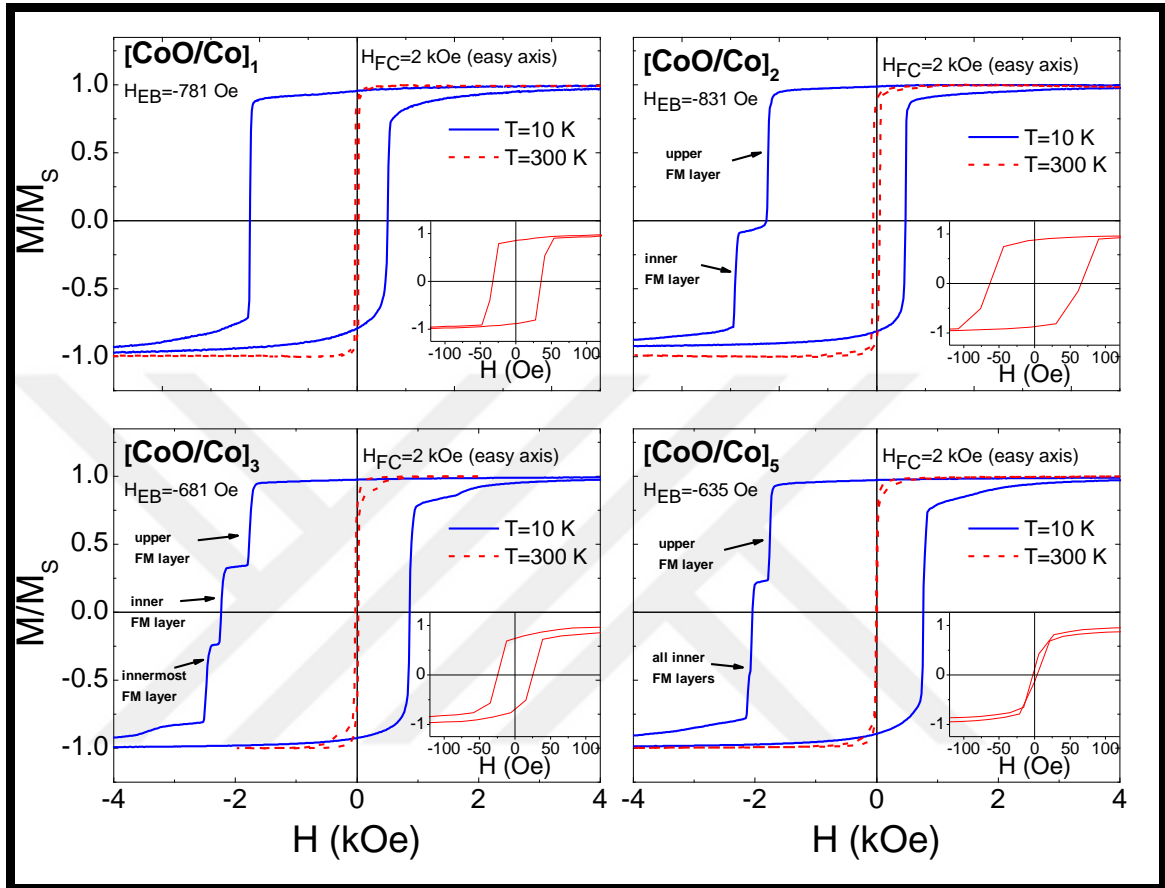


Figure 5.14. The hysteresis loops normalized to saturation magnetization at room temperature (RT) (dashed lines) and at 10 K after field cooling (solid lines) of the samples.

Insets with red solid lines show the central parts of RT symmetric hysteresis loops.

Reproduced from [205] with the permission of AIP Publishing.

Figure 5.15 shows the characteristic temperature evolution of magnitudes of both positive and negative coercive fields. At the beginning, absolute values of the coercive fields are the same with decreasing temperature. But after a certain point, a bifurcation occurs on field values. The temperature at and below which the separation of the coercive fields is observed is called as the ‘blocking’ temperature T_B . The blocking temperature in the present systems is around 200 K. Above the blocking temperature, the loops are symmetric and the exchange bias fields are zero. The dependence of the exchange bias and the coercive fields on temperature for all samples are summarized in Figure 5.15.

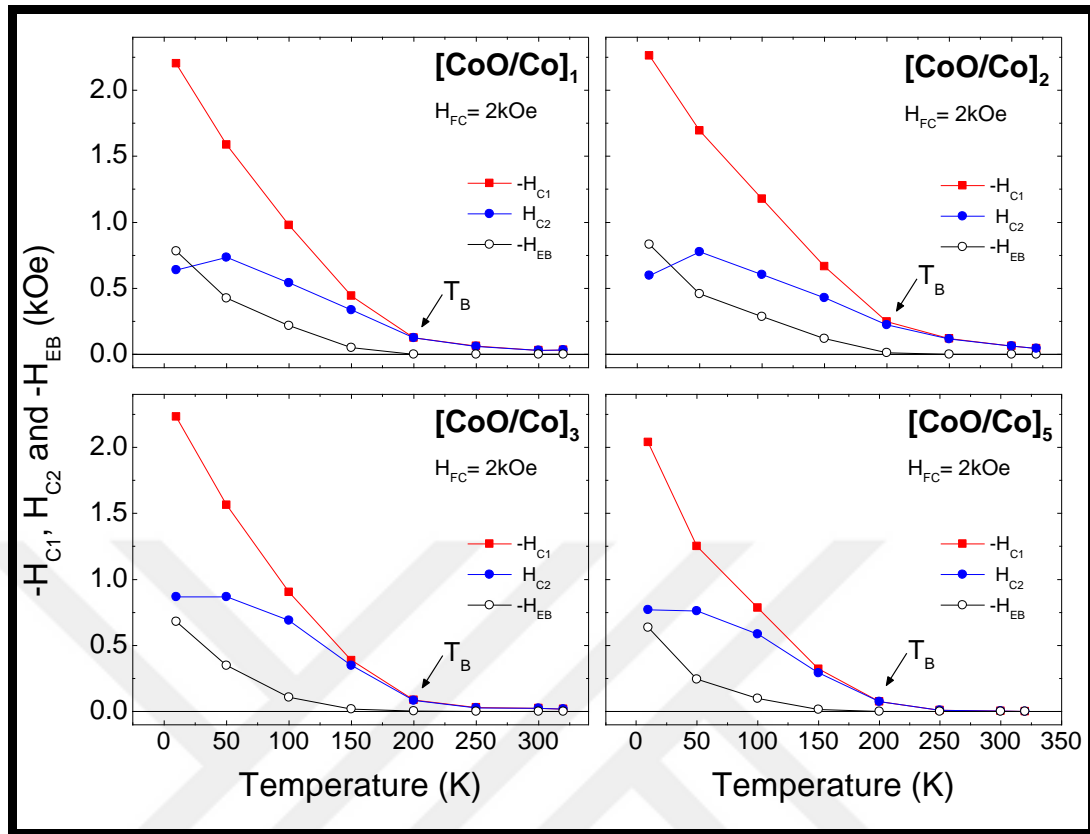


Figure 5.15. Temperature dependence of magnitudes of coercive fields ($-H_{C1}$ and H_{C2}) and exchange bias field ($-H_{EB}$) for $[\text{CoO}/\text{Co}]_n$ multilayers [205].

Since exchange bias is observed as a shift in the hysteresis loop, the exchange bias field values can be calculated from the shift of coercive fields by using the well known formula

$$H_{EB} = \frac{H_{C1} + H_{C2}}{2} \quad (5.1)$$

Here H_{C1} represents the intersection of the hysteresis loop with the magnetic field axis on the descending part whereas H_{C2} is the value on the ascending part. In all the samples, H_{C1} is negative and H_{C2} is positive that $-H_{C1}$ and H_{C2} are plotted in Figure 5.14 to represent the absolute values, or magnitudes, of these two coercive fields. The total coercive field defined as the half-width of the hysteresis loop is given by

$$H_C = \frac{-H_{C1} + H_{C2}}{2} \quad (5.2)$$

Since $|H_{C1}| > H_{C2}$ and since H_{C1} is negative, the exchange bias field values $H_{EB} = (H_{C1} + H_{C2})/2$ are negative and that gives us a shift of hysteresis loop towards negative values on the magnetic field axis. This is also the reason why $-H_{EB}$ is plotted in Figure 5.15 to represent the magnitude of exchange bias.



6. DISCUSSION

In-plane FMR spectra of polycrystalline $[\text{Co}/\text{CoO}]_n$ samples used in this study revealed two-fold symmetry with two collinear and opposite easy directions forming an easy axis and two hard directions in the same manner for 360° in plane rotation as shown in Figure 5.9. It is not expected of a polycrystalline structure to exhibit such kind of a uniaxial magneto crystalline anisotropy. This unexpected behaviour of $[\text{Co}/\text{CoO}]_n$ polycrystalline thin films is explained by growth conditions and called as growth induced or geometric (oblique) anisotropy [209-211]. For vacuum deposited thin metallic films, a fiber axis structure is formed varying from the normal to the substrate during the evaporation. That fiber axis tilts in a similar direction of incidence to that of the metallic flux. As the fiber axis was no longer normal to the plane of the film, depending on the geometric location of the evaporating filament, so-called geometric anisotropy was induced.

The onset of exchange bias with decreasing temperatures refers to the blocking temperature T_B and its value is expected to be very close to the Néel temperature T_N of AFM material depending on its thickness [5, 124-128] and stoichiometry [129-132]. In this study, this value is lower than the expected bulk value for CoO. Néel temperature of bulk CoO is around 290 K and observed blocking temperatures for all four polycrystalline $[\text{Co}/\text{CoO}]_n$ samples were around 200 K. Two arguments can be stressed to account for the observed low T_B of polycrystalline $[\text{Co}/\text{CoO}]_n$ samples. It is reported in the literature that homogeneity range of CoO from Co_1O_1 to Co_3O_4 can change the T_N of the material [129-132]. The T_N of Co_1O_1 is 291 K while that of Co_3O_4 is 34 K. Since XPS data revealed coexistence of different cobalt oxide phases in AFM layer causing nonstoichiometry, the T_N of the $[\text{Co}/\text{CoO}]_n$ samples should be reduced below to 291 K and this reduction translates to low T_B because the upper limit of the T_B is fixed by T_N . Blocking temperature is also strongly related with the AFM layer thickness up to a limiting transition thickness to the bulk properties depending on material. This dependence of T_N on AFM CoO layer thickness was related to a finite-size scaling effect [124]. Studies for CoO show that T_N reduces below 20 nm with decreasing thickness and thus T_B reduces [5, 125, 126]. Since we on the average have 15 nm AFM CoO layer thickness for each sample, a lower T_B is expected. Caution should be taken, however, because a neutron diffraction study [127]

revealed that for CoO layer thicknesses less than 9 nm, reduced T_B is not associated with reduced T_N . A study conducted on CoNiO/NiFe exchange bias system also revealed that the blocking temperature of the AFM layer is dependent on the deposition conditions such as the substrate bias and the sputtering pressure which was also thought to be related to finite size scaling phenomena [212].

The effect of increase in the number of FM-AFM interfaces on exchange bias field is detailed in this study. For single bilayer system, standard exchange bias hysteresis loop was observed. However, additional steps were observed for hysteresis loops of other bilayers. Two, three and again two steps emerged in the hysteresis loops of double, triple and quintuple bilayer samples respectively. In all cases the outer ferromagnetic Co layers have just one antiferromagnetic CoO neighbour and inner ferromagnetic Co layers have two antiferromagnetic CoO neighbours. The pinning effects of two separate AFM neighbours on a single FM layer cause the magnetization reversal to happen at higher negative coercive fields. As a result, exchange bias field increases for the inner Co layers and this behaviour causes an additional step in the hysteresis loop. Considering only the number of pinning AFM neighbours maximum two steps for all samples are reasonable because one FM layer can only have one or two AFM neighbours in the thin film stack. The third steps can be explained by the nonuniform distribution of layer thicknesses, as shown in TEM images (Figure 5.4). This is reported in the literature that both FM and AFM layer thicknesses affect the exchange bias field [5, 6, 99, 115, 213]. It is asserted that the thickness of AFM materials up to 20nm is effective on the exchange bias effect in a positive manner [5]. For the hysteresis loop of triple bilayer, inner and innermost layers have different thicknesses. The innermost and a bit thinner FM Co layer has thicker AFM CoO neighbours than the next Co layer above it that can increase the exchange bias effect and cause one more step as compared to double bilayer system. The thickness distribution within the quintuple bilayer system, however, is more uniform as compared to the triple bilayer system, causing all the inner FM layers to have more or less the same coercive field to have their magnetization reversals together. As a result, the steps in the exchange bias hysteresis loops can be based on the number of AFM neighbouring interfaces of FM material and the differences between the thicknesses of the layers.

Apart from the absence of step-like behaviour in the ascending branches of hysteresis loops, there is another asymmetry between the ascending and descending branches even in the single bilayer system. This kind of asymmetric behaviour was indicated to be intrinsic to the exchange biased systems with different magnetization reversal pathways, e.g. domain wall motion or coherent rotation, at each branch of the hysteresis loop [96, 102, 214]. The asymmetry is affected by the relative orientation of the FM anisotropy and the induced unidirectional anisotropy directions, competition between the magnitudes of these anisotropies and the angle made by the hysteresis magnetic field and the unidirectional anisotropy direction [215]. The hysteresis curves for all samples show relatively sharp changes during the magnetization reversals of FM layers along the descending branches and more rounded features on the ascending parts. This seems to suggest that first reversal happens via a domain wall movement and the subsequent reversals to the positive magnetization by rotation [216]. One must be cautious, however, that our VSM magnetometry system is only sensitive to the projection of magnetization along the hysteresis magnetic field, carrying no information on the perpendicular magnetization component, that distinguishing between domain nucleation-propagation and magnetization rotation is rather questionable. Angle dependent measurements of the hysteresis loops and numerical simulations may illuminate the problem more satisfactorily to give insight to the role of competing anisotropies. We also expect that our inability to perfectly align the unidirectional anisotropy direction and the FM uniaxial anisotropy axis experimentally causing noncollinearity might also have induced an asymmetric character [214].

Our fundamental FMR theoretical analysis showed clearly that ω_0 as obtained by equation (4.67) is the resonance frequency of the FM material and it is a dynamical quantity dependent upon the orientation of the film with respect to the DC magnetic field, the magnitude of the DC field, magnetic anisotropies, etc. Thus, we concluded that varying the orientation and DC field value causes the material to gain a particular value of ω_0 and for a specific set of parameters it is equal to ω of the driving field which in turn creates a resonance as the name ferromagnetic resonance implies.

Our work on FMR theory of multilayer structures provided us a framework to write down the dynamical magnetization components in a linearized model. Our step by step calculations makes it clear how the elements of the C -matrix can be modelled and

calculated, along with the range of magnetic layer number i and the total number of FM layers N in the multilayer stack. The restrictions on i and N identified and clarified in the main text are important for a solution algorithm. It is the hope of the author that this step by step analysis, which might seem to be over detailed, might provide some clear idea on how those hidden intermediate steps in the published papers can actually be dealt with. The analyses can be extended for different geometries from in-plane to out-of-plane by the procedures outlined and, by a choice of proper energy terms, FMR data can be simulated to extract magnetic properties of the FM materials.



7. CONCLUSION

In this work, we have studied polycrystalline $[\text{Co}/\text{CoO}]_n$ multilayers with different number of repetitions n and tried to probe their exchange bias and magnetic properties. A uniaxial magnetic anisotropy in the film plane was observed for the as produced polycrystalline $[\text{Co}/\text{CoO}]_n$ thin films at room temperature and the observed uniaxial anisotropy was explained by geometric (or oblique) anisotropy due to film growth. The out-of-plane room temperature FMR results indicated that the surface normal is a hard axis and that the FM layers have slightly different anisotropies close to film normal. In all the multilayer samples, exchange bias is observed under field cooling switching anisotropy from uniaxial to unidirectional. The blocking temperature (T_B) below which EB emerges was found to be around 200 K and its lower value than the bulk Néel temperature T_N is explained by the nonstoichiometry due to varying phases of cobalt oxide, finite-size scaling effects and the deposition conditions of the AFM layers. For multi bilayer systems, additional steps are observed in the exchange biased hysteresis loops and this behaviour is related to incoherent magnetization reversals of individual layers due to (i) two kinds of interfaces made by the FM layers in contact with two AFM neighbours from above and below, except the uppermost FM Co with a single AFM neighbour and (ii) varying thicknesses of FM and AFM layers as was observed in previous studies. The separate spin-flips were observed in one shot. The observed asymmetries in the hysteresis loops were connected to magnetization reversal pathways, competing anisotropies, noncollinearities between the uniaxial anisotropy of the FM film and unidirectional anisotropy direction that is expected after the field cooling procedure. Theoretical work on ferromagnetic resonance demonstrated how the resonance condition can be obtained and FMR study on multilayers resulted in a linearized model with clear restrictions on the use of recursive relationships in the calculation of the matrix elements of the linear model in obtaining the dynamical susceptibility.

REFERENCES

1. W. H. Meiklejohn and C. P. Bean. New Magnetic Anisotropy. *Physical Review*, 102:1413-1414, 1956.
2. W. H. Meiklejohn and C. P. Bean. New Magnetic Anisotropy. *Physical Review*, 105:904-913, 1957.
3. T. R. Gao, Z. Shi, S. M. Zhou, R. Chantrell, P. Asselin, X. J. Bai, J. Du, and Z. Z. Zhang. Exchange Bias, Training Effect, Hysteretic Behaviour of Angular Dependence, and Rotational Hysteresis Loss in NiFe/FeMn Bilayer: Effect of Antiferromagnet Layer Thickness. *Journal of Applied Physics*, 105:053913, 2009.
4. W. H. Meiklejohn. Exchange Anisotropy - A Review. *Journal of Applied Physics*, 33:1328-1335, 1962.
5. J. Nogués, I. K. Schuller. Exchange Bias. *Journal of Magnetism and Magnetic Materials*, 192:203-232, 1999.
6. A. E. Berkowitz, K. Takano. Exchange Anisotropy - A Review. *Journal of Magnetism and Magnetic Materials*, 200:552-570, 1999.
7. M. Kiwi. Exchange Bias Theory. *Journal of Magnetism and Magnetic Materials*, 234:584-595, 2001.
8. R. L. Stamps. Mechanisms for Exchange Bias. *Journal of Physics D: Applied Physics*, 33:R247-R268, 2000.
9. F. Radu and H. Zabel. Exchange Bias Effect of Ferro-/Antiferromagnetic Heterostructures. In: H. Zabel and S. D. Bader, editors, *Magnetic Heterostructures: Advances and Perspectives in Spinstructures and Spintransport*, pages 97-184. Springer Tracts in Modern Physics (227), Springer-Verlag, Berlin-Heidelberg, 2008.

10. C. Binek. *Ising-type Antiferromagnets: Model Systems in Statistical Physics and in the Magnetism of Exchange Bias*, Springer Tracts in Modern Physics (196), Springer-Verlag, Berlin-Heidelberg, 2003.
11. J. Nogués, J. Sort, V. Langlais, S. Doppiu, B. Dieny, J. S. Muñoz, S. Surinach, M. D. Baro, S. Stoyanov, Y. Zhang. Exchange Bias in Ferromagnetic Nanoparticles Embedded in an Antiferromagnetic Matrix. *International Journal of Nanotechnology*, 2:23-42, 2005.
12. I. K. Schuller. Unusual Phenomena in Exchange-Biased Nanostructures. *MRS (Materials Research Society) Bulletin*, 29:642-646, 2004.
13. R. Coehoorn. Giant Magnetoresistance and Magnetic Interactions in Exchange-Biased Spin Valves. In: K. H. J. Buschow, editor, *Handbook of Magnetic Materials Volume 15*, pages:1-197, Elsevier North-Holland, The Netherlands, 2003.
14. J. Nogués, J. Sort, V. Langlais, V. Skumryev, S. Suriñach, J.S. Muñoz, M.D. Baró. Exchange Bias in Nanostructures. *Physics Reports*, 422:65-117, 2005.
15. J. F. Bobo, L. Gabillet and M. Bibes. Recent Advances in Nanomagnetism and Spin Electronics. *Journal of Physics: Condensed Matter*, 16:S471-S496, 2004.
16. M. N. Baibich, J. M. Broto, A. Fert, F. Nguyen Van Dau, F. Petroff, P. Etienne, G. Creuzet, A. Friederich, and J. Chazelas. Giant Magnetoresistance of (001)Fe/(001)Cr Magnetic Superlattices. *Physical Review Letters*, 61:2472-2475, 1988.
17. G. Binasch, P. Grünberg, F. Saurenbach, and W. Zinn. Enhanced Magnetoresistance in Layered Magnetic Structures with Antiferromagnetic Interlayer Exchange. *Physical Review B*, 39:4828-4830, 1989.
18. S. S. P. Parkin, N. More, and K.P. Roche. Oscillations In Exchange Coupling and Magnetoresistance in Metallic Superlattice Structures: Co/Ru, Co/Cr, and Fe/Cr. *Physical Review Letters*, 64:2304-2307, 1990.

19. B. Dieny, V. S. Speriosu, S. S. P. Parkin, B. A. Gurney, D. R. Wilhoit, and D. Mauri. Giant Magnetoresistance in Soft Ferromagnetic Multilayers. *Physical Review B*, 43:1297-1300, 1991.
20. S. S. P. Parkin, R. Bhadra, and K. P. Roche. Oscillatory Magnetic Exchange Coupling Through Thin Copper Layers. *Physical Review Letters*, 66:2152-2155, 1991.
21. A. Fert, P. Grünberg, A. Barthélémy, F. Petroff, W. Zinn. Layered Magnetic Structures: Interlayer Exchange Coupling and Giant Magnetoresistance. *Journal of Magnetism and Magnetic Materials*, 140-144:1-8, 1995.
22. P. Grünberg. Layered Magnetic Structures: History, Facts and Figures. *Journal of Magnetism and Magnetic Materials*, 226-230:1688-1693, 2001.
23. P. A. Grünberg. Exchange Anisotropy, Interlayer Exchange Coupling and GMR in Research and Application. *Sensors and Actuators A: Physical*, 91:153-160, 2001.
24. E. Y. Tsymbal and D. G. Pettifor. Perspectives of Giant Magnetoresistance. In: H. Ehrenreich and F. Spaepen, editors, *Solid State Physics, Vol 56*, pages 113-237. Solid State Physics (56), Elsevier Academic Press Inc, San Diego-USA, 2001.
25. P.A. Grünberg. Nobel Lecture: From Spin Waves to Giant Magnetoresistance and Beyond. *Reviews of Modern Physics*, 80:1534-1540, 2008.
26. A. Barthélémy, A. Fert, J-P. Contour, M. Bowen, V. Cros, J. M. De Teresa, A. Hamzic, J. C. Faini, J. M. George, J. Grollier, F. Montaigne, F. Pailloux, F. Petroff, C. Vouille. Magnetoresistance and Spin Electronics. *Journal of Magnetism and Magnetic Materials*, 242-245:68-76, 2002.
27. M. Julliere. Tunneling Between Ferromagnetic Films. *Physics Letters A*, 54:225-226, 1975.

28. J. C. Slonczewski. Conductance and Exchange Coupling of Two Ferromagnets Separated by a Tunneling Barrier. *Physical Review B*, 39:6995-7002, 1989.
29. J. S. Moodera, L. R. Kinder, T. M. Wong, and R. Meservey. Large Magnetoresistance at Room Temperature in Ferromagnetic Thin Film Tunnel Junctions. *Physical Review Letters*, 74:3273-3276, 1995.
30. T. Miyazaki, N. Tezuka. Giant Magnetic Tunneling Effect in Fe/Al₂O₃/Fe Junction. *Journal of Magnetism and Magnetic Materials*, 139:L231-L234, 1995.
31. R. C. Sousa, J. J. Sun, V. Soares, P. P. Freitas, A. Kling, M. F. da Silva, and J. C. Soares. Large Tunneling Magnetoresistance Enhancement by Thermal Anneal. *Applied Physics Letters*, 73:3288-3290, 1998.
32. J. S. Moodera, G. Mathon. Spin Polarized Tunneling in Ferromagnetic Junctions. *Journal of Magnetism and Magnetic Materials*, 200:248-273, 1999.
33. S. Parkin, K. P. Roche, M. G. Samant, P. M. Rice, R. B. Beyers, R. E. Scheuerlein, E. J. O'Sullivan, S. L. Brown, J. Bucchigano, D. W. Abraham, Yu Lu, M. Rooks, P. L. Trouilloud, R. A. Wanner, and W. J. Gallagher. Exchange-Biased Magnetic Tunnel Junctions and Application to Nonvolatile Magnetic Random Access Memory (invited). *Journal of Applied Physics*, 85:5828-5833, 1999.
34. S. Cardoso, V. Gehanno, R. Ferreira, P. P. Freitas. Ion Beam Deposition and Oxidation of Spin-Dependent Tunnel Junctions. *IEEE Transactions on Magnetics*, 35:2952-2954, 1999.
35. M. Bowen, V. Cros, F. Petroff, A. Fert, C. Martínez Boubeta, J. L. Costa-Krämer, J. V. Anguita, A. Cebollada, F. Briones, F. Güell, F. Peiró, and A. Cornet. Large Magnetoresistance in Fe/MgO/FeCo(001) Epitaxial Tunnel Junctions on GaAs(001). *Applied Physics Letters*, 79:1655-1657, 2001.

36. W. H. Butler, X.-G. Zhang, T. C. Schulthess, and J. M. MacLaren. Spin-Dependent Tunneling Conductance of Fe/MgO/Fe Sandwiches. *Physical Review B*, 63:054416, 2001.
37. J. Mathon and A. Umerski. Theory Of Tunneling Magnetoresistance of an Epitaxial Fe/MgO/Fe(001) Junction. *Physical Review B*, 63:220403:1-4, 2001.
38. S. Yuasa, T. Nagahama, A. Fukushima, Y. Suzuki, and K. Ando. Giant Room-Temperature Magnetoresistance in Single-Crystal Fe/MgO/Fe Magnetic Tunnel Junctions. *Nature Materials*, 3:868-871, 2004.
39. S. Yuasa, A. Fukushima, H. Kubota, Y. Suzuki, and K. Ando. Giant Tunneling Magnetoresistance Up to 410% At Room Temperature in Fully Epitaxial Co/MgO/Co Magnetic Tunnel Junctions With bcc Co(001) Electrodes. *Applied Physics Letters*, 89:042505, 2006.
40. S. Yuasa, D. D. Djayaprawira. Giant Tunnel Magnetoresistance in Magnetic Tunnel Junctions With A Crystalline MgO(001) Barrier. *Journal of Physics D: Applied Physics*, 40:R337-R354, 2007.
41. Y. M. Lee, J. Hayakawa, S. Ikeda, F. Matsukura, H. Ohno. Effect of Electrode Composition on The Tunnel Magnetoresistance of Pseudo-Spin-Valve Magnetic Tunnel Junction With a MgO Tunnel Barrier. *Applied Physics Letters*, 90:212507, 2007.
42. B. Dieny, R. C. Sousa, J. Herault, C. Pappas, G. Prenat, U. Ebels, D. Houssameddine, B. Rodmacq, S. Auffret, L. D. Buda-Prejbeanu, M. C. Cyrille, B. Delaet, O. Redon, C. Ducruet, J-P. Nozieres, I. L. Pre. Spin-Transfer Effect and Its Use in Spintronic Components. *International Journal of Nanotechnology*, 7:591-614, 2010.
43. A. Schuhl, D. Lacour. Spin Dependent Transport: GMR & TMR. *Comptes Rendus Physique*, 6:945-955, 2005.
44. I. Žutić, J. Fabian, and S. Das Sarma. Spintronics: Fundamentals and Applications. *Reviews of Modern Physics*, 76:323-410, 2004.

45. C. Chappert, A. Fert, F. N. Van Dau. The Emergence Of Spin Electronics in Data Storage. *Nature Materials*, 6:813-823, 2007.
46. S. D. Bader, S. S. P. Parkin. Spintronics. *Annual Review of Condensed Matter Physics*, 1:71-88, 2010.
47. A. Hirohata, K. Takanashi. Future Perspectives for Spintronic Devices. *Journal of Physics D: Applied Physics*, 47:19300, 2014.
48. J. G. Zhu. Magnetoresistive Random Access Memory: The Path to Competitiveness and Scalability. *Proceedings of the IEEE*, 96:1786-1798, 2008.
49. D. Apalkov, B. Dieny, J. M. Slaughter. Magnetoresistive Random Access Memory. *Proceedings of the IEEE*, 104:1796-1830, 2016.
50. B. Dieny, V. S. Speriosu, S. S. P. Parkin, B. A. Gurnay, P. Baumgart and D. R. Wilhoit. Magnetotransport Properties of Magnetically Soft Spin-Valve Structures. *Journal of Applied Physics*, 69:4774-4779, 1991.
51. M. Y. Khan, C.-B. Wu and W. Kuch. Pinned Magnetic Moments in Exchange Bias: Role of the Antiferromagnetic Bulk Spin Structure. *Physical Review B*, 89:094427, 2014.
52. W. Kuch, L. I. Chelaru, F. Offi, J. Wang, M. Kotsugi and J. Kirschner. Tuning the Magnetic Coupling Across Ultrathin Antiferromagnetic Films by Controlling Atomic-Scale Roughness. *Nature Materials*, 5:128-133, 2006.
53. J. Wang, T. Sannomiya, J. Shi and Y. Nakamura. Influence of Interface Roughness on the Exchange Bias of Co/CoO Multilayers. *Journal of Applied Physics*, 113:17D707, 2013.
54. F. Y. Yang and C. L. Chien. Spiraling Spin Structure in an Exchange-Coupled Antiferromagnetic Layer. *Physical Review Letters*, 85:2597-2600, 2000.

55. R. Morales, Z.-P. Li, J. Olamit, K.Liu, J. M. Alameda and I. K. Schuller. Role of the Antiferromagnetic Bulk Spin Structure on Exchange Bias. *Physical Review Letters*, 102:097201, 2009.
56. M. G. Blamire, M. Ali, C.-W. Leung, C. H. Marrows and B. J. Hickey. Exchange Bias and Blocking Temperature in Co/FeMn/CuNi Trilayers. *Physical Review Letters*, 98:217202, 2007.
57. E. Restrepo-Parra, J. D. Agudelo-Giraldo, J. Restrepo. Thickness and Bilayer Number Dependence on Exchange Bias in Ferromagnetic/Antiferromagnetic Multilayers Based on $\text{La}_{1-x}\text{Ca}_x\text{MnO}_3$. *Physica B*, 440:61-66, 2014.
58. C. Kittel. *Introduction to Solid State Physics, 8th Edition*, John Wiley & Sons Inc., USA, 2005.
59. B. D. Cullity, C. D. Graham. *Introduction to Magnetic Materials-Second Edition*, IEEE Press-John Wiley & Sons Inc., Hoboken, New Jersey, USA, 2009.
60. J. M. D. Coey. *Magnetism and Magnetic Materials*, Cambridge University Press, New York, USA, 2009.
61. N. A. Spaldin. *Magnetic Materials: Fundamentals and Applications, Second Edition*, Cambridge University Press, New York, USA, 2011.
62. W. F. Brown, Jr. *Magnetostatic Principles in Ferromagnetism*, North-Holland Publishing Company, Amsterdam, 1962.
63. T. Iwata. A Diagonal Sum Rule Concerning Demagnetization Tensors in Composite Bodies. *Journal of Applied Physics*, 39:3094-3097, 1968.
64. What-then-how, “Magnetic Phenomena and Their Interpretation-Classical Approach (Magnetic Properties of Materials) Part 1”, <http://what-when-how.com/electronic-properties-of-materials/magnetic-phenomena-and-their-interpretationc>

lassical-approach-magnetic-properties-of-materials-part-1/ [retrieved 9 October 2017].

65. L. Z. Yuan. Recent Advances in Exchange Bias of Layered Magnetic FM/AFM Systems. *Science China: Physics, Mechanics and Astronomy*, 56:61-69, 2013.
66. S. Gangopadhyay, G. C. Hadjipanayis, C. M. Sorensen and K. J. Klabunde. Effect of Exchange Anisotropy of the Hysteresis Behaviour of Co Particles. *Nanostructured Materials*, 1:449-456, 1992.
67. S. Gangopadhyay, G. C. Hadjipanayis, C. M. Sorensen and K. J. Klabunde. Magnetic Properties of Ultrafine Co Particles. *IEEE Transactions on Magnetics*, 28:3174-3176, 1992.
68. S. Gangopadhyay, G. C. Hadjipanayis, C. M. Sorensen and K. J. Klabunde. Exchange Anisotropy in Oxide Passivated Co Fine Particles. *Journal of Applied Physics*, 73:6964-6966, 1993.
69. D. S. Geoghegan, P. G. McCormick and R. Street. Mechanically Alloyed Antiferromagnetic-Ferromagnetic Exchange Coupled Nano-Composites. *Materials Science Forum*, 179-181:629-634, 1995.
70. H-M. Lin, C. M. Hsu, Y.D. Yao, Y. Y. Chen, T. T. Kuan, F. A. Yang, and C. Y. Tung. Magnetic Study of Both Nitrided And Oxidized Co Particles. *Nanostructured Materials*, 6:977-980, 1995.
71. M. Spasova, U. Wiedwald, M. Farle, T. Radetic, U. Dahmen, M. Hilgendorff and M. Giersig. Temperature Dependence of Exchange Anisotropy in Monodisperse Cobalt Nanoparticles With a Cobalt Oxide Shell. *Journal of Magnetism and Magnetic Materials*, 272-276:1508-1509 (2004).
72. A. N. Dobrynin, D. N. Ievlev, K. Temst, P. Lievens, J. Margueritat, J. Gonzalo, C. N. Afonso, S. Q. Zhou, A. Vantomme, E. Piscopiello and G. Van Tendeloo. Critical Size

For Exchange Bias in Ferromagnetic-Antiferromagnetic Particles. *Applied Physics Letters*, 87:012501, 2005.

73. S. E. Inderhees, J. A. Borchers, K. S. Green, M. S. Kim, K. Sun, G. L. Strycker and M. C. Aronson. Manipulating The Magnetic Structure of Co Core/CoO Shell Nanoparticles: Implications For Controlling the Exchange Bias. *Physical Review Letters*, 101:117202, 2008.

74. M. Feyngenson, Y. Yiu, A. Kou, K. S. Kim and M. C. Aronson. Controlling the Exchange Bias Field in Co Core/CoO Shell Nanoparticles. *Physical Review B*, 81:195445, 2010.

75. V. Skumryev, S. Stoyanov, Y. Zhang, G. Hadjipanayis, D. Givord, J. Nogués. Beating the Superparamagnetic Limit With Exchange Bias. *Nature*, 423:850-853, 2003.

76. Y. D. Yao, Y. Y. Chen, C. M. Hsu, H. M. Lin, C. Y. Tu, M. F. Tai, D. H. Wang, K. T. Wu and C. T. Suo. Thermal and Magnetic Studies on Nanocrystalline Ni. *Nanostructured Materials*, 6:933-936, 1995 .

77. Y. D. Yao, Y. Y. Chen, M. F. Tai, D. H. Wang and H. M. Lin. Magnetic Anisotropy Effects in Nano-Cluster Nickel Particles. *Materials Science and Engineering: A*, 217-218:281-285, 1996.

78. J. Löffler, W. Wagner, H. Van Swygenhoven, J. Meier, B. Doudin, J.-Ph. Ansermet. Magnetic Properties of Nanostructured Ferromagnetic Metals. *Materials Science Forum*, 235-238:699-704, 1997.

79. J. Löffler, W. Wagner, H. Van Swygenhoven and A. Wiedenmann. Nanoscale Characterization Of Magnetic Properties in Nanostructured Fe, Ni and Co by Small-Angle Neutron Scattering. *Nanostructured Materials*, 9:331-334, 1997.

80. S. A. Makhlof, H. Al-Attar, R. H. Kodama. Particle Size and Temperature Dependence of Exchange Bias in NiO Nanoparticles. *Solid State Communications* 145:1-4, 2008.
81. A. C. Johnston-Peck, J. Wang and J. B. Tracy. Synthesis and Structural and Magnetic Characterization of Ni(core)/NiO(shell) Nanoparticles. *ACS Nano*, 3:1077-1084, 2009.
82. A. Kremenović, B. Jančar, M. Ristić, M. Vučinić-Vasić, J. Rogan, A. Pačevski and B. Antić. Exchange-Bias and Grain-Surface Relaxations in Nanostructured NiO/Ni Induced by a Particle Size Reduction. *The Journal of Physical Chemistry C*, 116:4356-4364, 2012.
83. R. K. Zheng, G. H. Wen, K. K. Fung and X. X. Zhang. Giant Exchange Bias and The Vertical Shifts of Hysteresis Loops in γ -Fe₂O₃ Coated Fe Nanoparticles. *Journal of Applied Physics* 95:5244-5246, 2004.
84. R. K. Zheng, G. H. Wen, K. K. Fung and X. X. Zhang. Training Effect Of Exchange Bias in γ -Fe₂O₃ Coated Fe Nanoparticles. *Physical Review B*, 69:214431, 2004.
85. L. Del Bianco, D. Fiorani, A. M. Testa, E. Bonetti and L. Signorini. Field-Cooling Dependence of Exchange Bias in a Granular System of Fe Nanoparticles Embedded in an Fe Oxide Matrix. *Physical Review B*, 70:052401, 2004.
86. Q. K. Ong, X.-M. Lin and A. Wei. The Role Of Frozen Spins in the Exchange Anisotropy of Core-Shell Fe@Fe₃O₄ Nanoparticles. *Journal of Physical Chemistry C: Nanomater Interfaces*, 115: 2665-2672, 2011.
87. A. Kostopoulou, F. Thétiot, I. Tsiaoussis, M. Androulidaki, P. D. Cozzoli and A. Lappas. Colloidal Anisotropic ZnO-Fe@Fe_xO_y Nanoarchitectures With Interface-Mediated Exchange-Bias and Band-Edge Ultraviolet Fluorescence. *Chemistry of Materials*, 24:2722-2732, 2012.

88. C. M. Hsu, H.-M. Lin, K.-R. Tsai, P.-Y. Lee. High Resolution Transmission Electron Microscopy and Magnetic Properties of Nanocrystalline Iron Particles With Oxidized and Nitrided Surfaces. *Journal of Applied Physics*, 76:4793-4799, 1994.
89. M. Ali, P. Adie, C. H. Marrows, D. Greig, B. J. Hickey and R. L. Stamps. Exchange Bias Using a Spin Glass. *Nature Materials*, 6:70-75, 2007.
90. S. Karmakar, S. Taran, E. Bose, B. K. Chaudhuri, C. P. Sun, C. L. Huang, and H. D. Yang. Evidence Of Intrinsic Exchange Bias and Its Origin in Spin-Glass-Like Disordered $L_{0.5}Sr_{0.5}MnO_3$ Manganites (L=Y, $Y_{0.5}Sm_{0.5}$ and $Y_{0.5}La_{0.5}$). *Physical Review B*, 77:144409, 2008.
91. T. Zhang and M. Dressel. Grain-Size Effects on the Charge Ordering and Exchange Bias in $Pr_{0.5}Ca_{0.5}MnO_3$: The Role of Spin Configuration. *Physical Review B*, 80:014435, 2009.
92. X. Zhang, S. Tang and Y. Du. Synthesis, Characterization, and Exchange Bias Effect in Single Crystalline $Li_{0.44}MnO_2$ Nanoribbons. *The Journal of Physical Chemistry C*, 115:2644-2649, 2011.
93. V. Markovich, R. Puzniak, D. Mogilyansky, X. Wu, K. Suzuki, I. Fita, A. Wisniewski, S. Chen and G. Gorodetsky. Exchange Bias Effect in $La_{0.2}Ca_{0.8}MnO_3$ Antiferromagnetic Nanoparticles With Two Ferromagnetic-Like Contributions. *The Journal of Physical Chemistry C*, 115:1582-1591, 2011.
94. M. Takahashi, A. Yanai, S. Taguchi and T. Suzuki. A Study Of Exchange Anisotropy in Co-CoO Evaporated Thin Films. *Japanese Journal of Applied Physics*, 19:1093-1106, 1980.
95. L. Smardz, U. Köbler and W. Zinn. Temperature and Thickness Dependence of Unidirectional Magnetic Anisotropy Effects in Co/CoO Thin Films. *Vacuum*, 42:283-285, 1991.

96. M. R. Fitzsimmons, P. Yashar, C. Leighton, Ivan K. Schuller, J. Nogués, C. F. Majkrzak and J. A. Dura. Asymmetric Magnetization Reversal in Exchange-Biased Hysteresis Loops. *Physical Review Letters*, 54:3986-3989, 2000.
97. C. Leighton, M. R. Fitzsimmons, A. Hoffmann, J. Dura, C. F. Majkrzak, M. S. Lund, and Ivan K. Schuller. Thickness-Dependent Coercive Mechanisms in Exchange-Biased Bilayers. *Physical Review B*, 65:064403, 2002.
98. F. Radu, M. Etzkorn, V. Leiner, T. Schmitte, A. Schreyer, K. Westerholt, H. Zabel. Polarised Neutron Reflectometry Study of Co/CoO Exchange-Biased Multilayers. *Applied Physics A: Materials Science & Processing*. 74(Supplement 1):S1570-S1572, 2002.
99. F. Radu, M. Etzkorn, R. Siebrecht, T. Schmitte, K. Westerholt, and H. Zabel. Interfacial Domain Formation During Magnetization Reversal in Exchange-Biased CoO/Co Bilayers. *Physical Review B*, 67:134409, 2003.
100. M. Ali, C. H. Marrows, M. Al-Jawad, B. J. Hickey, A. Misra, U. Nowak and K. D. Usadel. Antiferromagnetic Layer Thickness Dependence of The IrMn/Co Exchange-Bias System. *Physical Review B*, 68:214420, 2003.
101. L. W. Martin, Y.-H. Chiu, M. B. Holcomb, M. Huijben, P. Yu, S. J. Han, D. Lee, S. X. Wang, R. Ramesh. Nanoscale Control of Exchange Bias With BiFeO₃ Thin Films. *Nano Letters*, 8:2050-2055, 2008.
102. Y. Liu, S.-G. Wang, Y. Li, N. Li, S. Liu, N. Chen, M.-H. Li and G.-H. Yu. Asymmetric Magnetization Reversal and Its Dual Origin in Co/FeMn Out-of-Plane Induced Exchanged Bias Systems. *Physical Review B*, 84:104436, 2011.
103. E. Demirci, M. Öztürk, E. Sınır, U. Ulucan, N. Akdoğan, O. Öztürk, M. Erkovan. Temperature-Dependent Exchange Bias Properties of Polycrystalline Pt_xCo_{1-x}/CoO Bilayers. *Thin Solid Films*, 550:595-601, 2014.

104. Y. J. Chen, D. K. Lottis, E. D. Dahlberg, J. N. Kuznia, A. M. Wowchak, and P. I. Cohen. Exchange Effects in Molecular-Beam-Epitaxy Grown Iron Films. *Journal of Applied Physics*, 69:4523-4525, 1991.
105. C. Tsang, N. Heiman and K. Lee. Exchange Induced Unidirectional Anisotropy At FeMn-Ni₈₀Fe₂₀ Interfaces. *Journal of Applied Physics*, 52:2471-2473, 1981.
106. M. Tsunoda, M. Konoto, K. Uneyama and M. Takahashi. Effect of Surface Cleaning of Substrate on the Exchange Coupling Field in Ni-Fe/25 at % Ni-Mn Films. *IEEE Transactions on Magnetics*, 33:3688-3690, 1997.
107. M. Tsunoda, Y. Tsuchiya, M. Konoto and M. Takahashi. Microstructure of Antiferromagnetic Layer Affecting on Magnetic Exchange Coupling in Trilayered Ni-Fe/25 At % Ni-Mn/Ni-Fe Films. *Journal of Magnetism and Magnetic Materials*, 171:29-44, 1997.
108. C. L. Lin, J. M. Sivertsen, and J. H. Judy. Magnetic Properties Of NiFe Films Exchange-Coupled With NiO. *IEEE Transactions on Magnetics*, 31:4091-4093, 1995.
109. T. J. Klemmer, V. R. Inturi, M. K. Minor, and J. A. Barnard. Exchange Induced Unidirectional Anisotropy Observed Using Cr-Al Antiferromagnetic Films. *Applied Physics Letters*, 70:2915-2917, 1997.
110. D. V. Dimitrov, S. Zhang, J. Q. Xiao, G. C. Hadjipanayis and C. Prados. Effect of Exchange Interactions At Antiferromagnetic/Ferromagnetic Interfaces on Exchange Bias and Coercivity. *Physical Review B*, 58:12090-12094, 1998.
111. S. M. Zhou, K. Liu, and C. L. Chien. Dependence of Exchange Coupling in Permalloy/Cr₈₂Al₁₈ Bilayers on the Constituent Layer Thickness. *Journal of Applied Physics*, 87:6659-6661, 2000.
112. M. D. Stiles and R. D. McMichael. Coercivity in Exchange-Bias Bilayers. *Physical Review B*, 63:064405, 2001.

113. H. Xi and R. M. White. Antiferromagnetic Thickness Dependence of Exchange Biasing. *Physical Review B*, 61:80-83, 2000.
114. F. Liu. Exchange Bias in Patterned Nanostructures. *PhD Thesis, Department of Materials Science and Engineering, Massachusetts Institute of Technology, USA, February 2016.*
115. T. Ambrose and C. L. Chien. Dependence of Exchange Coupling on Antiferromagnetic Layer Thickness in NiFe/CoO Bilayers. *Journal of Applied Physics*, 83:6822-6824, 1998.
116. J. Nogués, D. Lederman, T. J. Moran, I. K. Schuller and K. V. Rao. Large Exchange Bias and Its Connection to Interface Structure in FeF₂-Fe Bilayers. *Applied Physics Letters* 68:3186-3188, 1996.
117. D. Lederman, J. Nogués and I. K. Schuller. Exchange Anisotropy and the Antiferromagnetic Surface Order Parameter. *Physical Review B*, 56:2332-2335, 1997.
118. V. P. Nascimento, E. C. Passamani, A. D. Alvarenga, F. Pelegrini, A. Biondo, E. B. Saitovitch. Influence of the Roughness on the Exchange Bias Effect of NiFe/FeMn/NiFe Trilayers. *Journal of Magnetism and Magnetic Materials*, 320:e272-e274, 2008.
119. E. Restrepo-Parra, G. Orozco-Hernandez, J. Urrea-Serna, J. F. Jurado, J. C. Vargas-Hernandez, J. C. Riano-Rojas, J. Restrepo. Interface Roughness Influence on Exchange Bias Effect in La_{2/3}Ca_{1/3}MnO₃/ La_{1/3}Ca_{2/3}MnO₃ Bilayers. *Journal of Materials Science*, 45:6763-6768, 2010.
120. J. Moritz, P. Bacher, and B. Dieny. Numerical Study of the Influence of Interfacial Roughness on the Exchange Bias Properties of Ferromagnetic/Antiferromagnetic Bilayers. *Physical Review B*, 94:104425, 2016.

121. A. Maitre, D. Ledue and R. Patte. Interfacial Roughness and Temperature Effects on Exchange Bias Properties in Coupled Ferromagnetic/Antiferromagnetic Bilayers. *Journal of Magnetism and Magnetic Materials*, 324:403-409, 2012.
122. D.-H. Han, J.-G. Zhu, J. H. Judy and J. M. Sivertsen. Texture and Surface/Interface Topological Effects on the Exchange and Coercive Fields of NiFe/NiO Bilayers. *Journal of Applied Physics*, 81:340-343, 1997.
123. D.-H. Han, J.-G. Zhu and J. H. Judy. NiFe/NiO Bilayers With High Exchange Coupling and Low Coercive Fields. *Journal of Applied Physics*, 81:4996-4998, 1997.
124. T. Ambrose and C. L. Chien. Finitesize Scaling in Thin Antiferromagnetic CoO layers. *Journal of Applied Physics*, 79:5920-5922, 1996.
125. X. Y. Lang, W. T. Zheng and Q. Jiang. Dependence of the Blocking Temperature in Exchange Biased Ferromagnetic/Antiferromagnetic Bilayers on the Thickness of the Antiferromagnetic Layer. *Nanotechnology*, 18:155701, 2007.
126. M. Molina-Ruiz, A. F. Lopeandía, F. Pi, D. Givord, O. Bourgeois and J. Rodríguez-Viejo. Evidence of Finite-Size Effect on the Néel Temperature in Ultrathin Layers of CoO Nanograins. *Physical Review B*, 83:140407, 2011.
127. P. J. van der Zaag, L. F. Feiner, R. M. Wolf, J. A. Borchers, Y. Ijiri, R. W. Erwin. The Blocking and Néel Temperature in Exchange Biased Fe₃O₄/CoO Multilayers. *Physica B: Condensed Matter*, 276-278:638-639, 2000.
128. P. J. van der Zaag, Y. Ijiri, J. A. Borchers, L. F. Feiner, R. M. Wolf, J. M. Gaines, R. W. Erwin, M. A. Verheijen. Difference Between Blocking And Néel Temperatures in The Exchange Biased Fe₃O₄/CoO System. *Physical Review Letters*, 84:6102-6105, 2000.
129. N. Akdoğan, S. Kazan, B. Aktaş, M. Özdemir, H. İnam, M. Obaida, J. Dudek, K. Westerholt. Field Cooling-Induced Magnetic Anisotropy in Exchange Biased CoO/Fe

Bilayer Studied by Ferromagnetic Resonance. *Journal of Magnetism and Magnetic Materials*, 323:346-350, 2011.

130. E. Demirci, M. Öztürk, R. Topkaya, S. Kazan, N. Akdoğan, M. Obaida, K. Westerholt. Thickness and Temperature Dependence of Exchange Bias in Co/CoO Bilayers. *Journal of Superconductivity and Novel Magnetism*, 25:2591-2595, 2012.

131. G. Nowak, A. Remhof, F. Radu, A. Nefedov, H.-W. Becker and H. Zabel. Structural and Magnetic Properties of Stoichiometric Epitaxial CoO/Fe Exchange-Bias Bilayers. *Physical Review B*, 75:174405, 2007.

132. M. Öztürk, E. Demirci, R. Topkaya, S. Kazan, N. Akdoğan, M. Obaida, K. Westerholt. Effect of Exchange Bias on Magnetic Anisotropies in Fe/CoO. *Journal of Superconductivity and Novel Magnetism*, 25:2597-2603, 2012.

133. J. Nogués, D. Lederman, T. J. Moran and I. K. Schuller. Positive Exchange Bias in FeF₂-Fe Bilayers. *Physical Review Letters*, 76:4624-4627, 1996.

134. J. Nogués, L. Morellon, C. Leighton, M. R. Ibarra and I. K. Schuller. Antiferromagnetic Spin Flop and Exchange Bias. *Physical Review B*, 61:R6455-R6458, 2000.

135. T. Nozaki, M. Oida, T. Ashida, N. Shimomura, T. Shibata and M. Sahashi. Positive Exchange Bias Observed in Pt-Inserted Cr₂O₃/Co Exchange Coupled Bilayers. *Applied Physics Letters*, 105:212406, 2014.

136. D. Paccard, C. Schlenker, O. Massenet, R. Montmory and A. Yelon. A New Property of Ferromagnetic-Antiferromagnetic Coupling. *Physica Status Solidi (B)*, 16:301-310, 1966.

137. C. Binek. Training of the Exchange-Bias Effect: A Simple Analytical Approach. *Physical Review B*, 70:014421, 2004.

138. F. Radu. Fundamental Aspects of Exchange Bias Effect in AF/F Bilayers and Multilayers. *PhD Thesis, Department of Physics and Astronomy, Ruhr-Universitat Bochum, Germany, 2005.*
139. J. H.E. Griffiths. Anomalous High-Frequency Resistance of Ferromagnetic Metals. *Nature*, 158:670-671, 1946.
140. K. J. Standley. James Griffiths and Ferromagnetic Resonance. *Physics Bulletin*, 34:115-118, 1983.
141. W. A. Yager, Y. M. Bozorth. Ferromagnetic Resonance At Microwave Frequencies. *Physical Review*, 72:80-81, 1947.
142. C. Kittel. Interpretation of Anomalous Larmor Frequencies in Ferromagnetic Resonance Experiment. *Physical Review*, 71:270-271, 1947.
143. C. Kittel. On the Theory of Ferromagnetic Resonance Absorption. *Physical Review*, 73:155-161, 1948.
144. J. H. Van Vleck. Concerning the Theory of Ferromagnetic Resonance Absorption. *Physical Review*, 78:266-274, 1950.
145. L. D. Landau, E. M. Lifshitz. On the Theory of the Dispersion of Magnetic Permeability in Ferromagnetic Bodies. *Phys. Z. Sowjet*, 8:153-169, 1935.
146. T. L. Gilbert. A Phenomenological Theory of Damping in Ferromagnetic Materials. *IEEE Transactions on Magnetics*, 40:3443-3449, 2004.
147. F. Bloch. Nuclear Induction. *Physical Review*, 70:460-474, 1946.
148. N. Bloembergen. On the Ferromagnetic Resonance in Nickel And Supermalloy. *Physical Review*, 78:572-580, 1950.

149. D. Polder. VIII. On the Theory of Ferromagnetic Resonance. *The London, Edinburgh, and Dublin Philosophical Magazine and Journal of Science*, 40:99-115, 1949.
150. L. R. Walker. Magnetostatic Modes in Ferromagnetic Resonance. *Physical Review*, 105:390-399, 1957.
151. G. T. Rado and J. R. Weertman. Spin-Wave Resonance in a Ferromagnetic Metal. *Journal of Physics and Chemistry of Solids*, 11: 315-333, 1959.
152. T. G. Phillips and H. M. Rosenberg. Spin Waves in Ferromagnets. *Reports on Progress in Physics*, 29:285-332, 1966.
153. S. V. Vonsovskii, editor. *Ferromagnetic Resonance: The Phenomenon of Resonant Absorption of a High Frequency Magnetic Field in Ferromagnetic Substances*, Pergamon Press Ltd., 1966.
154. M. Sparks. Ferromagnetic Resonance in Thin Films III. Theory of Mode Intensities. *Physical Review B*, 1:3869-3880, 1970.
155. V. Kambersky and C. E. Patton. Spin-Wave Relaxation and Phenomenological Damping in Ferromagnetic Resonance. *Physical Review B*, 11:2668-2672, 1975.
156. S. E. Barnes. Theory of Electron Spin Resonance of Magnetic Ions in Metals. *Advances in Physics*, 30:801-938, 1981.
157. G. T. Rado. Theory of Ferromagnetic Resonance and Static Magnetization in Ultrathin Crystals. *Physical Review B*, 26:295-304, 1982.
158. P. E. Wigen. Microwave Properties of Magnetic Garnet Thin Films. *Thin Solid Films*, 114:135-186, 1984.
159. B. Heinrich, J. F. Cochran and R. Hasegawa. FMR Linebroadening in Metals Due to Two-Magnon Scattering. *Journal of Applied Physics*, 57:3690-3692, 1985.

160. J. F. Cochran, B. Heinrich and A. S. Arrott. Ferromagnetic Resonance in a System Composed of a Ferromagnetic Substrate and an Exchange-Coupled Thin Ferromagnetic Overlayer. *Physical Review B*, 34:7788-7801, 1986.
161. C. Chappert, K. Le Dang, P. Beauvillain, H. Hurdequint and D. Renard. Ferromagnetic Resonance Studies of Very Thin Cobalt Films on a Gold Substrate. *Physical Review B*, 34:3192-3197, 1986.
162. S. W. McKnight and C. Vittoria. Ferromagnetic Resonance in Magnetic Multilayer Structures. *Physical Review B*, 36:8574-8581, 1987.
163. R. F. Soohoo. Ferromagnetic and Spin Wave Resonance in Multilayer Films. *Journal of Applied Physics*, 63:3829, 1988.
164. L. Baselgia, M. Warden, F. Waldner, S. L. Hutton, J. H. Drumheller, Y. Q. He, P. E. Wigen and M. Marysko. Derivation of the Resonance Frequency from the Free Energy of Ferromagnets. *Physical Review B*, 38:2237-2242, 1988.
165. J. B. Sokoloff. Theory of the Microwave-Frequency Magnetic Susceptibility of Insulating Ferri- and Ferromagnets. *Journal of Applied Physics*, 66:3187-3191, 1989.
166. Z. Celinski and B. Heinrich. Ferromagnetic Resonance Linewidth of Fe Ultrathin Films Grown on a bcc Substrate. *Journal of Applied Physics*, 70:5935-5937, 1991.
167. B. Heinrich and J. F. Cochran. Ultrathin Metallic Magnetic Films: Magnetic Anisotropies and Exchange Interactions. *Advances in Physics*, 42:523-639, 1993.
168. B. Aktaş, Y. Öner and H. Z. Durusoy. A Spin-Wave Resonance Study on Reentrant NiMn Films. *Journal of Magnetism and Magnetic Materials*, 119:339-352, 1993.
169. B. Aktaş, M. Özdemir. Simulated Spin Wave Resonance Absorption Curves for Ferromagnetic Thin Films and Application to NiMn Films. *Physica B*, 193:125-138, 1994.

170. J. O. Artman. Comment on “Anisotropy Studies of Molecular-Beam-Epitaxy-Grown Co(111) Thin Films by Ferromagnetic Resonance” [J. Appl. Phys. 75, 6492 (1994)]. *Journal of Applied Physics*, 77:5484-5485, 1995.
171. M. Özdemir, B. Aktaş, Y. Öner, T. Sato and T. Ando. Anomalous Anisotropy of Re-Entrant Ni₇₇Mn₂₃ Film. *Journal of Physics: Condensed Matter*, 9:6433-6445, 1997.
172. A. G. Gurevich and G. A. Melkov. *Magnetization Oscillations and Waves*, CRC Press, Florida, USA, 1996.
173. Y. Öner, M. Özdemir, B. Aktaş, C. Topaçlı, E. A. Harris and S. Senoussi. The Role of Pt Impurities on Both Bulk and Surface Anisotropies in Amorphous NiMn Films. *Journal of Magnetism and Magnetic Materials*, 170:129-142, 1997.
174. M. Özdemir, B. Aktaş, Y. Öner, T. Sato and T. Ando. A Spin-Wave Resonance Study on Reentrant Ni₇₇Mn₂₃ Films. *Journal of Magnetism and Magnetic Materials*, 164:53-60, 1996.
175. M. Farle. Ferromagnetic Resonance of Ultrathin Metallic Layers. *Reports on Progress in Physics*, 61:755-826, 1998.
176. H. Suhl. Theory of the Magnetic Damping Constant. *IEEE Transactions on Magnetics*, 34:1834-1838, 1998.
177. W. Platow, A. N. Anisimov, G. L. Dunifer, M. Farle and K. Baberschke. Correlations Between Ferromagnetic-Resonance Linewidths and Sample Quality in the Study of Metallic Ultrathin Films. *Physical Review B*, 58:5611-5621, 1998.
178. A. Ercole, E. T. M. Cernohan, G. Lauhoff and J. A. C. Bland. Temperature Dependent Spin-Wave Behaviour in Co/CoO Bilayers. *Journal of Magnetism and Magnetic Materials*, 198-199:534-536, 1999.

179. P. J. Silva, M. Colina, J. R. Fermin. Temperature Dependence of Ferromagnetic Resonance of Al/Fe Bilayers. *Physica B*, 322:308-311, 2002.
180. R. J. Hicken, A. Barman, V. V. Kruglyak and S. Ladak. Optical Ferromagnetic Resonance Studies of Thin Film Magnetic Structures. *Journal of Physics D: Applied Physics*, 36:2183-2192, 2003.
181. H. Moradi. Temperature Dependence of the Linewidth of Spin-Waves in Co/CoO Bilayers. *Journal of Magnetism and Magnetic Materials*, 278:317-322, 2004.
182. R. D. McMichael, P. Krivosik. Classical Model of Extrinsic Ferromagnetic Resonance Linewidth in Ultrathin Films. *IEEE Transactions on Magnetics*, 40:2-11, 2004.
183. F. Giesen. Magnetization Dynamics of Nanostructured Ferromagnetic Rings and Rectangular Elements. *PhD Thesis, Institute of Applied Physics, University of Hamburg, Germany*, 2005.
184. B. Z. Rameev, A. Gupta, F. Yıldız, L. R. Tagirov, B. Aktaş. Strain-Induced Magnetic Anisotropies in Epitaxial CrO₂ Thin Films Probed by FMR Technique. *Journal of Magnetism and Magnetic Materials*, 300:e526-e529, 2006.
185. Kh. Zakeri, J. Lindner, I. Barsukov, R. Meckenstock, M. Farle, U. von Hörsten, H. Wende and W. Keune. Spin Dynamics in Ferromagnets: Gilbert Damping and Two-Magnon Scattering. *Physical Review B*, 76:104416, 2007.
186. R. Topkaya, M. Erkovan, A. Öztürk, O. Öztürk, B. Aktaş and M. Özdemir. Ferromagnetic Resonance Studies of Exchange Coupled Ultrathin Py/Cr/Py Trilayers. *Journal of Applied Physics*, 108:023910, 2010.
187. W. J. Fan, X. P. Qiu, Z. Shi, S. M. Zhou and Z. H. Cheng. Correlation Between Ferromagnetic Resonance Field Shift and Rotatable Anisotropy in Polycrystalline NiFe/FeMn Bilayers. *Thin Solid Films*, 518:2175-2178, 2010.

188. L. Tiu, T. Moriyama, D. C. Ralph and R. A. Buhrman. Spin-Torque Ferromagnetic Resonance Induced by the Spin Hall Effect. *Physical Review Letters*, 106:036601, 2011.
189. M. Charilaou, M. Winklhofer and A. U. Gehring. Simulation of Ferromagnetic Resonance Spectra of Linear Chains of Magnetite Nanocrystals. *Journal of Applied Physics*, 109:093903, 2011.
190. M. Erkovan, S. T. Öztürk, R. Topkaya, M. Özdemir, B. Aktaş and O. Öztürk. Ferromagnetic Resonance Investigation of Py/Cr Multilayer System. *Journal of Applied Physics*, 110:023908, 2011.
191. F. Macia, P. Warnicke, D. Bedau, M.-Y. Im, P. Fischer, D. A. Arena and A. D. Kent. Perpendicular Magnetic Anisotropy in Ultrathin Co|Ni Multilayer Films Studied with Ferromagnetic Resonance and Magnetic X-Ray Microspectroscopy. *Journal of Magnetism and Magnetic Materials*, 324:3629-3632, 2012.
192. J. Zhu, J. A. Katine, G. E. Rowlands, Y.-J. Chen, Z. Duan, J. G. Alzate, P. Upadhyaya, J. Langer, P. K. Amiri, K. L. Wang and I. N. Krivorotov. Voltage Induced Ferromagnetic Resonance in Magnetic Tunnel Junctions. *Physical Review Letters*, 108:197203, 2012.
193. C. T. Boone, H. T. Nembach, J. M. Shaw and T. J. Silva. Spin Transport Parameters in Metallic Multilayers Determined by Ferromagnetic Resonance Measurements of Spin-Pumping. *Journal of Applied Physics*, 113:153906, 2013.
194. R. Topkaya, S. Kazan, R. Yılgin, N. Akdoğan, M. Özdemir and B. Aktaş. Ferromagnetic Resonance Studies of Exchange Biased CoO/Fe Bilayer Grown on MgO Substrate. *Journal of Superconductivity and Novel Magnetism*. 27:1503-1512, 2014.
195. D. P. Gopman, C. L. Dennis, R. D. McMichael, X. Hao, Z. Wang, H. Gan, Y. Zhou, J. Zhang and Y. Huai. Enhanced Ferromagnetic Resonance Linewidth of the Free Layer in Perpendicular Magnetic Tunnel Junctions. *AIP Advances*, 7:055923, 2017.

196. K. Lenz, H. Wende, W. Kuck, K. Baberschke, K. Nagy and A. Janossy. Two-Magnon Scattering and Viscous Gilbert Damping in Ultrathin Ferromagnets. *Physical Review B*, 73:144424, 2006.
197. P. B. Visscher. Fokker-Planck Theory of Spin-Torque Switching: Effective Energy and Transition-State Rate Theory. *SPIE Proceedings*, 7036:70360B, 2008.
198. M. Özdemir. NiMn, NiMnPt ve CrFe Alaşım İnce Filmlerinde Elektron Spin Rezonans (ESR) ve Direnç ölçümleri. *PhD Thesis, Graduate School of Science, İstanbul Technical University*, Turkey, 1998.
199. D. S. Bartran. Limitations of Coherent Precession Models. *IEEE Transactions on Magnetics*, 42:1958-1962, 2006.
200. V. Golub, K. M. Reddy, V. Chernenko, P. Müllner, A. Punnoose and M. Ohtsuka. Ferromagnetic Resonance Properties and Anisotropy of Ni-Mn-Ga Thin Films of Different Thicknesses Deposited on Si Substrate. *Journal of Applied Physics*, 105:07A942, 2009.
201. Z. Celinski, K. B. Urquhart, B. Heinrich. Using Ferromagnetic Resonance to Measure the Magnetic Moments of Ultrathin Films. *Journal of Magnetism and Magnetic Materials*, 166:6-26, 1996.
202. J. Smit and H. G. Beljers. Ferromagnetic Resonance Absorption in BaFe₁₂O₁₉, a Highly Anisotropic Crystal. *Philips Res. Rep.*, 10:113-130, 1955.
203. O. Kohmoto, T. Tsuda and H. Kitamura. Ferromagnetic Resonance in Digital-Video ME Tapes. *Journal of Magnetism and Magnetic Materials*, 193:349-351, 1999.
204. P. E. Wigen and Z. Zhang. Ferromagnetic Resonance in Coupled Magnetic Multilayer Systems. *Brazilian Journal of Physics*, 22:267-282, 1992.
205. M. Öztürk, E. Sınır, E. Demirci, M. Erkovan, O. Öztürk and N. Akdoğan. Exchange bias properties of [Co/CoO]_n multilayers. *Journal of Applied Physics*, 112:093911, 2012.

206. G. A. Carson, M. H. Nassir and M. A. Langell. Epitaxial Growth of Co_3O_4 on $\text{CoO}(100)$. *Journal of Vacuum Science & Technology A*, 14:1637-1642, 1996.
207. N. N. Greenwood and A. Earnshaw. *Chemistry of the Elements, Second Edition*, Elsevier, Butterworth-Heinemann, 1997.
208. M. Hansen. *Constitution of Binary Alloys, Metallurgy and Metallurgic Engineering Series*, McGraw-Hill, 1958.
209. T. G. Knorr, R. W. Hoffman. Dependence of Geometric Magnetic Anisotropy in Thin Iron Films. *Physical Review*, 113:1039-1046, 1959.
210. F. Hellman, E. M. Gyorgy. Growth-Induced Magnetic Anisotropy in Amorphous Tb-Fe. *Physical Review Letters*, 68:1391-1394, 1992.
211. Y. Park, E. E. Fullerton and S. D. Bader. Growth Induced Uniaxial In-Plane Magnetic Anisotropy For Ultrathin Fe Deposited on $\text{MgO}(001)$ by Oblique-Incidence Molecular Beam Epitaxy. *Applied Physics Letters*, 66:2140-2142, 1995.
212. A. J. Devasahayam and M. H. Kryder. The Dependence of The Antiferromagnet/Ferromagnet Blocking Temperature on Antiferromagnet Thickness and Deposition Conditions. *Journal of Applied Physics*, 85:5519-5521, 1999.
213. M. Gruyters and D. Riegel. Strong Exchange Bias by a Single Layer of Independent Antiferromagnetic Grains: The CoO/Co Model System. *Physical Review B*, 63:052401, 2000.
214. J. Camarero, J. Sort, A. Hoffmann, J. M. Garcia-Martin, B. Dieny, R. Miranda and J. Nogués. Origin of the Asymmetric Magnetization Reversal Behaviour in Exchange-Biased Systems: Competing Anisotropies. *Physical Review Letters*, 95:057204, 2005.
215. E. Jiménez, J. Camarero, J. Sort, J. Nogués, A. Hoffmann, F. J. Teran, P. Perna, J. M. Garcia-Martin, B. Dieny and R. Miranda. Highly Asymmetric Magnetic Behaviour in

Exchange Biased Systems Induced by Noncollinear Field Cooling. *Applied Physics Letters*, 95:122508, 2009.

216. F. Radu, M. Etzkorn, T. Schmitte, R. Siebrecht, A. Schreyer, K. Westerholt and H. Zabel. Asymmetric Magnetization Reversal on Exchange Biased CoO/Co Bilayers. *Journal of Magnetism and Magnetic Materials*, 240:251-253, 2002.



APPENDIX A: CALCULATION OF ENERGY DENSITY TERMS

Ferromagnetic (FM) samples can be modelled by the following energy density expression

$$E = E_Z + E_d + E_{ani} + E_g \quad (\text{A.1})$$

where

E_Z : Zeeman energy density

E_d : Energy density due to the demagnetizing field (shape anisotropy)

E_{ani} : Bulk magnetocrystalline anisotropy energy density

E_g : Geometrical (oblique) anisotropy energy density

i. Zeeman Energy Density:

This energy density contribution is due to the scalar product $\vec{M} \cdot \vec{H}$ between the magnetization vector \vec{M} and the applied magnetic field \vec{H} . The components of \vec{M} and \vec{H} are given by (from Figure 4.2)

$$M_x = M \cdot \sin\theta \cdot \cos\phi$$

$$M_y = M \cdot \sin\theta \cdot \sin\phi$$

$$M_z = M \cdot \cos\theta$$

and

$$H_x = H \cdot \sin\theta_H \cdot \cos\phi_H$$

$$H_y = H \cdot \sin\theta_H \cdot \sin\phi_H$$

$$H_z = H \cdot \cos\theta_H$$

Zeeman energy density is given by

$$E_Z = -\vec{M} \cdot \vec{H} = -(M_x H_x + M_y H_y + M_z H_z)$$

By replacing the x , y and z components we get

$$E_Z = -[(M \sin \theta \cos \phi)(H \sin \theta_H \cos \phi_H) + (M \sin \theta \sin \phi)(H \sin \theta_H \sin \phi_H) + (M \cos \theta)(H \cos \theta_H)]$$

which after regrouping becomes

$$E_Z = -MH[\sin \theta \sin \theta_H (\cos \phi \cos \phi_H + \sin \phi \sin \phi_H) + \cos \theta \cos \theta_H]$$

The term $(\cos \phi \cos \phi_H + \sin \phi \sin \phi_H)$ is just equal to $\cos(\phi - \phi_H)$, therefore the Zeeman energy density finally becomes

$$E_Z = -MH[\sin \theta \sin \theta_H \cos(\phi - \phi_H) + \cos \theta \cos \theta_H] \quad (\text{A.2})$$

ii. Energy Density Due To Demagnetizing Field:

The demagnetizing field is the source of the shape anisotropy in FM samples which is caused by the magnetization in the sample [61], acting to oppose and thus reduce the magnetization and is given by

$$\vec{H}_d = -N_d \vec{M}$$

where N_d is the demagnetizing factor determined by the shape of the sample. We have three demagnetization factors which are related to each other by the constitutive relation

$$N_x + N_y + N_z = 4\pi$$

which is a well known identity stemming from the fact that the sum of the demagnetization factors in three orthogonal directions is 4π [62, 63]. For the sample geometry in thin film form as given in Figure 4.2, we have $N_x = N_y = 0$ which then implies that $N_z = 4\pi$.

Macroscopic demagnetizing field caused by the magnetization itself is opposite to the magnetization

$$H_d = -NM = -N_z M_z$$

The energy density that would give this demagnetizing field is

$$E_d = 2\pi M_z^2 = 2\pi M^2 \cos^2 \theta \quad (\text{A.3})$$

iii. Magnetocrystalline Anisotropy Energy Density:

This anisotropy is due to the spin-orbit interaction and it reflects the crystal symmetry of the sample. In polycrystalline and amorphous thin films, this energy is expected to average to zero. For a uniaxial crystal, the magnetocrystalline anisotropy can be given by [59, 61]

$$E_{ani} = K_1 \sin^2 \theta + K_2 \sin^4 \theta \quad (\text{A.4})$$

where θ is the angle between the easy axis of magnetization and the magnetization itself and the constants K_1 and K_2 are the anisotropy coefficients. If the crystal possesses a single easy-axis so that the magnetization can point either up or down, it has a uniaxial symmetry.

When the anisotropy constants are positive, the energy minimum occurs at $\theta = 0$ where the magnetization is along the easy-axis. Magnetocrystalline anisotropy is intrinsic to the material.

iv. Geometrical (Oblique) Anisotropy Energy Density:

Due to the film preparation technique, a growth induced or geometric anisotropy can be observed in the samples [209-211]. If we again refer to the Figure 4.2, we can establish an equation for this kind of anisotropy. If we denote the unit vector along \vec{M} by \hat{e}^m and the unit vector along the geometrical anisotropy \vec{K}_g by \hat{e}^g , the components of these two unit vectors will become as in Table A.1.

Table A.1. Components of the unit vectors for oblique anisotropy energy density calculation

$e_x^m = \sin\theta \cdot \cos\phi$	$e_x^g = \sin\theta_g \cdot \cos\phi_g$
$e_y^m = \sin\theta \cdot \sin\phi$	$e_y^g = \sin\theta_g \cdot \sin\phi_g$
$e_z^m = \cos\theta$	$e_z^g = \cos\theta_g$

If the angle between magnetization \vec{M} and the geometrical anisotropy field \vec{K}_g is denoted by β , then we have

$$\hat{e}^m \cdot \hat{e}^g = |\hat{e}^m| \cdot |\hat{e}^g| \cdot \cos\beta = \cos\beta = e_x^m e_x^g + e_y^m e_y^g + e_z^m e_z^g$$

where use is made of the properties of the dot product and that the magnitudes of the unit vectors are 1. By using the components in the table above, we get

$$\cos\beta = \sin\theta \cos\phi \sin\theta_g \cos\phi_g + \sin\theta \sin\phi \sin\theta_g \sin\phi_g + \cos\theta \cos\theta_g$$

If the β dependence of the geometrical anisotropy energy is given by

$$E_g = -K_g \cos^2\beta \quad (\text{A.5})$$

Then for $\phi_g = 0$

$$\cos\beta = \sin\theta \cos\phi \sin\theta_g + \cos\theta \cos\theta_g$$

which upon squaring becomes

$$\cos^2\beta = \sin^2\theta \sin^2\theta_g \cos^2\phi + \cos^2\theta \cos^2\theta_g + 2\sin\theta \cos\theta \sin\theta_g \cos\theta_g \cos\phi$$

From the identity $\sin(a+b) = \sin a \cos b + \sin b \cos a$, we get $\sin(2a) = 2\sin a \cos a$ which translates into $\sin a \cos a = (1/2)\sin(2a)$ which then can be used for $\sin\theta \cos\theta$ and $\sin\theta_g \cos\theta_g$ terms to obtain

$$\cos^2\beta = \sin^2\theta\sin^2\theta_g\cos^2\phi + \cos^2\theta\cos^2\theta_g + \frac{1}{2}\sin(2\theta)\sin(2\theta_g)\cos\phi$$

If now $\cos^2\phi = 1 - \sin^2\phi$ and $\cos^2\theta = 1 - \sin^2\theta$ are employed, after some manipulation we get

$$\begin{aligned} \cos^2\beta &= \sin^2\theta[\sin^2\theta_g - \cos^2\theta_g - \sin^2\theta_g\sin^2\phi] + \cos^2\theta_g + \frac{1}{2}\sin(2\theta)\sin(2\theta_g)\cos\phi \\ \Rightarrow \cos^2\beta &= -\sin^2\theta[(\cos^2\theta_g - \sin^2\theta_g) + \sin^2\theta_g\sin^2\phi] + \cos^2\theta_g \\ &\quad + \frac{1}{2}\sin(2\theta)\sin(2\theta_g)\cos\phi \end{aligned}$$

From the identity $\cos(a+b) = \cos a \cos b - \sin a \sin b$, we get $\cos(2a) = \cos a \cos a - \sin a \sin a$ which translates into $\cos(2a) = \cos^2 a - \sin^2 a$ which then can be used for $\cos^2\theta_g - \sin^2\theta_g$ term to obtain

$$\begin{aligned} \cos^2\beta &= -\sin^2\theta[\cos(2\theta_g) + \sin^2\theta_g\sin^2\phi] + \cos^2\theta_g \\ &\quad + \frac{1}{2}\sin(2\theta)\sin(2\theta_g)\cos\phi \end{aligned} \tag{A.6}$$

By combining equations (A.5) and (A.6) we obtain the energy term for the geometrical anisotropy:

$$\begin{aligned} E_g &= K_g \left[\sin^2\theta(\cos(2\theta_g) + \sin^2\theta_g\sin^2\phi) - \cos^2\theta_g \right. \\ &\quad \left. - \frac{1}{2}\sin(2\theta)\sin(2\theta_g)\cos\phi \right] \end{aligned} \tag{A.7}$$

v. Mixed Anisotropy Terms For Various Anisotropy Axes:

In some situations where the system under consideration is to be represented by different energy contributions, it is a good practice to develop the angular dependence of energy

terms so that further numerical studies can be completed with relative ease. In this section a couple of different scenarios will be discussed.

- Demagnetizing Field with a Possible Perpendicular Anisotropy:

Demagnetization energy from equation (A.3):

$$E_d = 2\pi M_z^2 = 2\pi M^2 \cos^2 \theta$$

Perpendicular anisotropy along the film thickness:

$$E_p = -K_p \cos^2 \theta$$

Since both E_d and E_p have the same angular dependence, they can be combined together to give

$$E_{eff-z} = 2\pi M^2 \cos^2 \theta - K_p \cos^2 \theta$$

which can be written as

$$E_{eff-z} = K_{eff-z} \cos^2 \theta \tag{A.8}$$

where

$$K_{eff-z} = 2\pi M^2 - K_p \tag{A.9}$$

is the effective anisotropy constant along the film normal (z-direction).

- Uniaxial Anisotropy

If the direction of magnetization is represented by the angles θ and ϕ and that of the uniaxial energy by θ_u and ϕ_u , the angle between the magnetization and the uniaxial anisotropy axis will be

$$\cos\alpha = \sin\theta\sin\theta_u\cos(\phi - \phi_u) + \cos\theta\cos\theta_u$$

which actually reads exactly from the angular part of equation (A.2) with exchanging θ_H and ϕ_H by θ_u and ϕ_u . Then for the uniaxial anisotropy energy we can write

$$E_u = -K_u\cos^2\alpha = -K_u[\sin\theta\sin\theta_u\cos(\phi - \phi_u) + \cos\theta\cos\theta_u]^2 \quad (\text{A.10})$$

which then can be utilised to account for uniaxial anisotropies along a given direction as given in the following examples:

- Uniaxial Anisotropy in x –direction:

This is the first example of an in-plane uniaxial anisotropy which is in the x –direction with respect to Figure 4.2. For this case, $\theta_u = \pi/2$ and $\phi_u = 0$ which then implies from equation (A.10) that

$$E_{u-x} = -K_u\sin^2\theta\cos^2\phi \quad (\text{A.11})$$

- Uniaxial Anisotropy in y –direction

This time $\theta_u = \pi/2$ and $\phi_u = \pi/2$ and equation (A.10) will read

$$E_{u-x} = -K_u\sin^2\theta\sin^2\phi \quad (\text{A.12})$$

➤ Uniaxial Anisotropy in the Film Plane

When the anisotropy axis is in the plane of the film (xy -plane), $\theta_u = \pi/2$ and equation (A.10) will become

$$E_{u-xy} = -K_u \sin^2 \theta \cos^2(\phi - \phi_u) \quad (\text{A.13})$$

If, for example, the anisotropy axis makes an angle $\phi_u = \pi/4$ with the x -axis, we will have

$$E_{u-xy} = -K_u \sin^2 \theta \cos^2\left(\phi - \frac{\pi}{4}\right) = -K_u \sin^2 \theta \left[\cos\left(\phi - \frac{\pi}{4}\right)\right]^2$$

which by the use of $\cos(a - b) = \cos a \cos b + \sin a \sin b$ becomes

$$E_{u-xy} = -K_u \sin^2 \theta \left[\cos \phi \cos \frac{\pi}{4} + \sin \phi \sin \frac{\pi}{4}\right]^2$$

$$\Rightarrow E_{u-xy}(\phi_u = \pi/4) = -\frac{K_u \sin^2 \theta}{2} (\cos \phi + \sin \phi)^2 \quad (\text{A.14})$$